FINAL REPORT

PULTRUSION PROCESS CHARACTERIZATION

NASA Contract NAS8-37193

Submitted by

James G. Vaughan and Robert M. Hackett

School of Engineering

The University of Mississippi

University, MS 38677

TABLE OF CONTENTS

LIST OF TABLES

LIST OF FIGURES

LIST OF FIGURES

PULTRUSION PROCESS CHARACTERIZATION

INTRODUCTION

Pultrusion is a process through which high-modulus, lightweight composite structural members such as beams, truss components, stiffeners, etc., are manufactured. The basic operation, simple in concept - complex in detail, consists of pulling high-strength high-modulus reinforcement fibers/mat through a thermosetting resin bath, and then through a heated die where the wetted fiber bundle cures, thus producing a structurally sound part exiting the die. In the case of the pultrusion of thermoplastic composites, the material enters the die in the form of impregnated rovings and is consolidated. During the pultrusion of thermosetting resin composites major process interactions occur between the chemical reaction occurring during "cure" inside the die, the die temperature profile, and the pull speed of the reinforcement.

The pultrusion process, though a well-developed processing art, lacks a fundamental scientific understanding. The objective of the present study was to determine, both experimentally and analytically, the process parameters most important in characterizing and optimizing the pultrusion of uniaxial fibers. The effects of process parameter interactions were experimentally examined as a function of the pultruded product properties. A numerical description based on these experimental results was developed. This work was lead by Dr. James Vaughan. An analytical model of the pultrusion process was also

developed; this work was lead by Dr. Robert Hackett. The objective of the modeling effort was the formulation of a two-dimensional heat transfer model and developing of solutions for the governing differential equations using the finite element method.

PROCESS DESCRIPTION

In the pultrusion of thermosetting resin composites reinforcing material is assembled and oriented to enter the die in the configuration necessary for the development of the desired mechanical properties of the produced structural member. Heat is supplied to the process by electrically heated metal platens. Cooling water at the die entrance controls the transition from ambient to the die temperature. Hydraulic pullers provide a continuous movement of the product. A chemical reaction process occurs within the die and is initiated by the application of heat to the chemically active resin. The reaction progresses while under the influence of pressure within the die. It is exothermic, and at some position within the die the relationship of heat flux is inverted and the degree of cure progresses to the point where shrinkage allows the part to release from the die wall.

Precise control of the thermal and chemical phenomena occurring within the die is of utmost importance. If the reaction proceeds too rapidly the composite can bond to the die surface. This results in a loss of production, a low-quality product, and possible damage to the die. Once the process is in progress, the pulling force must be regulated to ensure that the line speed does not vary, since speed fluctuations translate directly into variations in cure conditions.

Outwardly the process is deceptively simple in that the function is well-understood.

However, without an in-depth knowledge of the interaction of the various system variables, one cannot achieve efficient performance of the process. Essentially, only general qualitative information about what occurs inside the pultrusion die is presently available. In the liquid zone of the process, the temperature of the die exceeds that of the resin with the temperature of both increasing. Within the gel zone the peak exotherm of the resin is reached, usually being well above the temperature of the die. In effect, over the remainder of the process the die is drawing heat from the curing composite, thereby reducing thermal shock to the product upon its exit from the die. The material traveling through the process undergoes a number of dynamic changes as a result of the temperature environment within the die. The nature of these changes is manifested, to an extent, through the variation of the viscosity of the resin over the length of the die. Over the initial portion, the viscosity decreases as the temperature of the material increases through conduction. This reduction aids in the continuing wet-out of any unsaturated fibers. At the point at which the chemical reaction is initiated, the change in viscosity is reversed, and the viscosity rapidly increases through the stages of gelation and final cure. It is desirable for this reaction to occur under sufficient pressure to ensure composite integrity and to minimize internal porosity which can occur from vapor pressures within the reacting material.

The pressure at the material-die interface is a measurement of normal surface forces which, combined with the appropriate coefficients of friction, yield a measurement of frictional force, or resistance to pull. Pressures can be associated with the viscosity of the resin, the volumetric ratios of fiber and resin, the coefficient of thermal expansion of the materials, the cross-sectional geometry of the cavity, the length of die over which there is

material contact, the coefficients of friction of the die with respect to the liquid, gel and solid, and the degree of shrinkage of the solid. The efficiency of the process can be greatly enhanced through a better understanding of the pressure distribution.

The purpose of this introductory description has been to define the pultrusion process with respect to thermosetting resin systems, highlight the most important process variables, indicate the complex interdependence among these variables which renders an intuitive grasp of the process almost impossible to attain, and thus, emphasize the need for definition of process variable interactions in order to gain insight into the process.

The remainder of this report will be broken into two sections to discuss the work completed to better characterize the pultrusion process. Section 1 will deal with the experimental work performed to statistically characterize pultrusion. This work was directed by Dr. James G. Vaughan. Section II will present the finite element modeling studies conducted by Dr. Robert M. Hackett.

SECTION I

EXPERIMENTAL CHARACTERIZATION OF THE PULTRUSION PROCESS

EXPERIMENTAL CHARACTERIZATION OF THE PULTRUSION PROCESS

EXPERIMENTAL DESIGN OPTIMIZATION METHODS

An optimum process control - product performance ratio for the pultrusion process can only be achieved through a basic understanding and control of all the variables that influence the quality of the final product. To accomplish this objective, considerable time was spent in planning an experimental study to obtain the needed understanding. The experimental procedure had to be capable of determining all process control variables of importance, yet constrained due to the fact that the time for experimentation would be limited. The procedure had to take into account the fact that many of the process variables may interact in their overall effect on the product in a manner called "negative interaction". Negative interaction implies that at one process setting, an increase in a given control variable setting causes an increase in a measured product yield, but at another setting of a different variable, an increase in the first variable now causes a decrease in the product yield.

Reviewing standard plans of experimentation, it was apparent that classical one-factor-at-a-time experiments would not be useful. The classical concept of changing only one factor at a time to determine its effect on product yield cannot deal with interaction among variables, nor is there an accurate method of estimating experimental error. These factors

are known to be present in the pultrusion process. Also, the classical technique requires a great deal of experimental time with little understanding gained to show for the effort. Thus a better experimentation strategy was required.

The second broad class of experimental strategy used by engineers and scientists deals with statistical experimentation. Two major subdivisions of statistical experiments are the full factorial and the fractional or "incomplete" factorial approaches. Examination of the various statistically based experimental plans indicated that too many variables were probably of importance in the pultrusion process to use a full factorial experiment. In looking at various fractional factorial experiments suitable for fitting response surfaces, the central composite design technique [1] and the Box-Behnken method [2] are cited the most often. Both of these experimental designs are fractions of the 3^k factorials, but only require enough observations to estimate main and second-order interactions. Main factors are the process parameters themselves while second-order interactions are the interactions of one main process parameter with another main process parameter. For this study the central composite design showed the greatest possible benefit considering the number of possible pultrusion variables. For five process parameters of interest, the central composite design requires 32 experiments for analysis of all interactions up to second-order, whereas the Box-Behnken technique would require 47 experiments for similar analysis.

The central composite design for five process parameters consists of 16 multi-variable experiments, three mid-point experiments, and 13 star point experiments. These 32 experiments allow all main and two factor interactions to be determined without confounding for five process parameters. Thus the method allows the determination of the importance

of each process parameter, separately and in combination with each other process parameter. The experimental plan for the 32 experiments is listed in Table I. The plan in Table I is listed in standard statistical design order while the plan shown in Table II is listed in the random order as run.

In Tables I and II, the symbols "-2" and "+2" represent the lowest and highest normalized levels of the 5 factors, while "0" represents the center point of each factor range. The symbols "-1" and "1" are halfway between the "0" and "$\pm$2" points. The first 16 experiments constitute a 2^{5-1} resolution IV experiment. The last series of experiments as listed in Table I and II are the star point experiments. Statistical tests can be performed to verify that the variance in the experimental data is actually due to interactions and not to experimental error. The order in which these trials are run is randomized to eliminate systematic variation or bias in the experiment.

TABLE I
Central Composite Experimental Test Plan

Listed in Standard Experimental Order

Random Test #	Test Plan #	Normalized Test Parameters 1	2	3	4	5
16	1	-1	-1	-1	-1	1
1	2	1	-1	-1	-1	-1
11	3	-1	1	-1	-1	-1
17	4	1	1	-1	-1	1
5	5	-1	-1	1	-1	-1
10	6	1	-1	1	-1	1
12	7	-1	1	1	-1	1
18	8	1	1	1	-1	-1
8	9	-1	-1	-1	1	-1
2	10	1	-1	-1	1	1
7	11	-1	1	-1	1	1
9	12	1	1	-1	1	-1
6	13	-1	-1	1	1	1
14	14	1	-1	1	1	-1
15	15	-1	1	1	1	-1
13	16	1	1	1	1	1
3	17	0	0	0	0	0
4	18	0	0	0	0	0
19	19	0	0	0	0	0
22	20	0	0	0	0	0
20	21	0	0	0	0	0
30	22	0	0	0	0	0
24	23	-2	0	0	0	0
27	24	0	-2	0	0	0
23	25	0	0	-2	0	0
31	26	0	0	0	-2	0
29	27	0	0	0	0	-2
21	28	2	0	0	0	0
26	29	0	2	0	0	0
28	30	0	0	2	0	0
25	31	0	0	0	2	0
32	32	0	0	0	0	2

TABLE II
Central Composite Experimental Test Plan

Listed in Random Experimental Order

Random Test #	Test Plan #	Normalized Test Parameters 1	2	3	4	5
1	2	1	-1	-1	-1	-1
2	10	1	-1	-1	1	1
3	17	0	0	0	0	0
4	18	0	0	0	0	0
5	5	-1	-1	1	-1	-1
6	13	-1	-1	1	1	1
7	11	-1	1	-1	1	1
8	9	-1	-1	-1	1	-1
9	12	1	1	-1	1	-1
10	6	1	-1	1	-1	1
11	3	-1	1	-1	-1	-1
12	7	-1	1	1	-1	1
13	16	1	1	1	1	1
14	14	1	-1	1	1	-1
15	15	-1	1	1	1	-1
16	1	-1	-1	-1	-1	1
17	4	1	1	-1	-1	1
18	8	1	1	1	-1	-1
19	19	0	0	0	0	0
20	21	0	0	0	0	0
21	28	2	0	0	0	0
22	20	0	0	0	0	0
23	25	0	0	-2	0	0
24	23	-2	0	0	0	0
25	31	0	0	0	2	0
26	29	0	2	0	0	0
27	24	0	-2	0	0	0
28	30	0	0	2	0	0
29	27	0	0	0	0	-2
30	22	0	0	0	0	0
31	26	0	0	0	-2	0
32	32	0	0	0	0	2

EXPERIMENTAL PROCEDURE

The composite system chosen for study was the Shell EPON 9420/9470/537 epoxy system with graphite fiber. The polyacrylonitrile (PAN) base graphite fiber, type I AS4-W-12K, was manufactured by Hercules Inc. A formulation for the epoxy system is given in Table III. The epoxy resin was mixed daily for each series of experiments and held at approximately 70-75 F before being placed into the pultrusion resin bath. The pultruded product shape was a 1 x 1/8 inch rectangle.

Considerable time was spent in readying the NASA/MSFC pultruder for the experiments required for the statistical optimization trials. New rubber grips were obtained to better grip the graphite fibers for initial pulling through the die. New alignment blocks, for preparing the fibers into the proper shape before entering the die, were machined. Methods of running the fibers through the resin bath for maximum wet-out were examined.

From prove-in experiments, five operating parameters were considered most important for optimization of the pultrusion process. These five parameters were the die platen heating temperatures (zone 1 and zone 2), the percent fiber content in the pultruded product, the pull speed of the product, and the amount of clay filler in the epoxy. Prove-in experiments, along with the Shell literature for the EPON 9420 epoxy, had indicated that the platen temperature should reach 400 F (204 C). Previous experiments had indicated that fiber percentages (by volume) less than 59% would result in an under-developed product shape and amounts greater than 65% were not possible for continuous pulling at high speeds. Thus the control parameters, with their various operating extremes, were selected for the optimization experiments as shown in Table IV.

TABLE III
Formulation Table for the Shell EPON 9420 Epoxy System

		phr
A.	EPON 9420 resin	100
	EPON 537 accelerator	2.0
	AXEL INT 18-46 (internal release agent)	0.65
B.	ASP 400-P (clay filler)	20
C.	EPON 9470 curing agent	24.4

Mix all components of A. together for one minute. Add component B. to above and mix until homogenous (app. 5 minutes). Do not allow mix to heat due to mixing action. Add component C. and mix for no more than 2 to 3 minutes. Again allow no heat to be generated.

EPON is a registered trademark of Shell Chemical Company.
AXEL is a trademark of Axel Plastics Research Laboratories.
ASP 400-P is a product of Engelhard Minerals & Chemicals Corporation.

TABLE IV

Range of Pultrusion Process Parameters
for Central Composite Design Experiments

		Process Parameter Test Range				
		-2	-1	0	1	2
Process Parameter 1:	Filler (phr)	16	17	18	19	20
Process Parameter 2:	Graphite tows	101	103	105	107	109
	%	59.7	60.9	62.1	63.3	64.4
Process Parameter 3:	Pull Speed in/min	8	10	12	14	16
Process Parameter 4:	Zone 1 Temp (F)	350	360	370	380	390
Process Parameter 5:	Zone 2 Temp (F)	350	360	370	380	390

RESULTS AND DISCUSSION

Figure 1 shows internal processing temperature profiles of the die for four platen control point temperatures. The control set point temperatures for each of the four profiles is noted in the Figure legend. The four plotted profiles represent the four temperature extremes from the range of zone temperature settings listed in Table IV. As can be seen from the plotted data, the peak temperature inside the die is approximately 40 F higher than the die set point temperature. Part of the reason for this overshoot lies with the two thermocouples in each heating platen that are used to control the die temperature to the set point temperature. These two control thermocouples, for both the bottom and top heating platen, are located 10.3 inches and 24.9 inches from the platen edge at the die entrance. Due to the placement of the cartridge heating rods within the heating platens, the sensing thermocouples can not determine the heat build-up between the two heating zones. Thus the platens heat to the set point temperature as designed, but overshoot the set point temperature in the region between the two zone control thermocouples. Another reason for the overshoot is the heat released due to the epoxy cure exotherm. Temperature profile tests indicate that the curing of the epoxy generates an additional 10 to 20 F to the peak temperature.

The temperature profile is not centered at the middle of the heated die. In fact, the peak temperature of all four profiles is in a different die location. Water cooling was used to prevent rapid heat build-up in the entrance section of the die. This has an effect of keeping the entrance portion of the die cooler than the remaining areas. As product is pulled through the die, heat tends to be carried toward the exit end of the die thus making

this region hotter than the other regions. Even though the heated platen length is only 36 inches and the die only 30 inches, the temperature within the pultruded product remains high for quite some distance outside the die as can be seen in Figure 1.

In Figure 1 it can also be observed that the temperature profiles with zone 1 high exit the die at a lower temperature than when zone 1 is low and zone 2 is high. This is due to the location of the epoxy exotherm within the die. When zone 1 is held at a high temperature, the resin exotherm tends to occur much earlier in the die. Thus much heat is released in the front portion of the die and little heat is produced in the rear of the die. However, when the front of the die is kept cooler and the zone 2 is high, then the resin exotherms in the rear of the die keeping the back portion of the die hot. This is why the "L-H" temperature profile appears to hold a higher temperature longer than any of the other three profiles.

Viscosity measurements were made for all resin batches used in the 32 experiments. These viscosity measurements are shown in Figure 2. Many of the first experiments used the same resin mix so the viscosity measurements are plotted as the same value for these first experiments. Towards the end of the experimentation, viscosity measurements were also made on the resin at the end of the experiment. These final viscosity readings are also shown in Figure 2 for experiments 23 - 32. As can be seen, an increase in viscosity of approximately 1000 cps during the course of the experiment was typical.

Table V presents the range of pull pressures observed during the pultrusion of the 32 test experiments. These values were taken from the Pultrusion Technology, Inc. (PTI) readout on the main display panel which uses the hydraulic load on the puller to determine

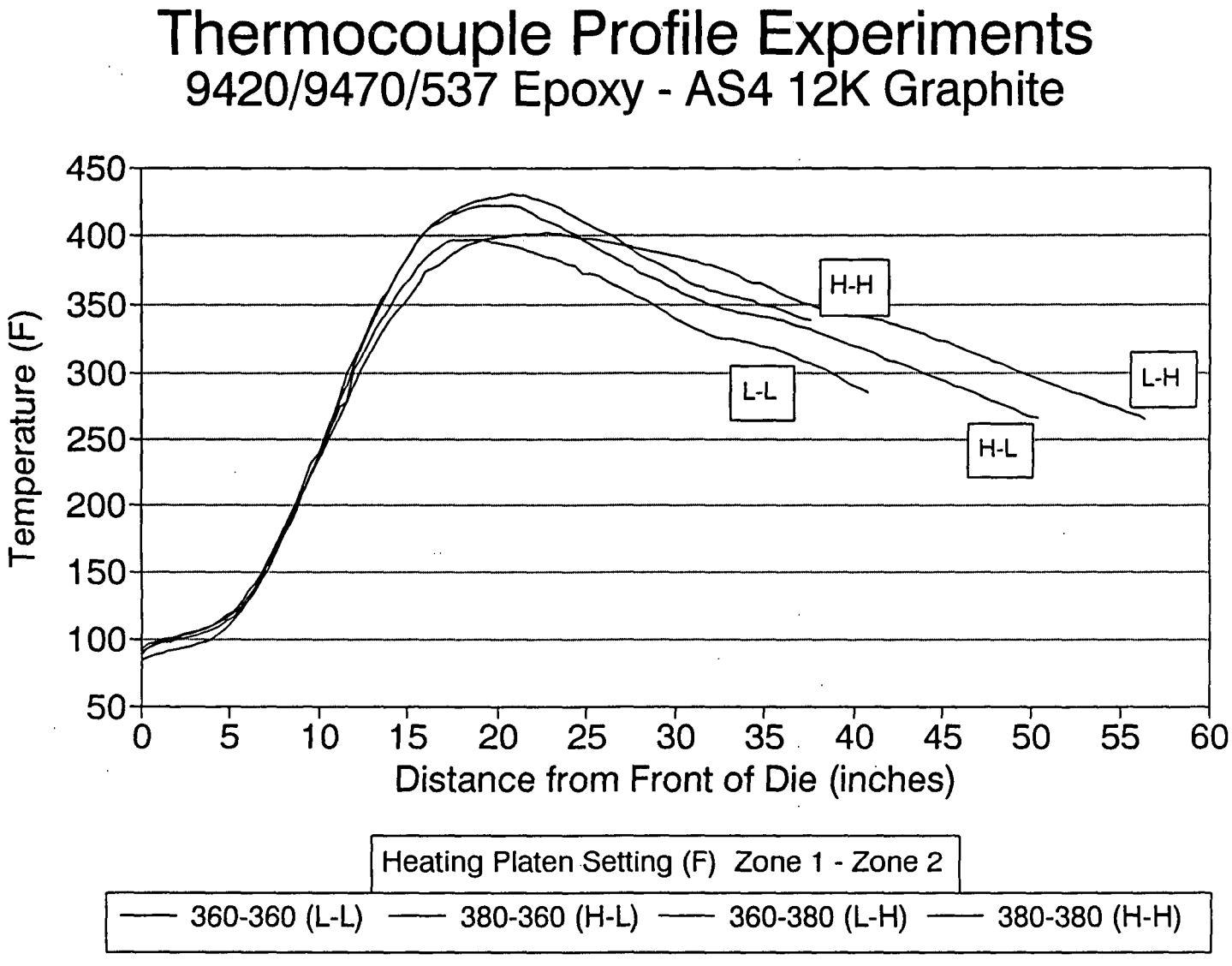

Figure 1. Temperature profile within pultrusion die as a function of the four extreme die zone temperature settings. Determined by passing a thermocouple through the pultrusion die.

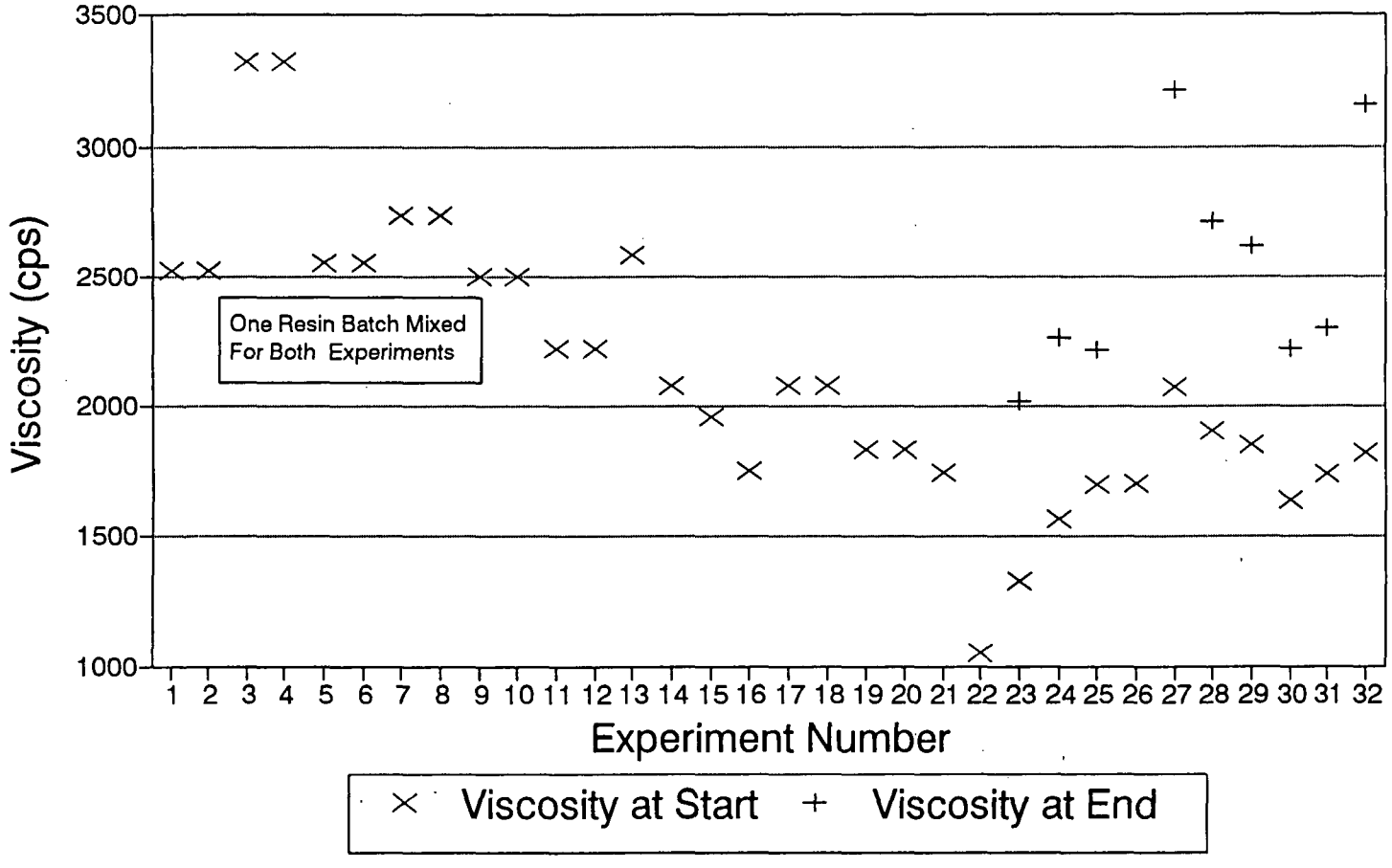

Figure 2. Viscosity as a function of experiment number. The viscosity of the first series of pultrusion experiments is the same since only one batch of resin was mixed for both sets of experiments. Viscosity at the end of the experiment was measured for experiments 23 - 32.

TABLE V

Pull Load for the 32 Pultrusion Experiments

Experiment Number	Pull Load (lbs)
1	Not Recorded
2	Not Recorded
3	1200 - 1700
4	1200 - 1700
5	4300 - 3500
6	6000 - 1400
7	2000 - 3000
8	3000 - 5000
9	3500 - 7600
10	8000 - 6250
11	2900 - 4000
12	5250 - 6000
13	7000 - 2500
14	2400 - 5000
15	2250 - 4500
16	1000
17	7600 - 9000
18	10000
19	2250 - 5000
20	2250 - 8000
21	1200
22	3750 - 6100
23	2000 - 1000
24	1200
25	2300 - 4000
26	2750
27	1300
28	3500 - 5500
29	1500
30	3300 - 1500
31	1200
32	3100 - 2400

pull load. As can be seen from the data in Table V a large variation in pull pressure occurred from these experiments. Where the pull pressure varied greatly within one run, the range of pull pressure observed is noted. If only one value is given for the pull pressure, then it was observed that the pull pressure did not vary by more than $\pm$ 200 pounds.

Fifty feet of 1 x 1/8 inch product were run for each pultrusion experiment. Ten sections, each five feet long were cut and labeled from the 50 feet of product. After all the pultrusion characterization experiments were completed, the following measurements were made on the 32 sets of pultruded product. Mechanical property tests were conducted for flexural shear strength (ASTM D790 Method II), and short-beam shear strength (ASTM D2344). Tensile strength - modulus (ASTM D3039) were also going to be conducted, but due to a delay in testing of the tensile samples, these data can not be included in this report. All tests were conducted at room temperature (approximately 75-85 F (24-30 C) except for the short-beam shear test which was conducted both at room temperature and at 350 F (177 C). Material samples for each test were selected from product produced every 10 feet of each experiment to determine if a major change in the process/property occurred during the time of the test. No change was observed.

Typical test results for the flexural shear tests are shown in Figure 3. In Figure 3 are plotted the flexural load versus the flexural displacement. The loading rate was 0.2 in/min. The data shown are for the five test samples of experiment 8, although similar curves were observed for all 32 experiments. Typical test results for the room temperature short-beam shear tests are shown in Figure 4; the high temperature (350 F) short-beam shear results are similar except for lower breaking stresses. The loading rate for the short-beam shear tests

was 0.05 in/min.

The data for all of the flexural test results are given in Figure 5. In Figure 5 the data are presented in the form of a maximum - minimum bar chart with the average of the tests results shown as a tick mark on the bar. Data for all 32 experiments are shown. A similar type of bar chart for the room temperature short-beam shear tests is shown in Figure 6 and the high temperature short-beam shear results in Figure 7.

All of the mechanical property test data, with averages and standard deviations, are given in Tables VI-VIII. As can be seen from Figures 5-7 and the data in Tables VI-VIII a large variation in test properties were observed. However, a simple examination of these data do not indicate any given pattern variation with regard to the five process parameters under investigation.

To further examine the effects of the pultrusion process parameters, a standard central composite design analysis was conducted. For these analyses, each of the average mechanical property values for each of the 32 experiments were used to determine a second order equation as a model of the pultrusion process. In these analyses all experimental runs were used with equal weight given to all equation coefficients. Table IX lists the coefficients for the experimental model. In Table IX it can be seen that many of the coefficients are not of major importance. By eliminating those coefficients of minor value and performing the fit analysis for those terms that produce a major influence in the experimental model, a reduced set of new fit coefficients can be developed. These reduced sets of equation coefficients are given in Table X for flexural strength, room temperature short-beam shear strength, and high temperature (350 F) short-beam shear strength. The R squared values

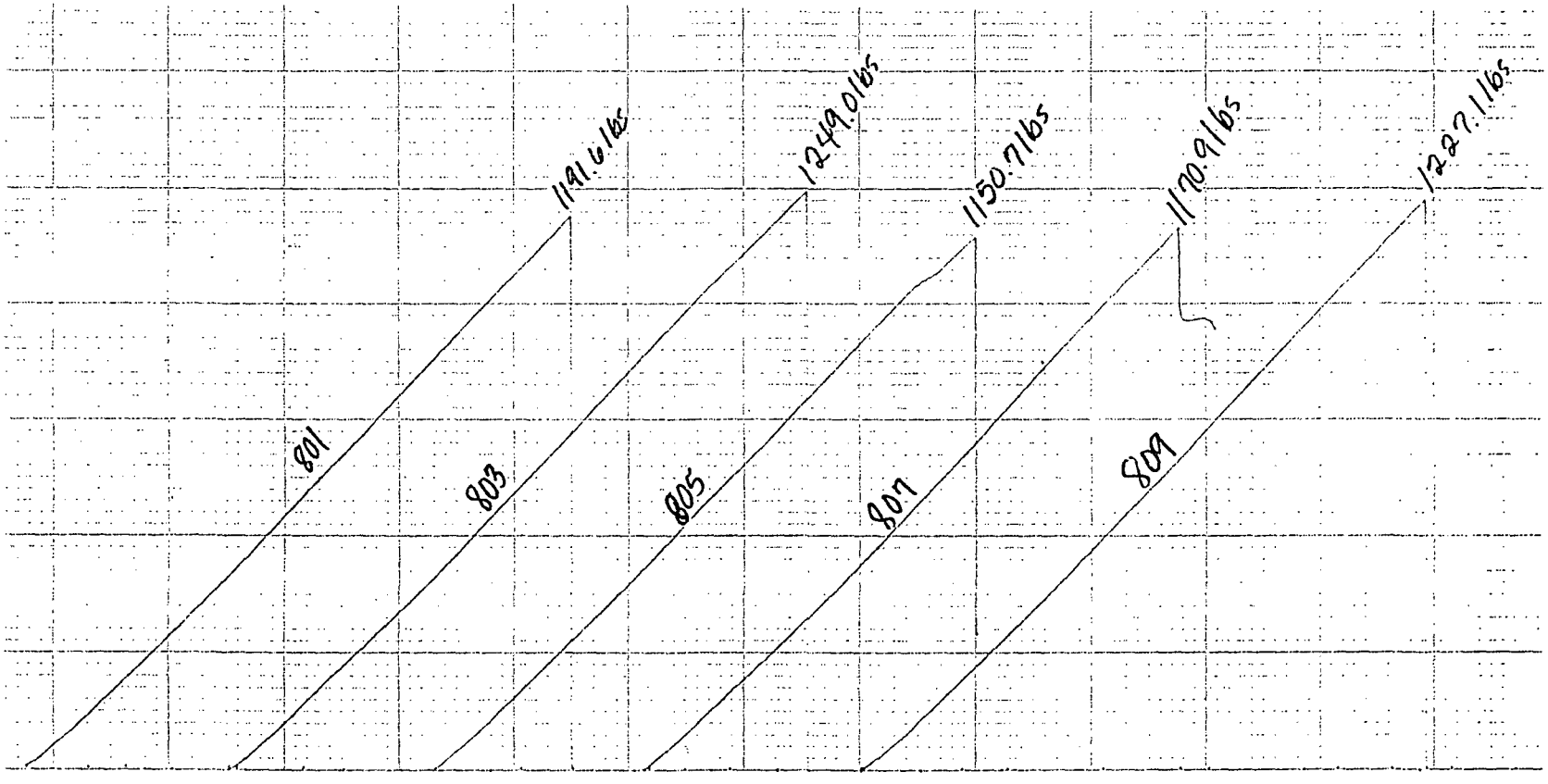

Figure 3. Typical results of flexural test plotting load versus displacement. Actual results shown are for experiment number eight.

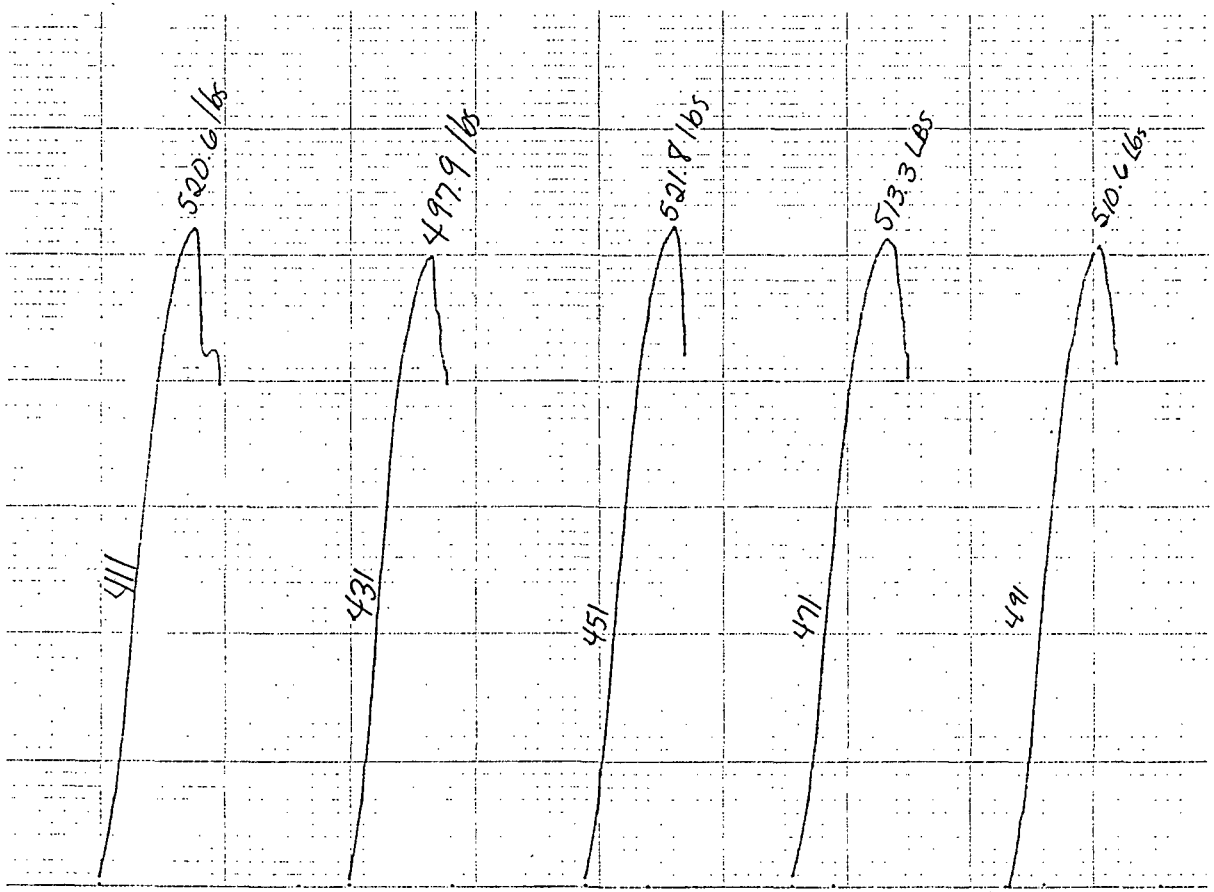

Figure 4. Typical results of short-beam shear test plotting load versus displacement. Actual results shown are for experiment number four.

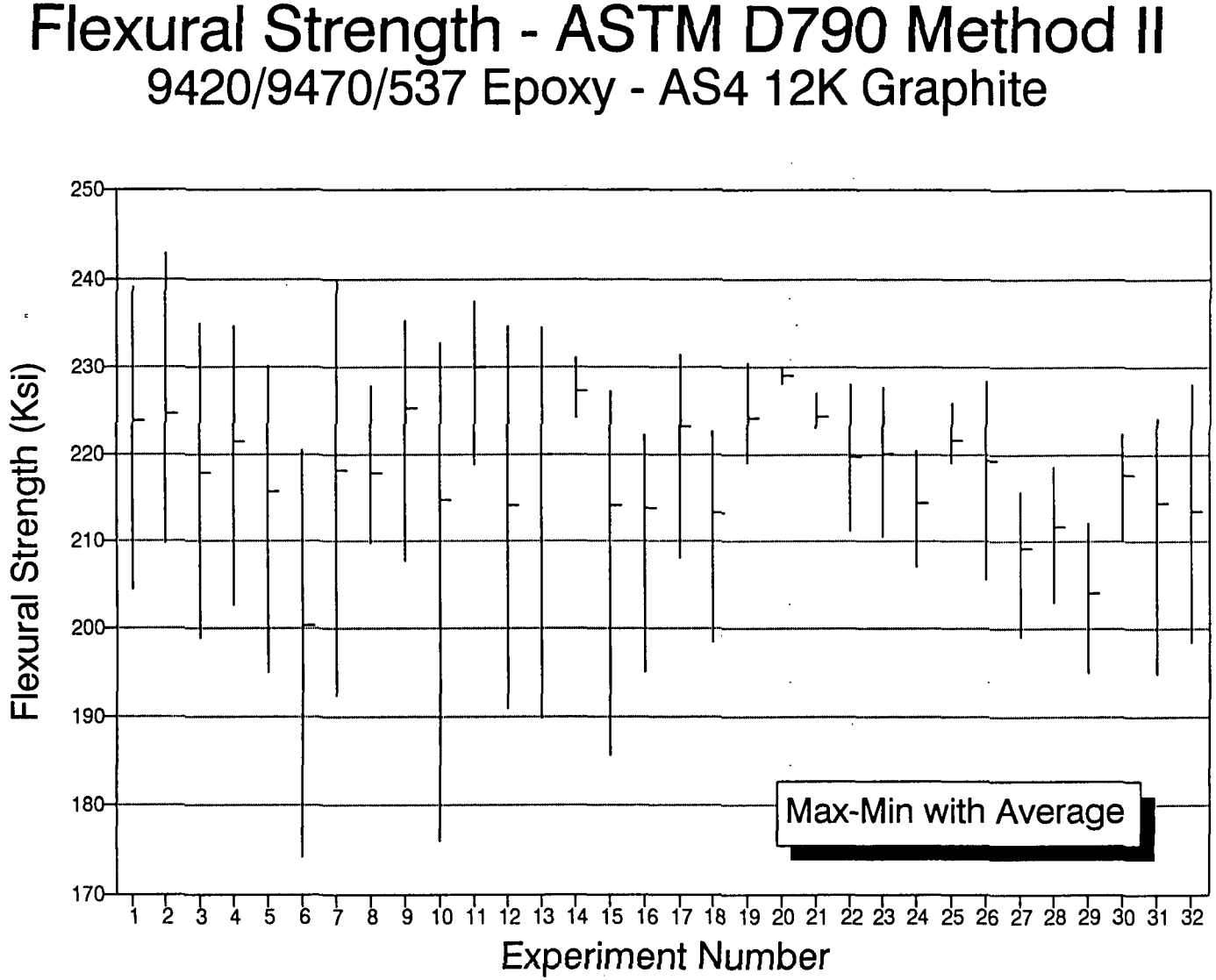

Figure 5. Plot of flexural strength for the 32 pultrusion experiments. Shown are the maximum and minimum values for those samples tested as well as the average of the test samples.

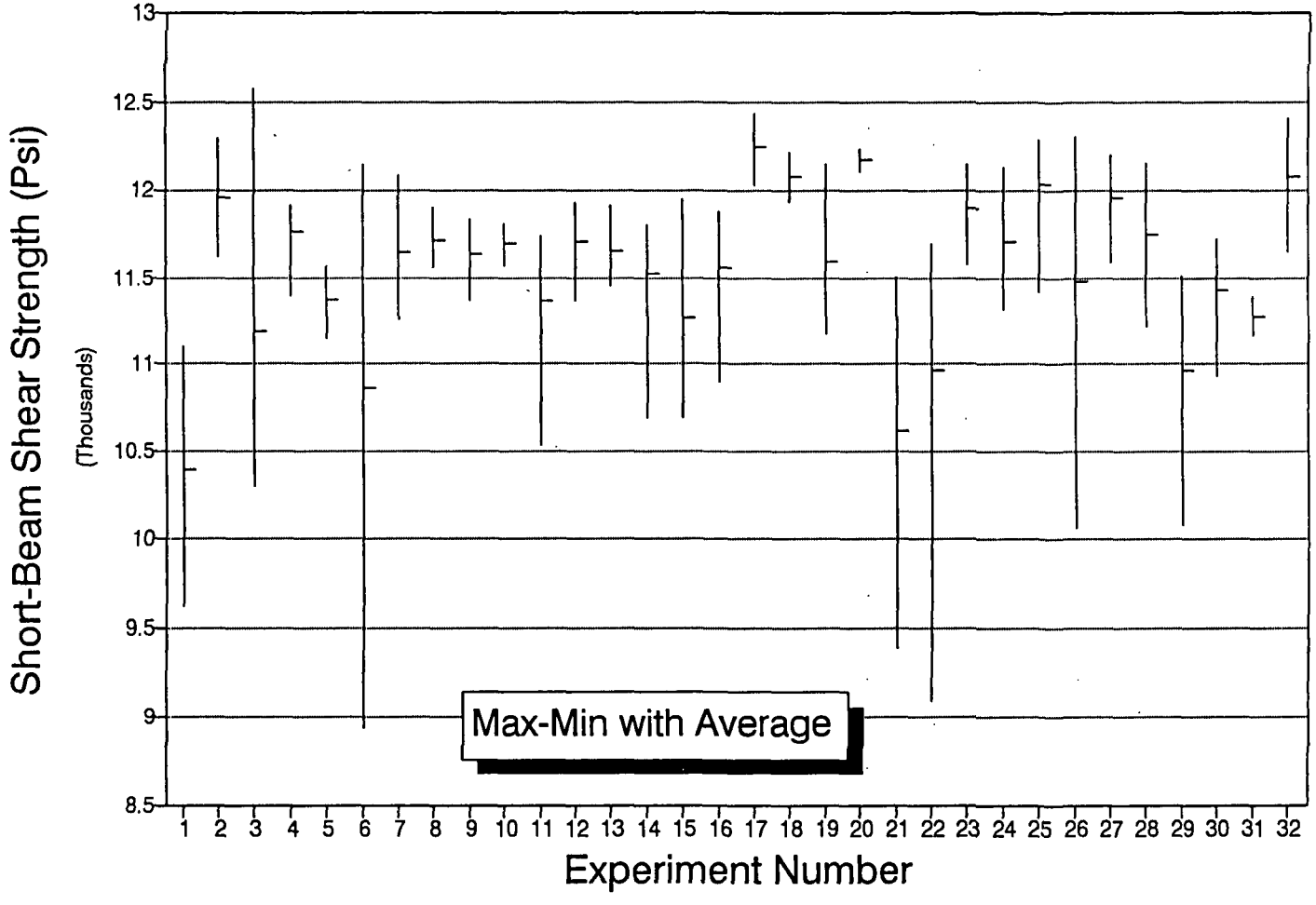

Figure 6. Plot of room temperature short-beam shear strength for the 32 pultrusion experiments. Shown are the maximum and minimum values for those samples tested as well as the average of the test samples.

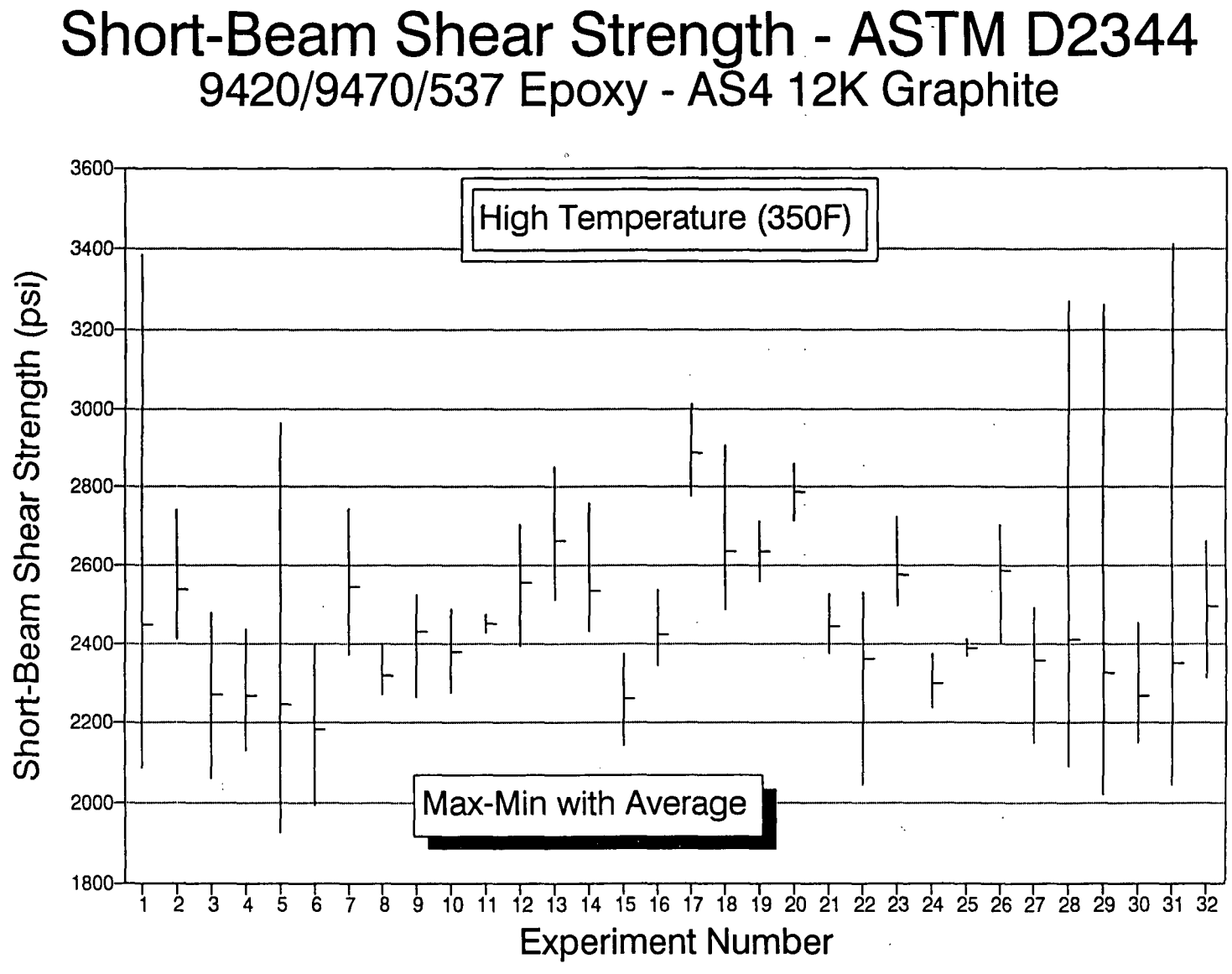

Figure 7. Plot of high temperature (350 F) short-beam shear strength for the 32 pultrusion experiments. Shown are the maximum and minimum values for those samples tested as well as the average of the test samples.

TABLE VI
Flexural Strength of Pultrusion Test Samples (ksi)

Random Test #	Individual Product Samples 1	2	3	4	5	STD.DEV.	AVG.
1	233.9	239.1	206.9	235.0	204.5	16.73	223.9
2	235.7	242.9	214.5	220.6	209.7	14.10	224.7
3	198.9	216.8	219.9	235.1	218.6	12.84	217.8
4	225.8	234.8	202.6	231.4	212.8	13.50	221.5
5	230.2	217.7	224.1	195.1	211.3	13.51	215.7
6	220.4	174.2	193.4	206.8	207.0	17.48	200.4
7	231.0	199.9	227.9	239.8	192.5	20.74	218.2
8	217.2	228.0	210.0	209.7	224.1	8.22	217.8
9	207.7	235.4	235.0	228.3	220.1	11.65	225.3
10	225.0	232.8	218.7	175.9	221.1	22.33	214.7
11	218.8	236.9	234.0	237.5	223.3	8.51	230.1
12	224.6	234.8	225.0	195.3	190.9	19.67	214.1
13	189.9	216.2	229.8	229.4	234.7	18.18	220.0
14	-	224.2	225.0	228.5	231.2	3.24	227.2
15	218.0	218.0	227.2	222.0	185.5	16.45	214.2
16	195.0	222.2	210.1	220.7	220.6	11.54	213.7
17	226.7	208.0	226.4	223.3	231.6	9.01	223.2
18	222.7	-	198.4	213.4	218.6	10.66	213.3
19	223.1	-	-	218.9	230.5	5.90	224.2
20	-	-	228.1	230.0	1.33	229.0	
21	224.5	227.1	223.0	223.0	224.1	1.66	224.3
22	-	217.0	228.1	222.5	211.2	7.27	219.7
23	210.5	227.8	225.7	216.7	219.7	6.98	220.1
24	220.4	207.0	210.3	214.2	220.3	5.96	214.4
25	218.9	225.9	223.3	219.4	220.7	2.95	221.6
26	205.6	216.3	223.9	228.4	222.3	8.83	219.3
27	214.9	199.0	207.4	208.8	215.8	6.75	209.2
28	218.6	212.1	203.0	216.8	208.1	6.36	211.7
29	195.1	201.6	208.5	203.3	212.1	6.55	204.1
30	210.0	222.4	220.6	217.2	-	5.48	217.6
31	220.7	224.2	219.4	194.8	212.8	11.68	214.4
32	224.0	207.8	198.5	208.8	228.1	12.27	213.4

TABLE VII
Short-Beam Shear Strength (psi) - Room Temperature

Random Test #	Individual Product Samples 1	2	3	4	5	STD.DEV.	AVG.
1	11,111	9,617	10,523	10,539	10,176	548	10,393
2	11,623	12,297	11,806	12,015	12,044	255	11,957
3	10,372	10,295	12,581	10,990	11,714	964	11,190
4	11,916	11,397	11,897	11,841	11,779	213	11,766
5	11,346	11,154	11,568	11,419	11,402	150	11,378
6	12,155	8,942	11,492	-	-	1,696	10,863
7	11,263	11,268	11,551	12,087	12,061	408	11,646
8	11,909	11,712	11,563	11,769	11,632	133	11,717
9	11,369	11,527	11,842	11,748	11,686	188	11,634
10	11,808	11,565	11,680	11,753	11,698	91	11,701
11	10,533	11,434	11,744	11,747	11,385	497	11,369
12	11,368	11,935	11,702	11,728	11,799	210	11,706
13	11,454	11,915	11,464	11,742	11,721	198	11,659
14	10,690	11,696	11,709	11,749	11,801	471	11,529
15	10,716	11,951	11,058	11,936	10,690	632	11,270
16	10,897	11,693	11,884	11,546	11,770	390	11,558
17	12,028	12,108	12,283	12,440	12,387	177	12,249
18	12,218	11,986	11,931	12,080	12,183	123	12,080
19	11,174	11,308	11,491	11,837	12,155	401	11,593
20	12,104	12,238	12,193	12,228	12,126	60	12,178
21	10,144	10,903	11,164	11,509	9,385	854	10,621
22	9,087	10,683	11,685	11,682	11,701	1,138	10,967
23	11,580	12,150	11,955	11,792	11,997	217	11,895
24	11,348	11,746	11,317	11,992	12,134	369	11,708
25	11,423	12,256	12,118	12,293	12,099	354	12,038
26	10,061	10,948	11,881	12,307	12,198	956	11,479
27	11,585	12,204	12,155	11,955	11,900	246	11,960
28	11,218	11,692	11,748	11,924	12,160	348	11,748
29	10,077	10,915	11,112	11,198	11,518	542	10,964
30	10,929	11,441	11,587	11,728	11,464	302	11,430
31	11,167	11,322	11,391	11,288	11,217	88	11,277
32	11,648	11,897	12,413	12,214	12,240	306	12,082

TABLE VIII
Short-Beam Shear Strength (psi) - High Temperature (350F)

Random Test #	Individual Product Samples 1	2	3	4	5	STD.DEV.	AVG.
1	2,251	2,086	2,285	2,232	3,385	529	2,448
2	2,491	2,539	2,741	2,409	2,514	123	2,539
3	2,200	2,059	2,477	2,314	2,295	154	2,269
4	2,351	2,197	2,127	2,437	2,223	125	2,267
5	2,965	1,927	2,111	2,274	1,959	424	2,247
6	2,398	1,991	2,157	-	-	205	2,182
7	2,744	2,369	2,536	2,592	2,472	140	2,543
8	2,397	2,367	2,281	2,272	2,270	60	2,317
9	2,264	2,478	2,524	2,460	2,424	100	2,430
10	2,419	2,489	2,369	2,273	2,344	81	2,379
11	2,474	2,424	2,435	2,471	2,449	22	2,451
12	2,575	2,539	2,704	2,556	2,390	112	2,553
13	2,609	2,713	2,852	2,510	2,629	128	2,662
14	2,554	2,454	2,472	2,428	2,758	134	2,533
15	2,270	2,318	2,374	2,141	2,198	93	2,260
16	2,427	2,538	2,433	2,367	2,341	76	2,421
17	2,906	2,883	2,865	3,013	2,778	85	2,889
18	2,907	2,704	2,530	2,484	2,542	174	2,633
19	2,559	2,644	2,571	2,686	2,714	69	2,635
20	2,746	2,712	2,859	2,858	2,758	68	2,787
21	2,374	2,479	2,527	2,447	2,390	63	2,444
22	2,044	2,273	2,530	2,456	2,493	202	2,359
23	2,562	2,725	2,533	2,565	2,497	88	2,577
24	2,344	2,247	2,236	2,291	2,376	60	2,299
25	2,367	2,371	2,381	2,413	2,412	22	2,389
26	2,399	2,641	2,580	2,705	2,603	114	2,586
27	2,248	2,438	2,462	2,491	2,148	151	2,357
28	2,223	2,089	2,096	3,274	2,355	497	2,407
29	3,261	2,019	2,100	2,134	2,115	525	2,326
30	2,147	2,288	2,197	2,251	2,453	117	2,267
31	3,415	2,066	2,103	2,044	2,128	596	2,351
32	2,483	2,312	2,472	2,542	2,662	127	2,494

TABLE IX
Coefficients for Experimental Mathematical Model

Complete Model

Equation Coefficients	Flexural Stress (ksi)	Short-Beam Shear Stress (psi)	Short-Beam Shear Stress (psi) 350 F
b(0)	220.75	11529.22	2422.15
b(a)	2.83	-19.96	76.21
b(b)	1.69	64.79	75.54
b(c)	-3.09	-26.29	-38.71
b(d)	0.56	56.79	-19.96
b(e)	-0.83	175.21	49.38
b(aa)	0.32	-97.59	-6.27
b(bb)	-0.96	41.16	18.73
b(cc)	-0.55	66.66	23.85
b(dd)	-0.02	25.66	-6.65
b(ee)	-2.33	-7.97	3.35
b(ab)	-2.36	97.94	4.69
b(ac)	0.84	113.06	24.44
b(ad)	2.82	54.44	11.56
b(ae)	1.52	118.19	0.06
b(bc)	-0.82	-1.81	11.19
b(bd)	-0.32	-139.44	-44.19
b(be)	1.48	-9.69	56.06
b(cd)	0.56	-183.06	12.81
b(ce)	-0.24	-164.06	-40.19
b(de)	-0.24	-126.19	-4.81

a => process parameter 1 = amount of filler (phr)
b => process parameter 2 = percent of graphite (%)
c => process parameter 3 = pull speed (in/min)
d => process parameter 4 = zone 1 die temperature (F)
e => process parameter 5 = zone 2 die temperature (F)

TABLE X
Coefficients for Experimental Mathematical Model

Reduced Set

Equation Coefficients	Flexural Stress (ksi)	Short-Beam Shear Stress (psi)	Short-Beam Shear Stress (psi) 350 F
b(0)	220.30	11550.16	2446.91
b(a)	3.67	-	76.21
b(b)	2.42	-	75.54
b(c)	-2.25	-	-38.71
b(d)	-	-	-
b(e)	-1.67	175.21	-
b(aa)	-	-	-
b(bb)	-	-	-
b(cc)	-	-	-
b(dd)	-	-	-
b(ee)	-2.15	-	-
b(ab)	-	-	-
b(ac)	2.13	-	-
b(ad)	-	-	-
b(ae)	-	-	-
b(bc)	-	-	-
b(bd)	-	-	-
b(be)	-	-	56.06
b(cd)	-	-183.06	-
b(ce)	-	-164.06	-
b(de)	-	-	-
R square	0.54	0.28	0.51

a => process parameter 1 = amount of filler (phr)
b => process parameter 2 = percent of graphite (%)
c => process parameter 3 = pull speed (in/min)
d => process parameter 4 = zone 1 die temperature (F)
e => process parameter 5 = zone 2 die temperature (F)

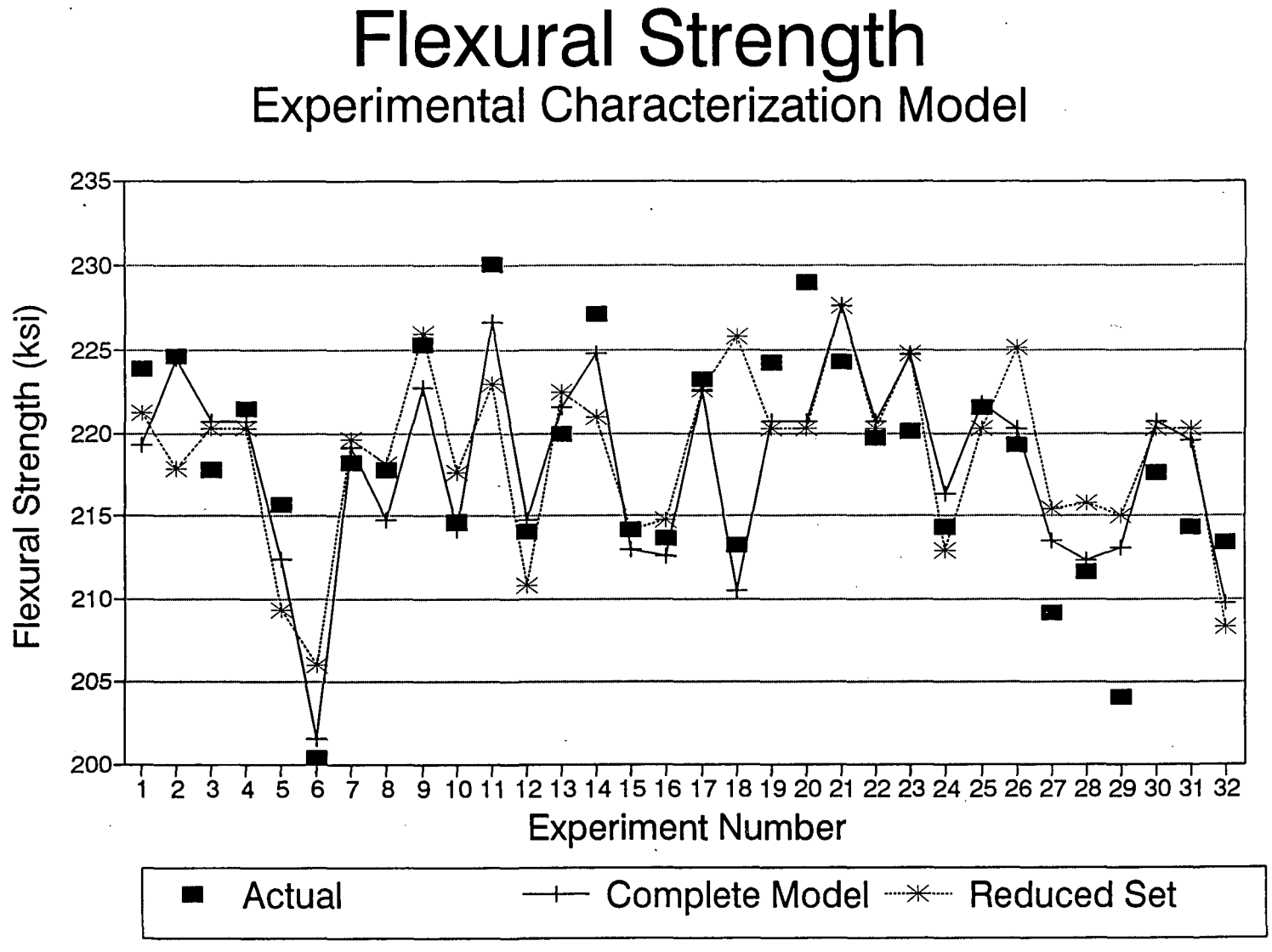

Figure 8. A comparison of flexural strengths predicted by the complete experimental model and a reduced set model to the measured flexural strengths.

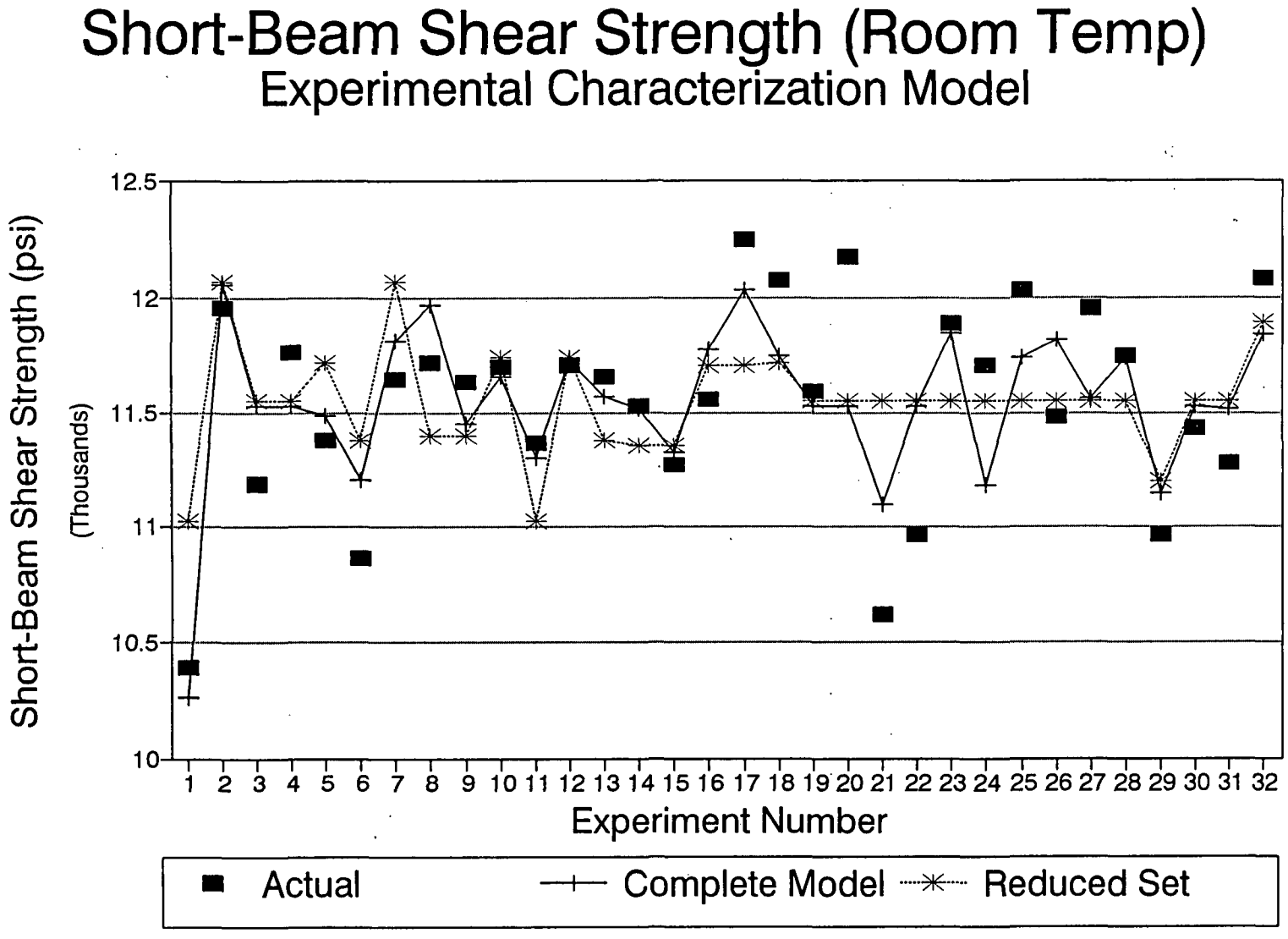

Figure 9. A comparison of short-beam shear strengths predicted by the complete experimental model and a reduced set model to the measured room temperature short-beam shear strengths.

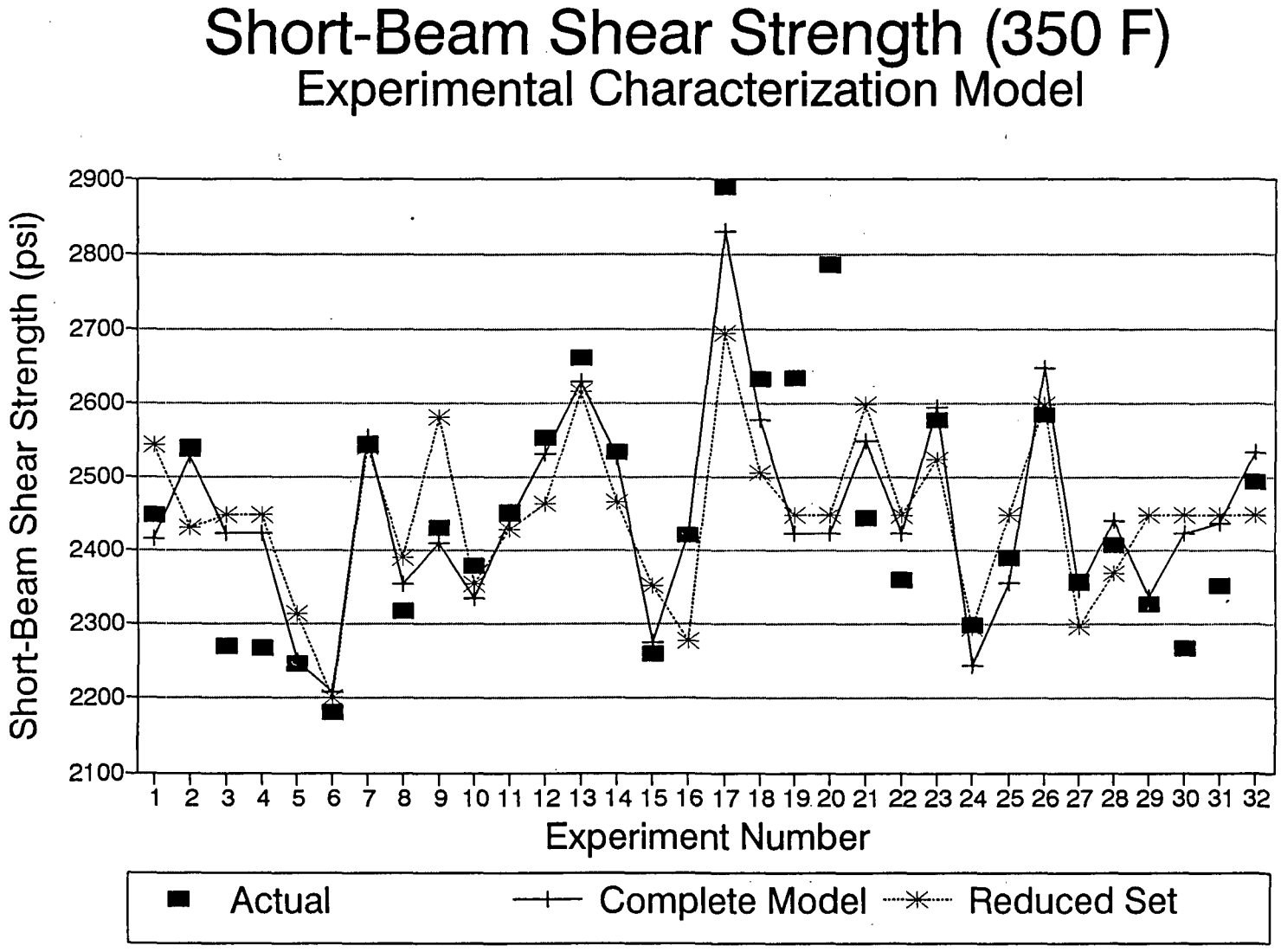

Figure 10. A comparison of short-beam shear strengths predicted by the complete experimental model and a reduced set model to the measured high temperature (350 F) short-beam shear strengths.

values are also given relating the quality of the fit. From the R squared values it can be seen that the room temperature short-beam strength have little statistical significance and thus they will not be discussed any further. The R squared values for flexural and high temperature short-beam shear, although not as high as one would like, can be considered for limited predictive cases. Figures 8-10 show the fit of the predictive model to the actual measured mechanical properties of flexural strength, room temperature short-beam shear strength, and high temperature (350 F) short-beam shear strength. Shown are the fit data for the complete model and the reduced set model. As can be seen, there are some trade-offs in the predictive fit when using the reduced coefficient set, but overall the reduced coefficient model fit is reasonable. The simplicity of the reduced model also helps in understanding the importance of the five process parameters.

The coefficients given in Table X for flexural strength indicate that the amount of filler, percent graphite, pull speed, and zone 2 temperature are important as are the interaction between the filler - pull speed and the zone 2 temperature squared. For high temperature short-beam shear strength, the amount of filler, the percentage of graphite, the pull speed, and the zone 2 temperature are important as is the interaction between the percent graphite - zone 2 temperature. Only the first zone of the die temperature does not appear as an important first order term. Thus continued development of the pultrusion will require further examination of all five process parameters with the exception of the first die temperature heating zone. It is understandable that the process parameters of importance for flexural strength (testing mainly fiber related properties) would be different than that for short-beam shear strength (testing mainly resin matrix related properties).

SUMMARY

An experimental characterization of the pultrusion process has been conducted for the composite material system of Shell EPON 9420/9470/537 epoxy with AS4-12K graphite. The results indicate that four processing parameters are important in determining the flexural and short-beam shear strength. These parameters are the amount of filler within the resin, the percent of graphite fiber in the material, the pull speed, and the second die temperature heating zone. The best mechanical properties are produced when the amount of filler and graphite are held high and the pull speed is reduced. There are mixed results for the effect of the second die temperature zone. A good experimental database has been development for continued studies into more advanced pultrusion characterization.

REFERENCES

1. *Statistical Design and Analysis of Experiments*, Robert Mason, Richard Gunst, and James Hess, John Wiley, 1989.

2. *The Collected Works of George E.P. Box, Volume 1*, edited by George C. Tiao,Wadsworth, 1985

SECTION II

TWO-DIMENSIONAL FINITE ELEMENT MODELING OF THE PULTRUSION OF FIBER/THERMOSETTING RESIN COMPOSITE MATERIALS

I. INTRODUCTION

Composite materials used in the fabrication of industrial products/components are under constant development. Applications vary from widely sold consumer products to high-performance aerospace components. Important research areas include the design of composites, performance optimization, and the prediction of composite material behavior.

The pultrusion of thermosetting plastics is a prevalent method for the manufacture of composite materials (Sumerak and Martin, 1984). It is a continuous process having a high potential for automation. It has the following potential advantages over other fabrication methods:

- higher production rates
- less scrap
- lower facility cost requirements
- lower direct labor cost requirements
- lower secondary finishing operation costs
- lower manufacturing cost

These are the reasons more and more material producers and researchers have been attracted to study, develop, and

improve the method in recent years.

A typical pultrusion process is simply described in Figure 1. Referring to the figure, the process requires a creel system which contains continuous reinforcement material, a resin tank which has a long gradual exit slope to ensure good fiber impregnation, a preform die which removes excess resin and forms the approximate desired cross section shape, a cure die which is heated to the required temperature to promote curing reaction, a pulling mechanism which is responsible for moving the product continuously at a constant speed, and a synchronized cut-off saw station which automatically clamps and cuts the part to the desired length.

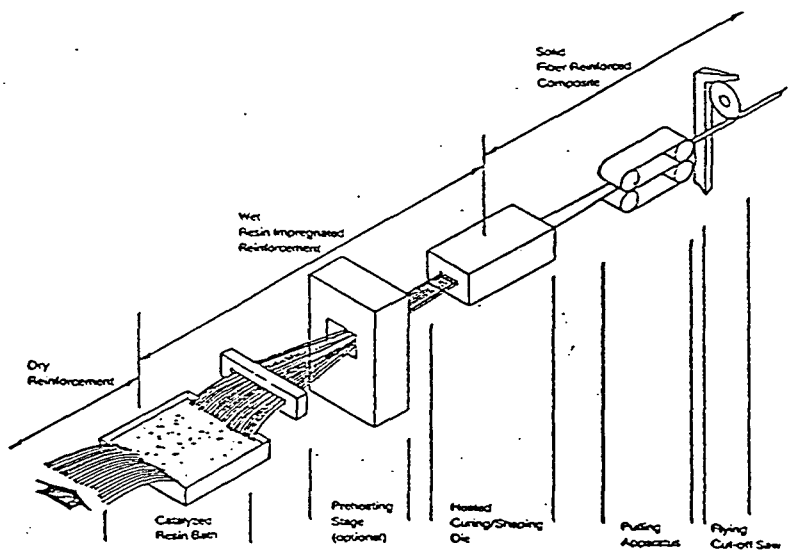

Figure 1. Schematic Diagram of the Pultrusion Process

In appearance the pultrusion process is quite simple. However, the interactive process variables are still not understood clearly and thoroughly (Sumerak and Martin, 1984). The main factors which influence the production capability and quality include the prescription of the matrix, the die temperature profile, the pultrusion machine speed (line speed), and the pulling force, with all except the prescription of the matrix being adjustable machine parameters. To make up a proper and effective formulation of resin requires in-depth chemical knowledge. It is fortunate that there are resin supplies on the market which satisfy different purposes (Shell Chemical Company, 1986). In most situations the duty of a pultrusion operator is to control the machine parameters. While machine parameters are independently adjustable, they are interactive in the sense that they act together to influence the curing characteristics of the material inside the die. It is well recognized that the mechanical properties of the pultruded composite material are affected directly by the degree-of-cure (Batch and Macosko, 1987). We know that the heat of reaction, which is the measure of degree-of-cure, may be expressed as a function of temperature. Temperature can be called the driving force of pultrusion. A sufficient degree-of-cure needs adequate reaction time, therefore it is important to select an appropriate line speed in order to ensure high quality. Thus precise control of the thermal

and chemical phenomena occurring within the die is of utmost importance.

A wide variety of component shapes can be manufactured through the pultrusion process. In this study only simple profile shapes are treated, thus a two-dimensional heat transfer model is applicable. Details of the formulation and development focus directly upon the pultrusion of thermosetting composite materials but the procedure and techniques presented here are also valid for the modeling of the pultrusion of thermoplastic composite materials. The finite element method is widely recognized as the state-or-the-art computational procedure for this class of problems (Lewis et al., 1981; Burnett, 1987). A two-dimensional finite element formulation capable of predicting the temperature profile and the degree-of-cure of the material is thus developed. Some numerical examples are also presented. The solutions show that the work done lays a good foundation for further study.

II. HEAT TRANSFER MODEL

A two-dimensional heat transfer model of the thermosetting pultrusion process is formulated and a numerical solution is developed using the finite element method. Because another important aspect of the pultrusion process, the degree-of-cure, is also a target of the study, the heat of reaction is included in the heat transfer model. The basic assumptions of the model are

- the process is steady-state
- the matrix and fiber have the same temperature at any point in the die
- the influence of pressure in the die on heat of reaction can be neglected
- for a rectangular cross section, the variation of temperature along the width of die can be ignored

Based upon the above assumptions, the governing differential equation of heat transfer can be expressed in Cartesian coordinates thusly

$$\rho cu\frac{\partial T}{\partial x} - \frac{\partial}{\partial x}(k_x\frac{\partial T}{\partial x}) - \frac{\partial}{\partial y}(k_y\frac{\partial T}{\partial y}) - H_u\rho m_m\frac{\partial \alpha}{\partial t} = 0 \qquad (1)$$

where

T = temperature of the material

k = thermal conductivity of the material

c = heat capacity of the material

u = pultrusion line speed

H_u = ultimate heat of reaction

m_m = mass fraction of matrix

α = degree-of-cure

ρ = density of the material

The independent variables x and y denote longitudinal and transverse directions, respectively. The rate of cure α is a function of temperature and degree-of-cure, therefore it is a function of position, thus satisfying the condition of steady state.

During pultrusion the top heat platen and bottom heat platen are controlled to be at same temperature, therefore the boundary conditions can be expressed as follows in the given coordinate system (refering to Figure 2)

$$T(0,y) = T_0 \tag{2a}$$

$$T(L,y) = T_D(L) \tag{2b}$$

$$T(x,\pm\frac{d}{2}) = T_D(x) \tag{2c}$$

where

T_0 = material temperature at the entrance of the die

T_D = die interface temperature

L = length of die

d = thickness of the material in the die

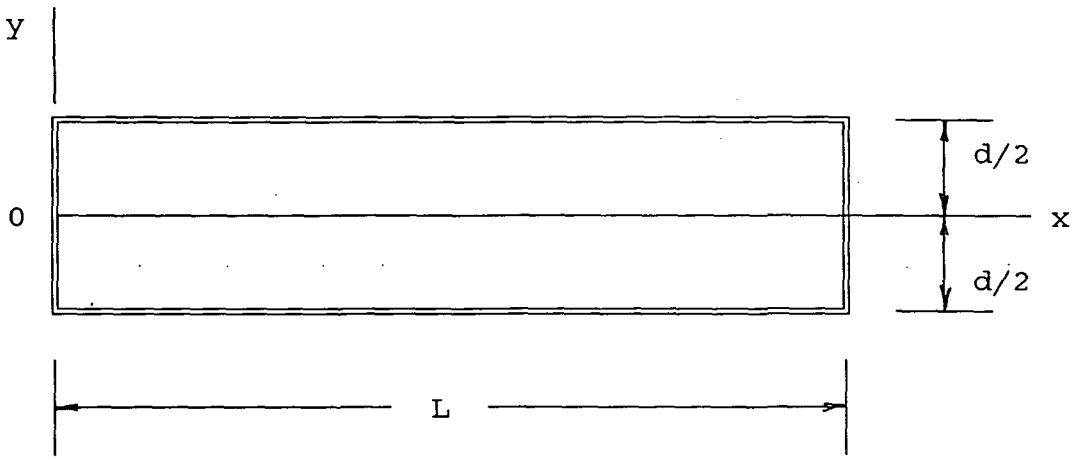

Figure 2. Coordinates of Die with Rectangular Cross Section

The boundary equation, Eq. (2c), is symmetric about the material mid-plane, y = 0, therefore we can assume that the temperature and the degree-of-cure are distributed symmetrically in the transverse direction. Considering the condition of contact resistance, it is more appropriate to change the temperature boundary condition to a convective boundary condition. Thus Eq. (2c) is replaced by the following condition

$$q_y(x,\pm\frac{d}{2}) = \pm h[T(x,\pm\frac{d}{2}) - T_D(x)] \tag{2d}$$

where

q_n = outward-normal component of heat flux at the boundary of $y = \pm d/2$

h = die-material interface convection coefficient

The thermal properties of the material can be approximated using the averaged values

$$\frac{1}{\rho} = \frac{m_m}{\rho_m} + \frac{1 - m_m}{\rho_f} \tag{3}$$

$$c = m_m[(1 - \alpha)c_u + \alpha c_c] + (1 - m_m)c_f \tag{4}$$

$$\frac{1}{k_x} = \frac{1 - v_f}{[(1-\alpha)k_u + \alpha k_c]} + \frac{v_f}{k_{fx}} \tag{5}$$

$$\frac{1}{k_y} = \frac{1 - v_f}{[(1-\alpha)k_u + \alpha k_c]} + \frac{v_f}{k_{fy}} \tag{6}$$

where the subscripts m and f refer to matrix and fiber, respectively; u and c refer to uncured and cured matrix, respectively; v_f is the fiber volume fraction; k_{fx} and k_{fy} are the thermal conductivities of the fiber, the former in the longitudinal direction and the latter in the transverse direction. The matrix density ρ_m depends on temperature and degree-of-cure

$$\rho_m = \frac{\rho_0}{1 + 3e(T - T_0) - \gamma\alpha} \tag{7}$$

In Eq. (7), ρ_0 is the matrix density at the temperature of T_0, e is the thermal expansion coefficient of the matrix, and γ is the shrinkage coefficient of the matrix due to the degree-of-cure. Thermal expansion of the fiber is ignored since its expansion coefficient is much less than that of the matrix.

From Eqs. (3) through (7), it is shown that all thermal properties of the material are assumed to be continuous functions of temperature and degree-of-cure. Therefore it is not necessary to use different governing equations to fit two or three different phase regions. This is convenient for solution because some work to satisfy the continuity of flux can be avoided.

For a die with a circular cross section, the axisymmetric case will be considered. This is consistent with the actual situation. At steady state the die interface temperature can be thought of as not varying along the direction of the circumference, therefore the assumption of axisymmetric distribution of material temperature is reasonable. Hence the heat transfer equation written in cylindrical coordinates can be simplified as follows

$$\rho cu\frac{\partial T}{\partial x} - \frac{\partial}{\partial x}(k_x\frac{\partial T}{\partial x}) - \frac{\partial}{\partial r}(k_r\frac{\partial T}{\partial r}) - \frac{1}{r}k_r\frac{\partial T}{\partial r} - H_u\rho m_m\frac{\partial \alpha}{\partial t} = 0 \tag{8}$$

where the subscript r represents the radial direction. The expressions of boundary conditions and thermal properties of the material are all similar to those in Cartesian coordinates.

To avoid a singularity during numerical calculations we rewrite Eq. (8),

$$\rho cu\frac{\partial T}{\partial x} - \frac{\partial}{\partial x}(k_x\frac{\partial T}{\partial x}) - \frac{1}{r}\frac{\partial}{\partial r}(rk_r\frac{\partial T}{\partial r}) - H_u\rho m_m\frac{\partial \alpha}{\partial t} = 0 \qquad (9)$$

Then, multiplying Eq. (9) by r,

$$\rho cur\frac{\partial T}{\partial x} - \frac{\partial}{\partial x}(rk_x\frac{\partial T}{\partial x} - \frac{\partial}{\partial r}(rk_r\frac{\partial T}{\partial r}) - H_u\rho m_m r\frac{\partial \alpha}{\partial t} = 0 \qquad (10)$$

Equation (10) is used to derive the formulation of the finite element method in the study. A one-dimensional heat transfer model is also treated, and the solution is compared with that of the two-dimensional model. The governing equation is from Hackett and Prasad (1989), with the heat of reaction added (Erhun and Advani, 1990)

$$\frac{\partial}{\partial x}(k_x\frac{\partial T}{\partial x}) - \rho cu\frac{\partial T}{\partial x} + \frac{2h}{d}(T_D - T) + H_u\rho m_m\frac{\partial \alpha}{\partial t} = 0 \qquad (11)$$

In Eq. (11), all thermal properties are determined using Eqs. (3) through (7). This is another point that is different from the formulation of Hackett and Prasad (1989).

III. CURING PROCESS MODEL

It is recognized that the mechanical properties of a thermosetting system depend strongly upon the crystalline structure of the reactants, or in other terms, on the cure of the matrix (Talbott and George, 1987). Curing propagation within the die during pultrusion is a complex chemical process which has not yet been clearly understood. But some efforts have been made to unveil the relationships among temperature, degree-of-cure, and rate-of-cure using simplified descriptions of the cure chemistry in combination with an appropriate cure model. In this study, formulas and data relative to the curing process are principly taken from Lee et al. (1982) and Lee and George (1987). The method obtained therefrom is suitable for characterizing a matrix containing catalysts. All the values and analytical expressions in this reference are based on experiments with Hercules 3501-6 resin.

The ultimate heat of reaction H_u is the amount of heat generated by curing the material from the beginning of the chemical reaction until the completion

$$H_u = \int_0^{t_d} \left(\frac{dQ}{dt}\right)_d dt \qquad (12)$$

where $(dQ/dt)_d$ is the instantaneous rate of heat generated during the reaction and t_d is the amount of time required to complete the reaction; the subscript d implies dynamic scanning. The constant H_u is independent of the heating rate. Lee et al. (1982) gives the value of the ultimate heat of reaction, measured by the method of dynamic scanning as

$$H_u = 473.6 \pm 5.4 \quad J/g \tag{13}$$

The rate-of-cure is a parameter that is assumed to be proportional to the rate-of-heat of the thermosetting matrix material

$$\frac{d\alpha}{dt} \equiv \frac{1}{H_u}\left(\frac{dQ}{dt}\right) \tag{14}$$

The degree-of-cure is defined as the integration of the rate-of-cure (Lee et al., 1982)

$$\alpha = \int_0^t \left(\frac{d\alpha}{dt}\right) dt = \frac{1}{H_u}\int_0^t \left(\frac{dQ}{dt}\right) dt \tag{15}$$

The value of α is always less than or equal to 1.

For convenient use in computer calculations, some analytical expressions were derived by Lee et al. (1982) to describe the rate-of-cure versus degree-of-cure and temperature

$$\frac{\partial \alpha}{\partial t} = (k_1 + k_2\alpha)(1 - \alpha)(B - \alpha), \quad \alpha \leq 0.3 \tag{16a}$$

$$\frac{\partial \alpha}{\partial t} = k_3(1 - \alpha), \quad \alpha > 0.3 \tag{16b}$$

where

$$k_1 = A_1 \exp\left(\frac{-\Delta E_1}{RT}\right) \tag{17a}$$

$$k_2 = A_2 \exp\left(\frac{-\Delta E_2}{RT}\right) \tag{17b}$$

$$k_3 = A_3 \exp\left(\frac{-\Delta E_3}{RT}\right) \tag{17c}$$

In Eqs. (17), A_1, A_2, A_3 are the pre-exponential factors, ΔE_1, ΔE_2, ΔE_3 are the activation energies, R is the universal gas constant, and T is the temperature measured by the Kelvin scale; the values of these constants are listed below

$$A_1 = 2.101 \times 10^9 \ \text{min}^{-1} \tag{18a}$$

$$A_2 = -2.014 \times 10^9 \ \text{min}^{-1} \tag{18b}$$

$$A_3 = 1.960 \times 10^5 \ \text{min}^{-1} \tag{18c}$$

$$\Delta E_1 = 8.07 \times 10^4 \quad J/mol \tag{19a}$$

$$\Delta E_2 = 7.78 \times 10^4 \quad J/mol \tag{19b}$$

$$R = 8.31441 \quad J/g\ mol.K \tag{20}$$

The constant B is independent of temperature and degree-of-cure; its value may be selected as follows

$$B = 0.47 \pm 0.07 \tag{21}$$

In this study, since only pultrusion at a steady state is treated, time becomes the dependant variable. The speed of matrix flow along the length of the die is assumed to be equal to the line speed and the speed of matrix flow in other directions can be thought of as zero. Thus time is only a function of x and the rate-of-cure can be rewritten as follows

$$\frac{\partial \alpha}{\partial t} = u \frac{\partial \alpha}{\partial x} \tag{22}$$

This formula will be used to replace it wherever it appears later.

IV. FINITE ELEMENT FORMULATION

In this study, the Galerkin weighted residual method is used to formulate the finite element method to solve the heat transfer equation. The general form of the typical element trial solution for temperature in Cartesian coordinates, $\bar{T}(x,y)$, is

$$\bar{T}(x,y) = \sum_{j=1}^{n} T_j \phi_j (x,y) \tag{23}$$

where n is the number of nodes in an element, T_j is the temperature at node j, and $\phi_j(x,y)$ is the shape function. The residual of Eq. (1) is

$$R(x,y) = \rho c u \frac{\partial \bar{T}}{\partial x} - \frac{\partial}{\partial x}(k_x \frac{\partial \bar{T}}{\partial x}) - \frac{\partial}{\partial x}(k_y \frac{\partial \bar{T}}{\partial y}) - H_u \rho m_m u \frac{\partial \hat{\alpha}}{\partial x} \tag{24}$$

where $u\partial\hat{\alpha}/\partial x$ is the trial solution of the rate-of-cure which has the same form as that of $\bar{T}$

$$u \frac{\partial \hat{\alpha}}{\partial x} = \sum_{j=1}^{n} u(\frac{\partial \alpha}{\partial x})_j \phi_j(x,y) \tag{25}$$

In Eq. (25), $u(\partial\alpha/\partial x)_j$ are the nodal values of rate-of-cure. The Galerkin method employs the trial functions as the weighting functions, thus the weighted residual equation for each node in an element can be written as

$$\iint_e R(x,y)\phi_i(x,y)dxdy =$$

$$\iint_e [\rho cu\frac{\partial \bar{T}}{\partial x} - \frac{\partial}{\partial x}(k_x\frac{\partial \bar{T}}{\partial x}) - \frac{\partial}{\partial y}(k_y\frac{\partial \bar{T}}{\partial y}) - H_u\rho m_m u\frac{\partial \hat{\alpha}}{\partial x}]\phi_i dxdy \qquad (26)$$

$$= 0, \qquad i = 1, 2, ..., n$$

where the subscript e implies integration over the domain of the element.

From the "chain rule" of differentiation we have

$$\frac{\partial}{\partial x}(k_x\frac{\partial \bar{T}}{\partial x})\phi_i = \frac{\partial}{\partial x}(k_x\frac{\partial \bar{T}}{\partial x}\phi_i) - k_x\frac{\partial \bar{T}}{\partial x}\frac{\partial \phi_i}{\partial x} \qquad (27a)$$

$$\frac{\partial}{\partial y}(k_y\frac{\partial \bar{T}}{\partial y})\phi_i = \frac{\partial}{\partial y}(k_y\frac{\partial \bar{T}}{\partial x}\phi_i) - k_y\frac{\partial \bar{T}}{\partial y}\frac{\partial \phi_i}{\partial y} \qquad (27b)$$

Substituting Eqs. (27) into Eq. (26) yields

$$\iint_e [\rho cu\frac{\partial \bar{T}}{\partial x}\phi_i + k_x\frac{\partial \bar{T}}{\partial x}\frac{\partial \phi_i}{\partial x} + k_y\frac{\partial \bar{T}}{\partial y}\frac{\partial \phi_i}{\partial y} - H_u\rho m_m u\frac{\partial \hat{\alpha}}{\partial x}]dxdy$$

$$-\iint_e [\frac{\partial}{\partial x}(k_x\frac{\partial \bar{T}}{\partial x}\phi_i) + \frac{\partial}{\partial y}(k_y\frac{\partial \bar{T}}{\partial y}\phi_i)]dxdy = 0 \qquad (28)$$

$$i = 1, 2, ..., n$$

The functions in the second integral in Eq. (28) are perfectly differentiable. Using the two-dimensional divergence theorem, the integral can be reduced to a line integration over the boundary of the element

$$-\iint[\frac{\partial}{\partial x}(k_x\frac{\partial\bar{T}}{\partial x}\phi_i) + \frac{\partial}{\partial y}(k_y\frac{\partial\bar{T}}{\partial y}\phi_i)]dxdy = \tag{29}$$

$$-\oint_c(k_x\frac{\partial\bar{T}}{\partial x}\phi_i\ell_x + k_y\frac{\partial\bar{T}}{\partial y}\phi_i\ell_y)ds$$

where ℓ_x and ℓ_y are the direction cosines of the outward unit normal to the element boundary, and s is the natural coordinate of the boundary.

The heat flux components in the x and y directions are

$$q_x = -k_x\frac{\partial T}{\partial x} \approx -k_x\frac{\partial\bar{T}}{\partial x} \tag{30a}$$

and

$$q_y = -k_y\frac{\partial T}{\partial y} \approx -k_y\frac{\partial\bar{T}}{\partial y} \tag{30b}$$

Using the expressions for q_x and q_y, the outward normal component of heat flux on the boundary is given by

$$q_n = q_x\ell_x + q_y\ell_y = -k_x\frac{\partial\bar{T}}{\partial x}\ell_x - k_y\frac{\partial\bar{T}}{\partial y}\ell_y \tag{31}$$

Substituting Eq. (31) into Eq. (29), we obtain the following closed-circuit line integration, referring to Figure 3,

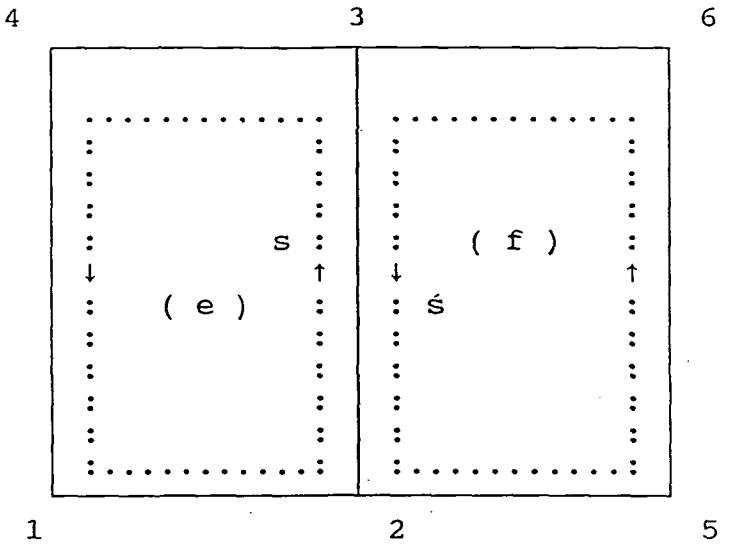

Figure 3. Notation for Interior Element Boundary Flux Integral

$$-\oint_e q_n \phi_i ds \tag{32}$$

In Figure 3, (e) and (f) are adjacent elements; s and ś are the routes of integration over the boundary of element (e) and element (f), respectively; they are all counterclockwise. The closed circuit integral of element (e) can be written as

$$\oint_e = \int_1^2 + \int_2^3 + \int_3^4 + \int_4^1 \tag{33}$$

In Eq. (33), 1, 2, 3, and 4 represent the nodal numbers of element (e). In the line integral on the right-hand side of Eq. (33), for example, $\int_1^2$ means integration along the route from node 1 to node 2; the others follow this pattern. Consider the line integral over the common boundary 2-3,

of heat flux and shape function, we have

$$q_{n_e} = -q_{n_f} \tag{34a}$$

$$\phi_i^{(e)} = \phi_i^{(f)} \tag{34b}$$

and from Figure 3, it is apparent that ds = -dś over segment 2-3. Thus the line integral over boundary 2-3 of element (e) can be changed as follows

$$\int_2^3 q_{n_e}\phi_i^{(e)}ds = -\int_3^2 (-q_{n_f})(\phi_i^{(f)})(-d\acute{s}) = -\int_3^2 q_{n_f}\phi_i^{(f)}d\acute{s} \tag{35}$$

Using superposition, the total sum of the heat flux over the internal boundary 2-3 is

$$\begin{aligned} &\int_2^3 q_{n_e}\phi_i^{(e)}ds + \int_3^2 q_{n_f}\phi_i^{(f)}d\acute{s} \\ &-\int_3^2 q_{n_f}\phi_i^{(f)}d\acute{s} + \int_3^2 q_{n_f}\phi_i^{(f)}d\acute{s} = 0 \end{aligned} \tag{36}$$

From this example we determine that for interior elements where all boundaries are internal, it is not necessary to calculate the closed circuit integral. Equation (28) is thus reduced to

$$\begin{aligned} &\iint_e [\rho c u\frac{\partial \bar{T}}{\partial x}\phi_i + k_x\frac{\partial \bar{T}}{\partial x}\frac{\partial \phi_i}{\partial x} + k_y\frac{\partial \bar{T}}{\partial y}\frac{\partial \phi_i}{\partial y}]dxdy = \\ &\iint_e H_u\rho m_m u\frac{\partial \hat{\alpha}}{\partial x}\phi_i dxdy \ , \qquad i = 1, 2, \ldots, n \end{aligned} \tag{37}$$

For exterior elements, only the line integral over the external boundary makes a contribution. In this derivation

external boundary makes a contribution. In this derivation the symmetric property of the system is used to reduce the amount of computation. The boundary equations change to

$$T(0,y) = T_o \tag{38a}$$

$$T(L,y) = T_D(L) \tag{38b}$$

$$T(x,\frac{d}{2}) = T_D(x) \tag{38c}$$

$$q_y(x,\frac{d}{2}) = h[T(x,\frac{d}{2}) - T_D(x)] \tag{38d}$$

$$q_y(x,0) = 0 \tag{38e}$$

Note that

$$q_n = h(\bar{T} - T_D) \tag{39}$$

The integration is thus changed to

$$\oint_e q_n \phi_i ds = \int_\Gamma h(\bar{T} - T_D)\phi_i ds \tag{40}$$

where Γ is the external boundary over which the temperature is unknown, and the heat flux q_n is not equal to zero. Substituting Eq. (40) into Eq. (28) and moving some terms from the left-hand side of the equation to the right-hand side yields

$$\iint_e [\rho cu \frac{\partial \bar{T}}{\partial x} \phi_i + k_x \frac{\partial \bar{T}}{\partial x} \frac{\partial \phi_i}{\partial x} + k_y \frac{\partial \bar{T}}{\partial y} \frac{\partial \phi_i}{\partial y}] dxdy + \int_\Gamma H \bar{T} \phi_i ds$$

$$= \iint_e H_u \rho m_m u \frac{\partial \hat{\alpha}}{\partial x} \phi_i dxdy + \int_\Gamma h T_D \phi_i ds \qquad (41)$$

$$i = 1, 2, ..., n$$

Substituting the trial function, Eq. (23), into Eq. (37) and Eq. (41), we get

$$\sum_{j=1}^{n} [\iint_e (k_x \frac{\partial \phi_i}{\partial x} \frac{\partial \phi_j}{\partial x} + k_y \frac{\partial \phi_i}{\partial y} \frac{\partial \phi_j}{\partial y} + \rho cu \phi_i \frac{\partial \phi_j}{\partial x}) dxdy] T_j$$

$$= \iint_e H_u \rho m_m u \frac{\partial \hat{\alpha}}{\partial x} \phi_i dxdy \quad , \qquad i = 1, 2, ..., n \qquad (42)$$

and

$$\sum_{j=1}^{n} \iint_e (k_x \frac{\partial \phi_i}{\partial x} \frac{\partial \phi_j}{\partial x} + k_y \frac{\partial \phi_i}{\partial y} \frac{\partial \phi_j}{\partial y} + \rho cu \phi_i \frac{\partial \phi_j}{\partial x}) dxdy +$$

$$\int_\Gamma h \phi_i \phi_j ds] T_j = \iint_e H_u \rho m_m u \frac{\partial \hat{\alpha}}{\partial x} \phi_i dxdy + \int_\Gamma h T_D \phi_i ds \qquad (43)$$

$$i = 1, 2, ..., n$$

where Eq. (42) is the residual equation for interior elements and Eq. (43) is the residual equation for exterior elements. They can be expressed in matrix form as

$$\begin{bmatrix} k_{11} & k_{12} & \cdots & k_{1n} \\ k_{21} & k_{22} & \cdots & k_{2n} \\ \vdots & \vdots & k_{ij} & \vdots \\ k_{n1} & k_{n2} & \cdots & k_{nn} \end{bmatrix} \begin{bmatrix} T_1 \\ T_2 \\ \vdots \\ T_n \end{bmatrix} = \begin{bmatrix} F_1 \\ F_2 \\ \vdots \\ F_n \end{bmatrix} \qquad (44)$$

where, for interior elements,

$$k_{ij} = \iint_e (k_x \frac{\partial \phi_i}{\partial x}\frac{\partial \phi_j}{\partial x} + k_y \frac{\partial \phi_i}{\partial y}\frac{\partial \phi_j}{\partial y} + \rho c u \phi_i \frac{\partial \phi_j}{\partial x}) dxdy \tag{45}$$

$$F_i = \iint_e H_u \rho m_m u \frac{\partial \hat{\alpha}}{\partial x} \phi_i dxdy \tag{46}$$

and, for exterior elements,

$$k_{ij} = \iint_e (k_x \frac{\partial \phi_i}{\partial x}\frac{\partial \phi_j}{\partial x} + k_y \frac{\partial \phi_i}{\partial y}\frac{\partial \phi_j}{\partial y} + \rho c u \phi_i \frac{\partial \phi_j}{\partial x}) dxdy + \int_\Gamma h \phi_i \phi_j ds \tag{47}$$

$$F_i = \iint_e H_u \rho m_m u \frac{\partial \hat{\alpha}}{\partial x} \phi_i dxdy + \int_\Gamma h T_D \phi_i ds \tag{48}$$

In this study we use the isoparametric quadrilateral element to solve the problem. First, let us consider the linear isoparametric quadrilateral element, that is to say n = 4 in Eq. (23). The shape functions for this element (refer to Figure 4), expressed in terms of element local coordinates, are given by

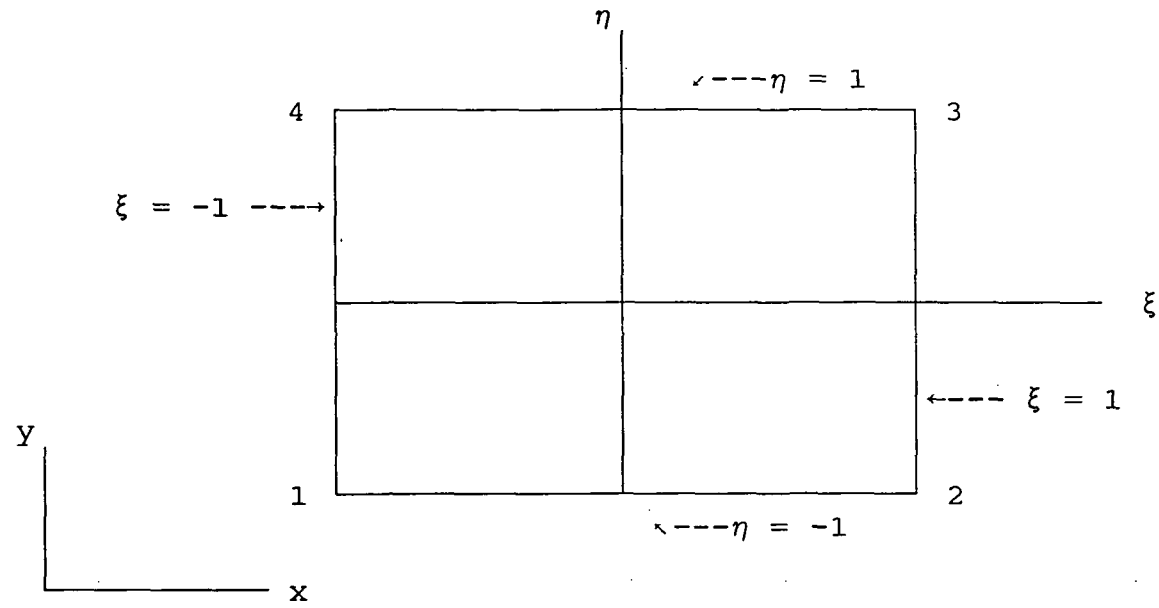

Figure 4. Element Local Coordinates

$$\phi_1(\xi,\eta) = \frac{1}{4}(1 - \xi)(1 - \eta) \tag{49a}$$

$$\phi_2(\xi,\eta) = \frac{1}{4}(1 + \xi)(1 - \eta) \tag{49b}$$

$$\phi_3(\xi,\eta) = \frac{1}{4}(1 + \xi)(1 + \eta) \tag{49c}$$

$$\phi_4(\xi,\eta) = \frac{1}{4}(1 - \xi)(1 + \eta) \tag{49d}$$

For an isoparametric element, the relationship between the global coordinates and local coordinates has the same form as the trial function

$$x = \sum_{j=1}^{4} x_j \phi_j(\xi,\eta) \tag{50a}$$

$$y = \sum_{j=1}^{4} y_j \phi_j(\xi,\eta) \tag{50b}$$

where x_j, y_j are the global coordinates of the nodes of the element. The coordinate transformation is determined by the Jacobian matrix which is given by

$$[J] = \begin{bmatrix} \frac{\partial x}{\partial \xi} & \frac{\partial y}{\partial \xi} \\ \frac{\partial x}{\partial \eta} & \frac{\partial y}{\partial \eta} \end{bmatrix} = \begin{bmatrix} J_{11} & J_{12} \\ J_{21} & J_{22} \end{bmatrix} \tag{51}$$

Note that in Eqs. (50), x and y are functions of ϕ_j. In order to obtain the elements of the Jacobian matrix we first have to know the derivatives of the shape functions $\phi_j(\xi,\eta)$. They are easily obtained from Eqs. (49).

$$\frac{\partial \phi_1}{\partial \xi} = -\frac{1}{4}(1 - \eta), \qquad \frac{\partial \phi_1}{\partial \eta} = -\frac{1}{4}(1 - \xi) \tag{52a}$$

$$\frac{\partial \phi_2}{\partial \xi} = \frac{1}{4}(1 - \eta), \qquad \frac{\partial \phi_2}{\partial \eta} = -\frac{1}{4}(1 + \xi) \tag{52b}$$

$$\frac{\partial \phi_3}{\partial \xi} = \frac{1}{4}(1 + \eta), \qquad \frac{\partial \phi_3}{\partial \eta} = \frac{1}{4}(1 + \xi) \tag{52c}$$

$$\frac{\partial \phi_4}{\partial \xi} = -\frac{1}{4}(1 + \eta), \qquad \frac{\partial \phi_4}{\partial \eta} = \frac{1}{4}(1 - \xi) \tag{52d}$$

Thus the elements of the Jacobian matrix can be written as follows

$$J_{11} = \sum_{j=1}^{4} x_j \frac{\partial \phi_j}{\partial \xi} = \frac{1}{4}[(x_2-x_1)(1-\eta) + (x_3-x_4)(1+\eta)] \tag{53a}$$

$$J_{12} = \sum_{j=1}^{4} y_j \frac{\partial \phi_j}{\partial \xi} = \frac{1}{4}[(y_2-y_1)(1-\eta) + (y_3-y_4)(1+\eta)] \tag{53b}$$

$$J_{21} = \sum_{j=1}^{4} x_j \frac{\partial \phi_j}{\partial \eta} = \frac{1}{4}[(x_4-x_1)(1-\xi) + (x_3-x_2)(1+\xi)] \tag{53c}$$

$$J_{22} = \sum_{j=1}^{4} y_j \frac{\partial \phi_j}{\partial \eta} = \frac{1}{4}[(y_4-y_1)(1-\xi) + (y_3-y_2)(1+\xi)] \tag{53d}$$

Using the "chain rule" of differentiation we have

$$\frac{\partial \phi_j}{\partial \xi} = \frac{\partial \phi_j}{\partial x}\frac{\partial x}{\partial \xi} + \frac{\partial \phi_j}{\partial y}\frac{\partial y}{\partial \xi} \tag{54a}$$

$$\frac{\partial \phi_j}{\partial \eta} = \frac{\partial \phi_j}{\partial x}\frac{\partial x}{\partial \eta} + \frac{\partial \phi_j}{\partial y}\frac{\partial y}{\partial \eta} \tag{54b}$$

which can be written in matrix form as

$$\begin{bmatrix} \frac{\partial \phi_j}{\partial \xi} \\ \frac{\partial \phi_j}{\partial \eta} \end{bmatrix} = \begin{bmatrix} \frac{\partial x}{\partial \xi} & \frac{\partial y}{\partial \xi} \\ \frac{\partial x}{\partial \eta} & \frac{\partial y}{\partial \eta} \end{bmatrix} \begin{bmatrix} \frac{\partial \phi_j}{\partial x} \\ \frac{\partial \phi_j}{\partial y} \end{bmatrix} = [J] \begin{bmatrix} \frac{\partial \phi_j}{\partial x} \\ \frac{\partial \phi_j}{\partial y} \end{bmatrix} \tag{55}$$

Inverting Eq. (55) yields

$$\begin{bmatrix} \frac{\partial \phi_j}{\partial x} \\ \frac{\partial \phi_j}{\partial y} \end{bmatrix} = [J]^{-1} \begin{bmatrix} \frac{\partial \phi_j}{\partial \xi} \\ \frac{\partial \phi_j}{\partial \eta} \end{bmatrix} \tag{56}$$

where

$$[J]^{-1} = \frac{1}{|J|}\begin{bmatrix} \frac{\partial y}{\partial \eta} & -\frac{\partial y}{\partial \xi} \\ -\frac{\partial x}{\partial \eta} & \frac{\partial x}{\partial \xi} \end{bmatrix} \tag{57}$$

and $|J|$ is the determinant of the Jacobian matrix, which can be written as

$$|J| = \frac{\partial x}{\partial \xi}\frac{\partial y}{\partial \eta} - \frac{\partial x}{\partial \eta}\frac{\partial y}{\partial \xi} \tag{58}$$

It is well known that after coordinate transformation the infinitesimal area element becomes

$$dA = dxdy = |J|d\xi d\eta \tag{59}$$

Equations (45) and (46) can now be rewritten in terms of local coordinates as

$$k_{ij} = \int_{-1}^{1}\int_{-1}^{1} (k_x \frac{\partial \phi_i}{\partial x}\frac{\partial \phi_j}{\partial x} + k_y \frac{\partial \phi_i}{\partial y}\frac{\partial \phi_j}{\partial y} + \rho c u \phi_i \frac{\partial \phi_j}{\partial x})|J|d\xi d\eta \tag{60a}$$

$$F_i = \int_{-1}^{1}\int_{-1}^{1} H_u \rho m_m u \frac{\partial \hat{\alpha}}{\partial x}\phi_i |J| \, d\xi d\eta \tag{60b}$$

For the exterior elements, referring to Figure 4, assuming that segment 3-4 is an external boundary, $\eta = 1$ on boundary 3-4; substituting $\eta = 1$ into the shape function expressions we then obtain

$$\phi_1^* = \phi_2^* = 0 \tag{61a}$$

$$\phi_3^* = \frac{1}{4}(1 + \xi)(1 + 1) = \frac{1}{2}(1 + \xi) \tag{61b}$$

$$\phi_4^* = \frac{1}{4}(1 - \xi)(1 + 1) = \frac{1}{2}(1 - \xi) \tag{61c}$$

where ϕ^* refers to shape functions on the boundary. In order to obtain the value of the line integral we need to derive the differential arc length ds

$$ds = \sqrt{dx^2 + dy^2} = \sqrt{(\frac{\partial x}{\partial \xi}d\xi + \frac{\partial x}{\partial \eta}d\eta)^2 + (\frac{\partial y}{\partial \xi}d\xi + \frac{\partial y}{\partial \eta}d\eta)^2} = \sqrt{J_{11}^2 + J_{12}^2}\, d\xi = \frac{1}{2}\sqrt{(x_3 - x_4)^2 + (y_3 - y_4)^2}\, d\xi = \frac{L^{(e)}}{2}d\xi \tag{62}$$

where $L^{(e)}$ is the length of segment of 3-4. Assuming that T_D is distributed linearly along the exterior boundary,

$$T_D = T_{D_3}\phi_3^* + T_{D_4}\phi_4^* \tag{63}$$

then we can obtain

$$\int_\Gamma hT_D\phi_i ds = \int_{-1}^{1} h(T_{D_3}\phi_3^* + T_{D_4}\phi_4^*)\phi_i^* \frac{L^{(e)}}{2}d\xi \tag{64}$$

From Eqs. (61), we know that when i = 1 or i = 2, Eq. (64) is equal to zero. Similarly we have

$$\int_\Gamma h\phi_i\phi_j ds = \int_{-1}^{1} h\phi_i^*\phi_j^* \frac{L^{(e)}}{2}d\xi \quad , \qquad i, j = 3,4 \tag{65}$$

Now, from Eqs. (47) and (48) we obtain

$$K_{ij} = \int_{-1}^{1}\int_{-1}^{1} (k_x \frac{\partial \phi_i}{\partial x}\frac{\partial \phi_j}{\partial x} + k_y \frac{\partial \phi_i}{\partial y}\frac{\partial \phi_j}{\partial y} + \rho c u \phi_i \frac{\partial \phi_j}{\partial x}) |J| d\xi d\eta + \int_{-1}^{1} h \phi_i^* \phi_j^* \frac{L^{(e)}}{2} d\xi \tag{66a}$$

and

$$F_i = \int_{-1}^{1}\int_{-1}^{1} H_u \rho m_m u \frac{\partial \hat{\alpha}}{\partial x} \phi_i |J| d\xi d\eta + \int_{-1}^{1} h(T_{D_k}\phi_k^* + T_{D_\ell}\phi_\ell^*)\phi_i^* \frac{L^{(e)}}{2} d\xi \tag{66b}$$

In Eqs. (66), for generality, we replace subscripts 3 and 4 with k and ℓ, respectively.

In the computer program we use bilinear Gauss-Legendre quadrature formulas to obtain the values of Eqs. (60) and Eqs. (66). The formulas for k_{ij} and F_i become

$$k_{ij} = \sum_{o=1}^{m}\sum_{p=1}^{m} W_o W_p [(k_x \frac{\partial \phi_i}{\partial x}\frac{\partial \phi_j}{\partial x} + k_y \frac{\partial \phi_i}{\partial y}\frac{\partial \phi_j}{\partial y} + \rho c u \phi_i \frac{\partial \phi_J}{\partial x}) |J|]_{(\xi_o, \eta_p)} \tag{67a}$$

$$F_i = \sum_{o=1}^{m}\sum_{p=1}^{m} W_o W_p [H_u \rho m_m u \frac{\partial \hat{\alpha}}{\partial x} \phi_i \ |J|]_{(\xi_o, \eta_p)} \tag{67b}$$

and

$$k_{ij} = \sum_{o=1}^{m}\sum_{p=1}^{m} W_o W_p [(k_x \frac{\partial \phi_i}{\partial x}\frac{\partial \phi_j}{\partial x} + k_y \frac{\partial \phi_i}{\partial y}\frac{\partial \phi_j}{\partial y} + \rho c u \phi_i \frac{\partial \phi_j}{\partial x}) \ |J|]_{(\xi_o, \eta_p)} + \sum_{o=1}^{m} W_o [h \phi_i^* \phi_j^* \frac{L^{(e)}}{2}]_{\xi_o} \tag{68a}$$

$$F_i = \sum_{o=1}^{m}\sum_{p=1}^{m} W_o W_p [H_u \rho m_m u \frac{\partial \hat{\alpha}}{\partial x}\phi_i |J|]_{(\xi_o,\eta_p)} + \sum_{o=1}^{m} [h(T_{D_k}\phi_k^* + T_{D_\ell}\phi_\ell^*)\phi_i^* \frac{L^{(c)}}{2}]_{\xi_o} \tag{68b}$$

where W_o and W_p are the weighting coefficients and ξ_o and η_p are the Gauss-point coordinates. In the computations we use a 2 × 2 Gauss quadrature; that is to say, m = 2, thus

$$W_o = W_p = 1 \tag{69a}$$

$$\xi_o = \eta_p = \pm\frac{\sqrt{3}}{3} \tag{69b}$$

In Eqs. (60), (66), (67), and (68), $\partial\phi/\partial x$ and $\partial\phi/\partial y$ are from Eq. (56) and $\partial\hat{\alpha}/\partial x$ is from Eq. (24). The material properties k_x, k_y, ρ, etc., can be thought as being constant within each element when the element is small.

Through the same procedure we derive the finite element formulation for the *axisymmetric model*. The boundary conditions now become

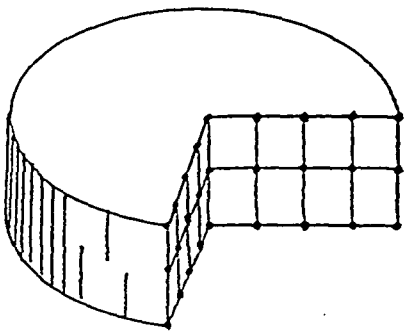

Figure 5. Axisymmetric Configuration of Isoparametric Element with Four Nodes

$$T(0,r) = T_0 \tag{70a}$$

$$T(L,r) = T_D(L) \tag{70b}$$

$$T(x,r_0) = T_D(x) \tag{70c}$$

$$q_r(x,r_0) = h[T(x,r_0) - T_D(x)] \tag{70d}$$

$$q_r(x,0) = 0 \tag{70e}$$

where r_o is the internal radius of the die. The element trial solution for temperature is

$$\bar{T}(x,r) = \sum_{j=1}^{n} T_j \phi_j(x,r) \tag{71}$$

Using Eq. (10), the weighted residual equation at node i in an annular element (referring to Figure 5) is

$$\iint_e [\rho cur\frac{\partial \bar{T}}{\partial x} - \frac{\partial}{\partial x}(rk_x\frac{\partial \bar{T}}{\partial x}) - \frac{\partial}{\partial r}(rk_r\frac{\partial \bar{T}}{\partial r}) - H_u\rho m_m ru\frac{\partial \hat{\alpha}}{\partial x}]\phi_i 2\pi dr dx = 0 , \quad i = 1, 2, ..., n \tag{72}$$

In Eq.(72), the common factor 2π can be cancelled. through integration by parts we obtain

$$-\iint_e \frac{\partial}{\partial x}(rk_x\frac{\partial \bar{T}}{\partial x})\phi_i dr dx = \iint_e rk_x\frac{\partial \bar{T}}{\partial x}\frac{\partial \phi_i}{\partial x} dr dx - \oint_e rk_x\frac{\partial \bar{T}}{\partial x}\phi_i n_x ds \tag{73a}$$

$$i = 1, 2, ..., n$$

$$-\iint_e \frac{\partial}{\partial r}(rk_r\frac{\partial \bar{T}}{\partial r})\phi_i drdx = \iint_e rk_r\frac{\partial \bar{T}}{\partial r}\frac{\partial \phi_i}{\partial r}drdx - \oint_e rk_r\frac{\partial \bar{T}}{\partial r}\phi_i n_r ds \qquad (73b)$$

$$i = 1, 2, \ldots, n$$

Substituting Eqs. (73) into the weighted residual equation and using boundary conditions to simplify the resulting expression, we obtain

$$\iint_e [\rho cur\frac{\partial \bar{T}}{\partial x} + rk_x\frac{\partial \bar{T}}{\partial x}\frac{\partial \phi_i}{\partial x} + rk_r\frac{\partial \bar{T}}{\partial r}\frac{\partial \phi_i}{\partial r}$$

$$- H_u\rho m_m ru\frac{\partial \hat{\alpha}}{\partial x}\phi_i]drdx + \int_\Gamma h(\bar{T} - T_D)\phi_i ds = 0 \qquad (74)$$

$$i = 1, 2, , \ldots, n$$

Then, substituting Eq. (71) into Eq. (74), expanding the resulting expression, and writing it in matrix form we have

$$[k_{ij}]_{n \times n}[T_i]_{n \times 1} = [F_i]_{n \times 1} \qquad (75)$$

where k_{ij} and F_i for interior elements and exterior elements are given respectively as

$$k_{ij} = \iint_e (k_x r\frac{\partial \phi_i}{\partial x}\frac{\partial \phi_j}{\partial x} + k_y r\frac{\partial \phi_i}{\partial r}\frac{\partial \phi_j}{\partial r} + \rho cur\phi_i\frac{\partial \phi_j}{\partial x}drdx \qquad (76a)$$

$$F_i = \iint_e H_u\rho m_m ur\frac{\partial \hat{\alpha}}{\partial x}\phi_i drdx \qquad (76b)$$

and

$$k_{ij} = \iint_e (k_x r \frac{\partial \phi_i}{\partial x}\frac{\partial \phi_j}{\partial x} + k_r r \frac{\partial \phi_i}{\partial r}\frac{\partial \phi_j}{\partial r} + \rho c u r \phi_i \frac{\partial \phi_j}{\partial x}) dr dx + \int_\Gamma h r \phi_i \phi_j ds \tag{77a}$$

$$F_i = \iint_e H_u \rho m_m u r \frac{\partial \hat{\alpha}}{\partial x} \phi_i dr dx + \int_\Gamma h r T_D \phi_i ds \tag{77b}$$

For a linear isoparametric quadrilateral element the geometric functions are

$$x = \sum_{j=1}^{4} x_j \phi_j(\xi,\eta) \tag{78a}$$

$$r = \sum_{j=1}^{4} r_j \phi_j(\xi,\eta) \tag{78b}$$

where the ϕ_j are exactly the same as in Eqs. (49). Expressing Eqs. (76) and Eqs. (77) in terms of local coordinates and applying the bilinear Guass-Legendre quadrature formulas, the final equations which can be used directly in the computer program are obtained and given by

$$k_{ij} = \sum_{o=1}^{2}\sum_{p=1}^{2} W_o W_p [(k_x r \frac{\partial \phi_i}{\partial x}\frac{\partial \phi_j}{\partial x} + k_r r \frac{\partial \phi_i}{\partial r}\frac{\partial \phi_j}{\partial r} + \rho c u r \phi_i \frac{\partial \phi_j}{\partial x}) |J|]_{(\xi_o \eta_p)} \tag{79a}$$

$$F_i = \sum_{o=1}^{2}\sum_{p=1}^{2} W_o W_p [H_u \rho m_m u r \frac{\partial \hat{\alpha}}{\partial x} \phi_i |J|]_{(\xi_o \eta_p)} \tag{79b}$$

and

$$k_{ij} = \sum_{o=1}^{2}\sum_{p=1}^{2} W_o W_p [(k_x r \frac{\partial \phi_i}{\partial x}\frac{\partial \phi_j}{\partial x} + k_r r \frac{\partial \phi_i}{\partial r}\frac{\partial \phi_j}{\partial r} + \rho c u r \phi_i \frac{\partial \phi_j}{\partial x})|J|]_{(\xi_o,\eta_p)} + \sum_{0=1}^{2} W_o [hr\phi_i^* \phi_j^* \frac{L^{(e)}}{2}]_{\xi_o} \quad (80a)$$

$$F_i = \sum_{o=1}^{2}\sum_{p=1}^{2} W_o W_p [H_u \rho m_m u r \frac{\partial \hat{\alpha}}{\partial x}\phi_i |J|]_{(\xi_o,\eta_p)} + \sum_{o=1}^{2} [rh(T_{D_k}\phi_k^* + T_{D_\ell}\phi_\ell^*)\phi_i^* \frac{L^{(e)}}{2}]_{\xi_o} \quad (80b)$$

where Eqs. (79) apply to interior elements and Eqs. (80) apply to exterior elements. In the equations, all indices have the same definitions as they were assigned relative to the Cartesian coordinates, except where r is used instead of y. Substituting Eqs. (79) or Eqs. (80) into Eq.(44), element heat transfer equations for an axisymetric condition will be formed.

The finite element method formulation for a one-dimensional heat transfer model is shown below. The equations are refined from Hackett and Prasad (1989). The element residual equations are

$$\begin{bmatrix} k_{ii} & k_{ij} \\ k_{ji} & k_{jj} \end{bmatrix} \begin{bmatrix} T_i \\ T_j \end{bmatrix} = \begin{bmatrix} F_i \\ F_j \end{bmatrix} \quad (81)$$

where

$$k_{ii} = \frac{k_x}{L^{(e)}} - \frac{\rho c u}{2} + \frac{2hL^{(e)}}{3d} \tag{82a}$$

$$k_{ij} = -\frac{k_x}{L^{(e)}} + \frac{\rho c u}{2} + \frac{hL^{(e)}}{3d} \tag{82b}$$

$$k_{ji} = -\frac{k_x}{L^{(e)}} - \frac{\rho c u}{2} + \frac{hL^{(e)}}{3d} \tag{82c}$$

$$k_{jj} = \frac{k_x}{L^{(e)}} + \frac{\rho c u}{2} + \frac{2hL^{(e)}}{3d} \tag{82d}$$

$$F_i = F_j = \frac{hL^{(e)}T_D}{d} + \frac{\rho m_m H_u \frac{\partial \hat{\alpha}}{\partial t} L^{(e)}}{2} \tag{83}$$

In the above equations, all material properties and rates-of-cure are functions of position but are treated as being constant within each element.

V. FORMULATION OF THE DEGREE-OF-CURE MODEL AND CALCULATION TECHNIQUE

In this study we use numerical integration to obtain the degree-of-cure solution. Beginning at the die entrance, the degree-of-cure in the transverse direction is set to zero, that is

$$\alpha(0,y) = 0 \tag{84}$$

From Eq. (17) through Eq. (21) we can obtain the rate-of-cure $\partial\alpha/\partial t$ through the temperature profile. Then, using Eq. (22) we can change rate-of-cure from the form of derivative with respect to time to the form of derivative with respect to the variable x

$$\frac{\partial\alpha}{\partial x} = \frac{1}{u}\frac{\partial\alpha}{\partial t} \tag{85}$$

Then a stepping procedure is used to integrate the gradient to find α further into the die

$$\alpha(x + dx,y) = \alpha(x,y) + \frac{1}{2}[\frac{\partial\alpha}{\partial x}(x,y) + \frac{\partial\alpha}{\partial x}(x + dx,y)]dx \tag{86}$$

Using the mesh of the finite element method, Eq. (86) may be rewritten as follows

$$\alpha(x_i + L^{(e)},y) = \alpha(x_i,y_i) + \frac{1}{2}[\frac{\partial\alpha}{\partial x}(x_i,y_i) + \frac{\partial\alpha}{\partial x}(x_i + L^{(e)},y_i)]L^{(e)} \tag{87}$$

where i is the nodal number. The profile for the degree-of-cure is determined through Eq. (87).

From the governing differential equation of heat transfer it is easily seen that temperature and degree-of-cure are coupled. We use the method of iteration to solve this problem. At first we set the degree-of-cure equal to zero everywhere. Thus it is not difficult to obtain the solution which will serve as the initial value. Depending on that value, the iteration will be developed successfully. The iteration procedure may be simply expressed as

1. Let $\alpha^{(1)} = 0$ to obtain $T^{(1)}$.
2. From $T^{(1)}$ obtain $\partial\alpha^{(2)}/\partial t$ and $\alpha^{(2)}$, then obtain $T^{(2)}$.
3. Repeat step 2 several times: from $T^{(j)}$ obtain $\partial\alpha^{(j+1)}/\partial t$ and $\alpha^{(j+1)}$, then obtain $T^{(j+1)}$; continue until the criterion for convergence is satisfied.

The criterion for convergence used in the computer program is that the difference in maximum temperatures in the die at a node obtained from two consecutive iterations be less than 10^{-2} °C. With this criterion, the number of iterations usually ranges from 4 to 8, depending on the different sets of die temperatures and line speed.

VI. NUMERICAL SOLUTION AND DISCUSSION

Three typical sets of die temperature profiles combined with three different line speeds are considered, using the finite element formulation derived in the previous rectangular and circular, are treated. All solutions of the above eighteen cases are satisfactory.

First, it should be pointed out that due to a lack of data, we use a temperature profile of the die interface, which was obtained with no material flow through the die, as the boundary condition. During pultrusion, the material near the die entrance will extract heat from the die and over the remainder of the die the material will release heat to the die. So, the actual temperature profile of the die interface during pultrusion may be somewhat different from that used in the paper. The error will be small because of the poor thermal conductivity of the composite material and it will not influence the general shape of the profile and the qualitative analysis. Comparing the temperature profile of the material with that of die interface, we can find some rule of temperature distribution. Over the beginning part of the die, the temperature of the die interface is higher

than that of the composite, the die providing heat to the material during the curing reaction. The length of this region depends on the line speed primarily; the higher the line speed, the longer is this region. Over the remainder of die, the temperature of the material is higher than that of the die interface due to the accumulation of heat of reaction. The die draws heat from the curing material, thereby reducing the thermal shock to the product upon its exit from the die.

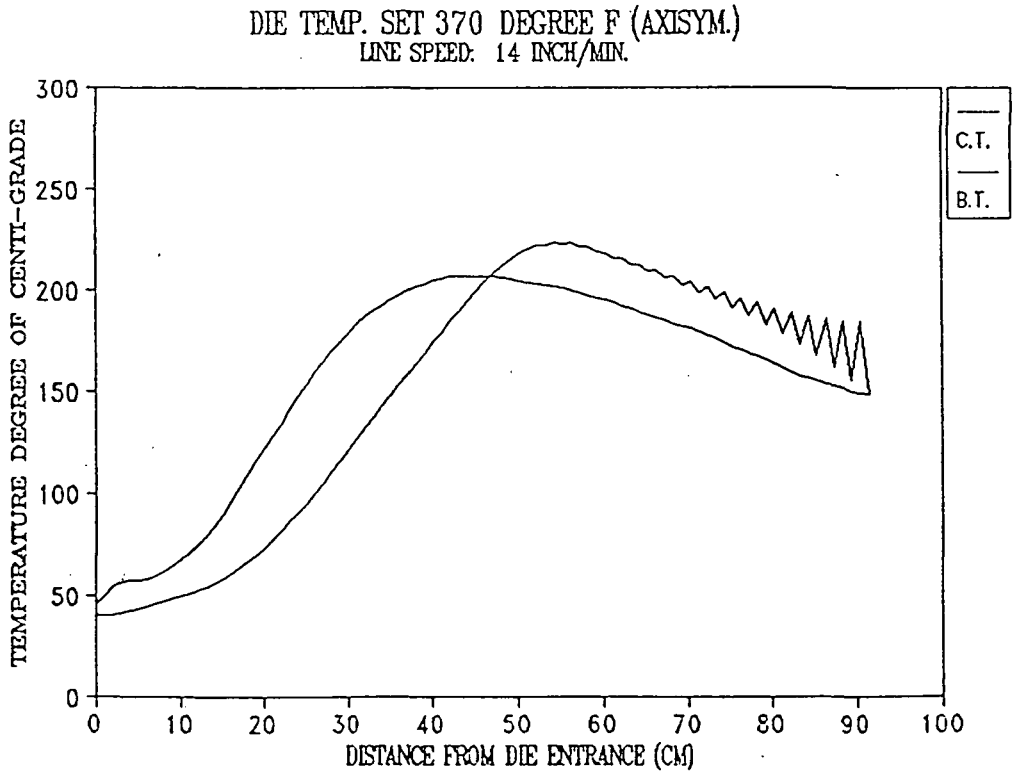

Figure 6. Temperature Profile of the Material

From Figure 6 we see that the centerline temperature of the composite is distinctly lower than the boundary temperature near the entrance of the die, even though the radius is less than 1 centimeter. The difference will be greater with increasing radius or thickness. This phenomenon explains the necessity of controlling a gentle gradient of die temperature near the entrance, otherwise a cured matrix skin may be formed on the die wall and a very poor product surface will result.

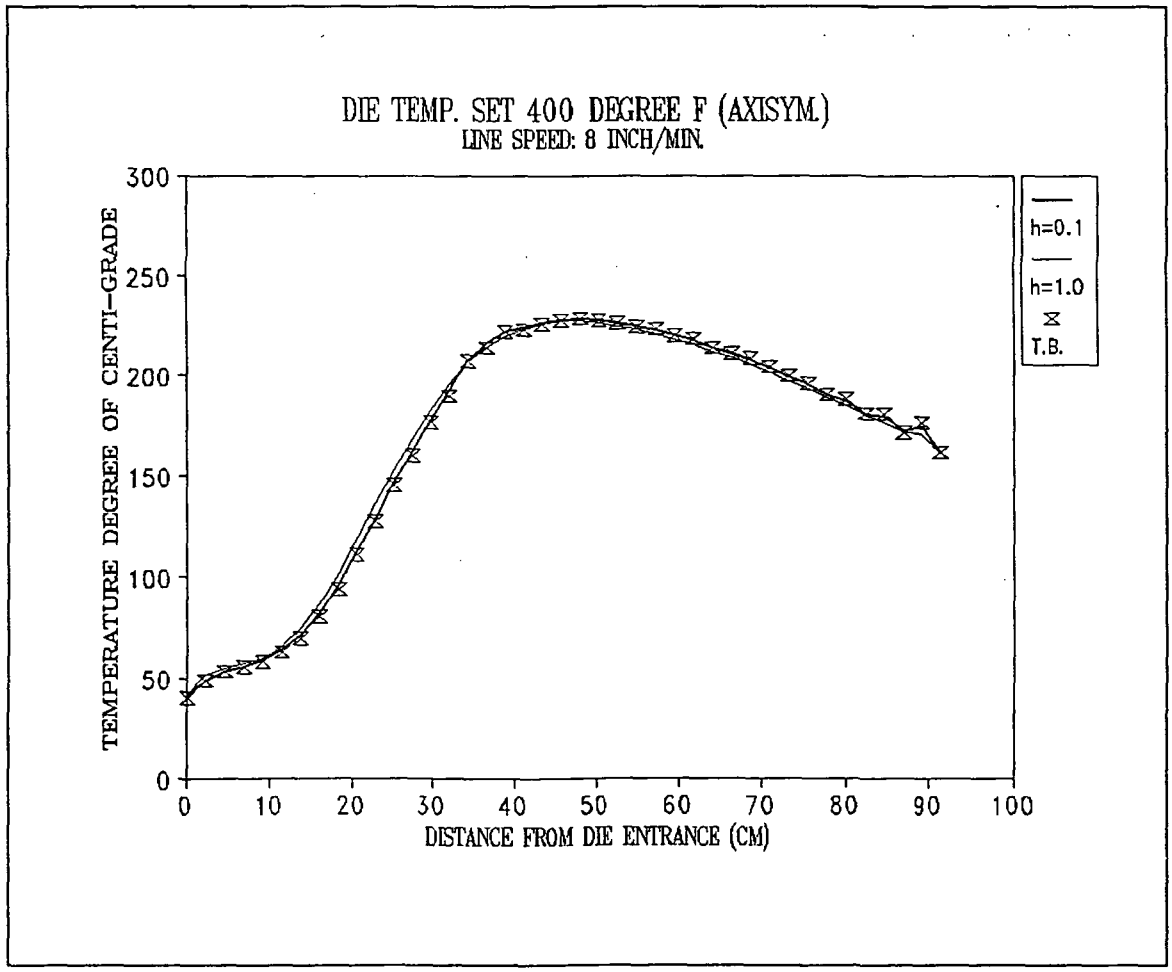

Figure 7. Temperature Profile Solved with Convective Boundary Conditions

The resulting material temperature profiles are obtained with temperature boundary conditions. Because the material in the die undergoes three different phases: liquid, gel, and solid, the value of the die-material interface convection coefficient is difficult to determine. This is an obstacle to applying convective boundary conditions. As examples, we calculate two cases with the coefficient h held constant over the whole domain of the die. We find that when h = 0.1, the solution is almost identical to the solution obtained with temperature boundary conditions. Another solution, with h = 1, is also very close to the solution obtained with temperature boundary conditions. This seems to indicate that within certain ranges, the variation of the convection coefficient does not greatly influence the temperature profile of the material From Figures 6 and 7, curve oscillations can be noted. This is caused by the convective term in the heat transfer equation. This term makes k_{ij} not equal to k_{ji} in the matrix [K]; that is to say, it makes the operator not self-adjoint (Zienkiewicz and Taylor, 1989). But if we adjust the boundary conditions properly, the numerical oscillations will be improved greatly. From analysis of the distribution of material temperature in the die, we know that the material temperature should be higher than the die temperature at the exit of the die. Therefore we change Eq. (2b) from a constant to a linear function of y and assume

that the centerline temperature is 8° C higher than the die temperature. The new results are shown in Figure 8.

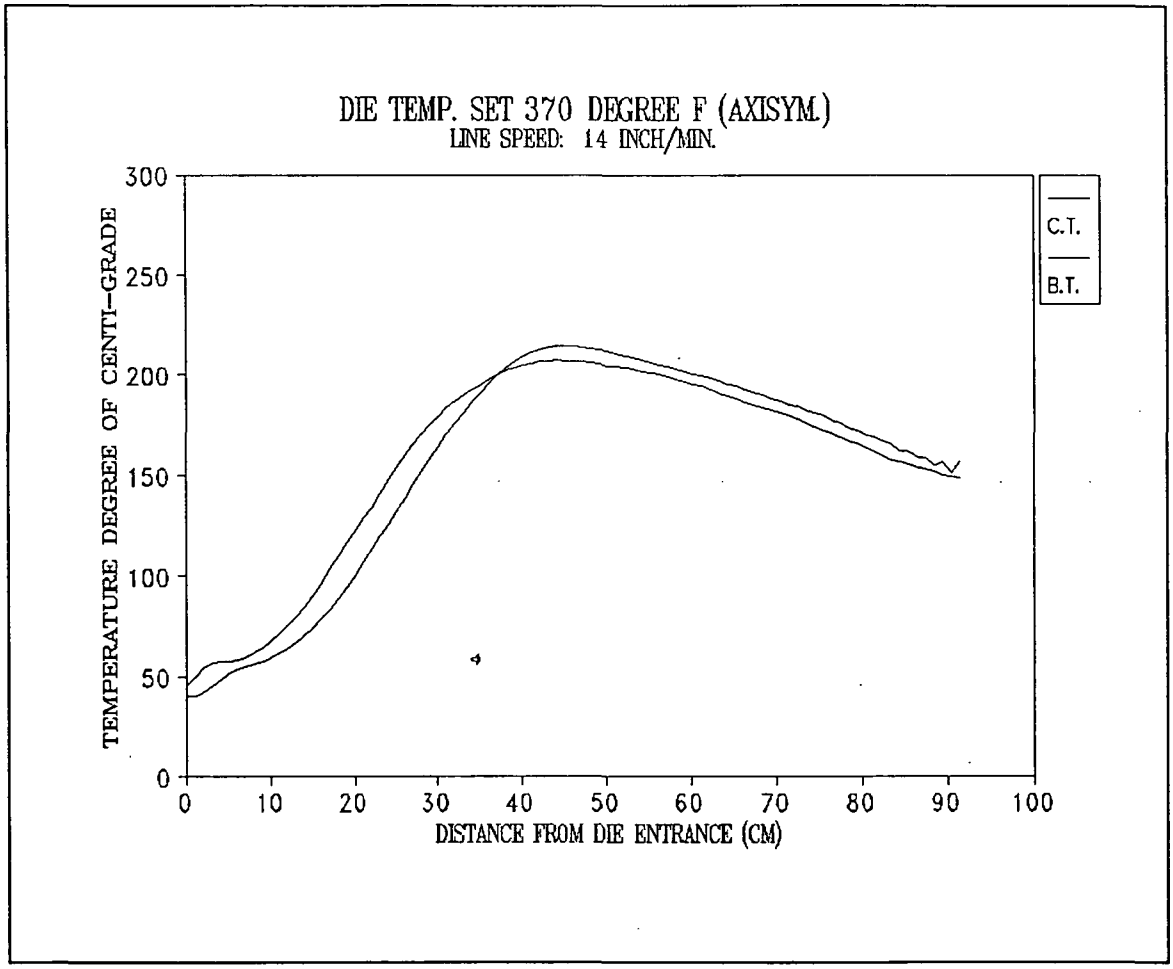

Figure 8. Temperature Profile Solved with Adjusted Boundary Conditions

Comparing the curve of degree-of-cure with a different line speed but with the same die temperature we find that when the line speed increases, the final degree-of-cure (the degree-of-cure at the die exit) decreases. In some cases the final degree-of-cure is too low to yield a qualified product. If a higher die temperature set is used, it is

possible to obtain a sufficiently cured composite material with a high line speed. This phenomenon shows that it is important to select an appropriate combination of die temperature set and line speed in order to produce a high quality as well as a high quantity of composite components. It should be explained that in the usual situation, the prescription of resin includes curing agent, curing agent

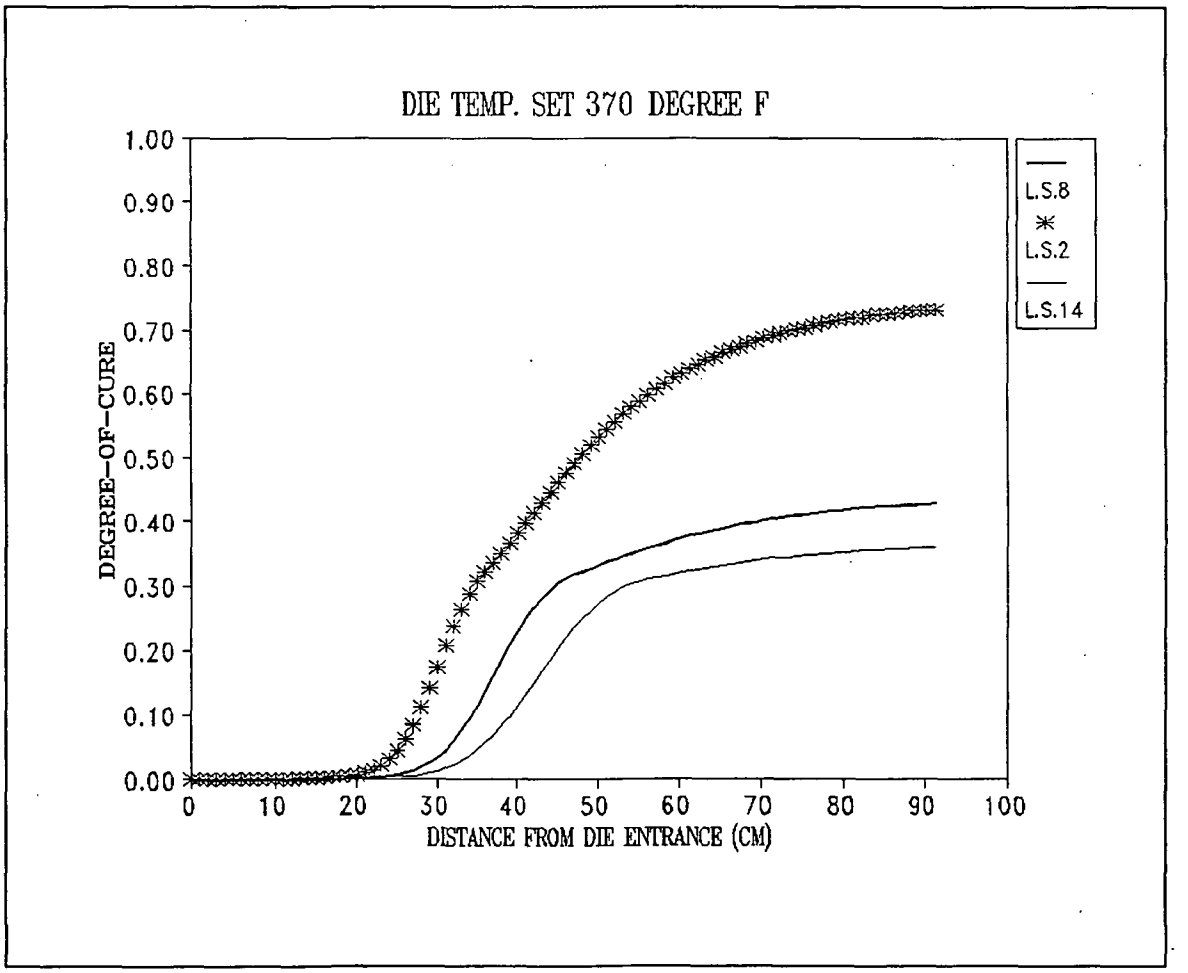

Figure 9. Profile of the Degree-of-Cure of the Material

accelerator, and the resin itself. But in this paper the curing process model is only based on the Hercules 3501-6

resin. So, in an actual pultrusion process, the speed-of-cure reaction will be faster and a higher line speed will be allowable. There are also other techniques for increasing the degree-of-cure of pultruded material, such as pre-heating before the material enters the die and post-heating after the material leaves the die. The details of these techniques are beyond the topic of this paper.

According to Batch and Macosko (1987), when the degree-of-cure is between 0.01 and 0.3, the matrix changes into the gel phase. Observing the degree-of-cure profile we see that the gel region in the die is located between 20 cm to 40 cm from the die entrance (relative to a 36-inch length die). Thus we can roughly divide the die into three regions: the first one-third of the die is the liquid region, the next one-sixth of the die is the gel region, and the last part of the die is the solid region. The position of peak exotherm of the material is usually located at the beginning of solid region. The relative positions of the sub-regions and the magnitude of material temperature may be varied based upon different prescriptions of resin and techniques utilized in processing, but the general rule of distribution is: in the liquid region, the temperature of the material is lower than that of the die and its average slop is gentle; in the gel region, the material temperature rapidly rises from lower than the die temperature to higher than the die temperature and its gradient is relatively sharp; in the

solid region, the material temperature is higher than that of the die and its average slope is gentle.

We know that the resin pressure model is another important sub-model of the pultrusion process. If a problem concerned with the resin pressure model is to be solved, the viscosity of the resin along the die must first be known. If the profile of the material temperature has been obtained, it is easy to determine the viscosity using the formula given by Lee et al. (1982),

$$\mu = \mu_\infty \exp(U/RT + K\alpha) \quad , \qquad \alpha \leq 0.5 \tag{88}$$

where μ is the viscosity, μ_∞ is a constant, U is the activation energy for the viscosity, and K is a constant which is independent of temperature

$$K = 14.1 \pm 1.2 \tag{89a}$$

$$\mu_\infty = 7.93 \times 10^{-14} \quad \text{Pa·s} \tag{89b}$$

$$U = 9.08 \times 10^{4} \quad \text{J/mol} \tag{89c}$$

As mentioned earlier, the data of Lee et al., (1982) are based upon the Hercules 3501-6 resin system, but the form of the formula is general because it is well known that viscosity is a function of temperature. In this paper we didn't calculate the value of viscosity, but here merely mention another use of the temperature profile.

We also calculated the 3 x 3 cases using the one-dimensional model and compared the solutions with the bulk

temperature profile as well as with the bulk degree-of-cure profile obtained with the two-dimensional model.

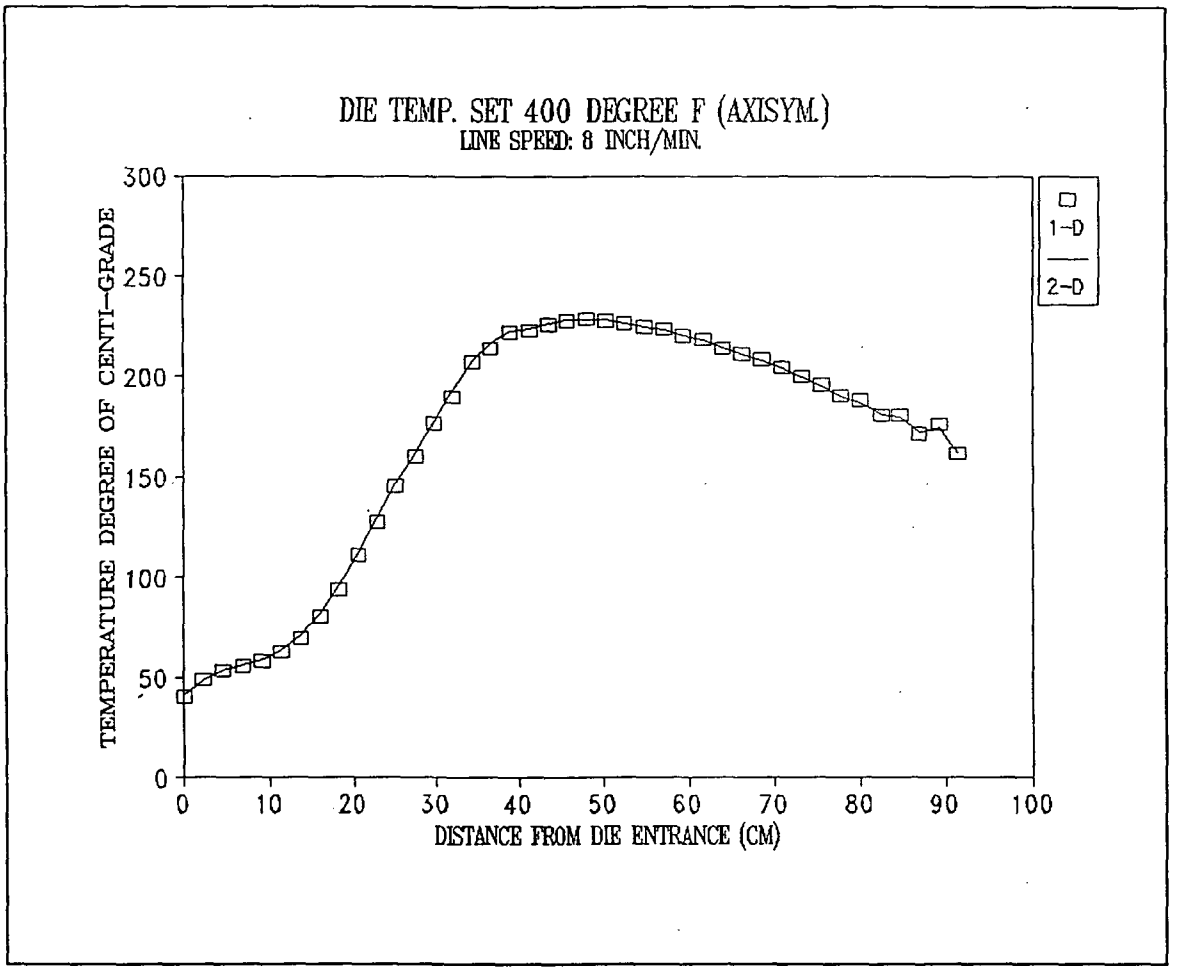

Figure 10. Temperature Profile of the One-Dimensional Model

We find that the differences between the results obtained with the one-dimensional model and those obtained with the two-dimensional model are very slight. If one is not interested in the variation of temperature and degree-of-cure in the direction of thickness, using the one-dimensional model is recommended since it is more convenient.

REFERENCES

Batch, G.L. and C.W. Macosko, 1987. "A Computer Analysis of Temperature and Pressure Distributions in a Pultrusion Die," 42nd Annual Conference, Composites Institute, The Society of the Plastics Industry, Inc.

Burnett, D.S. 1987. Finite Element Analysis, Addison-Wesley Publishing Company.

Erhun, M. and S.G. Advani, 1990. "A Predictive Model for Heat Flow During Crystallization of Semi-Crystalline Polymers," Journal of Thermoplastic Composite Materials, 3: 90-109.

Hackett, R.M. and S.N. Prasad, 1989. "Pultrusion Process Modeling," Advances in Thermoplastic Matrix Composite Materials. American Society for Testing and Material, 62-70.

Lee, W.I.,C.L. Alfred and S.S. George, 1982. "Heat of Reaction, Degree of Cure, and Viscosity of Hercules 3501-6 Resin," Journal of Composite Materials, 16: 510-520.

Lee, W.I. and S.S. George, 1987. "A Model of the Manufacturing Process of Thermoplastic Matrix Composites," Journal of Composite Materials, 21: 1017-1055.

Lewis, R.W., K. Morgan and O.C. Zienkiewicz, 1981. Numerical Methods in Heat Transfer. John Wiley & Sons Ltd.

Shell Chemical Company, 1986. "Pultrusion with EPON Epoxy Resin," Technical Bulletin.

Sumerak, J. and J. Martin, 1984. "Pultrusion Process Variables and Their Effective upon Manufacturing Capability," 39th Annual SPI Conference.

Talbott, M.F. and S.S. George, 1987. "The Effects of Crystallinity on the Mechanical Properties of Peek Polymer and Graphite Fiber Reinforced Peek," Journal of Composite Materials, 21: 1056-1081

Zienkiewicz, O.C. and R.L. Taylor, 1989. The Finite Element Method (Fourth Edition). Mcgraw-Hill Book Company (UK) Limited.

APPENDIX

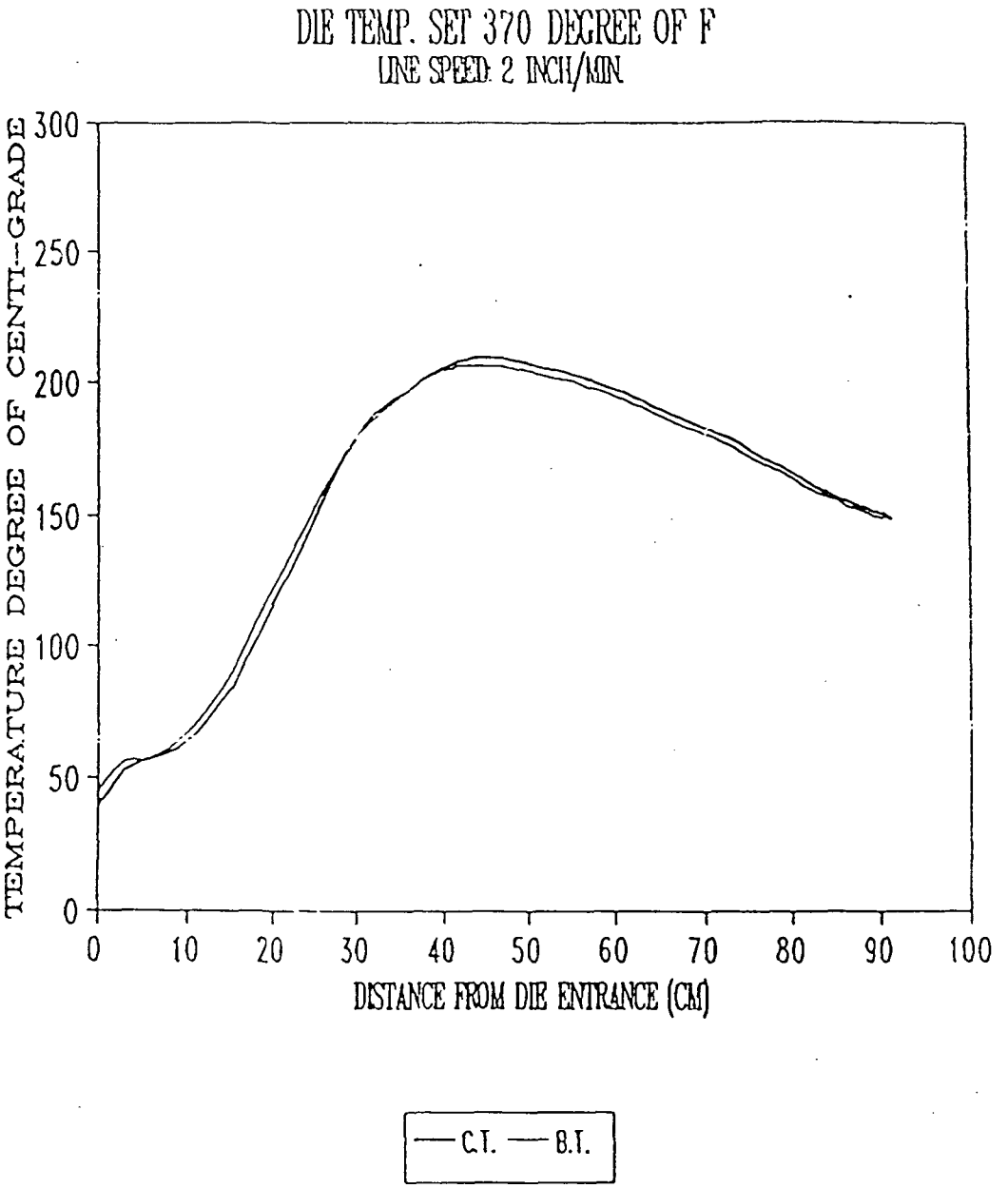
DIE TEMP. SET 370 DEGREE OF F
LINE SPEED: 2 INCH/MIN
TEMPERATURE DEGREE OF CENTI--GRADE
300
250
200
150
100
50
0
0
10
20
30
40
50
60
70
80
90
100
DISTANCE FROM DIE ENTRANCE (CM)
C.I.
B.I.

Figure A-1

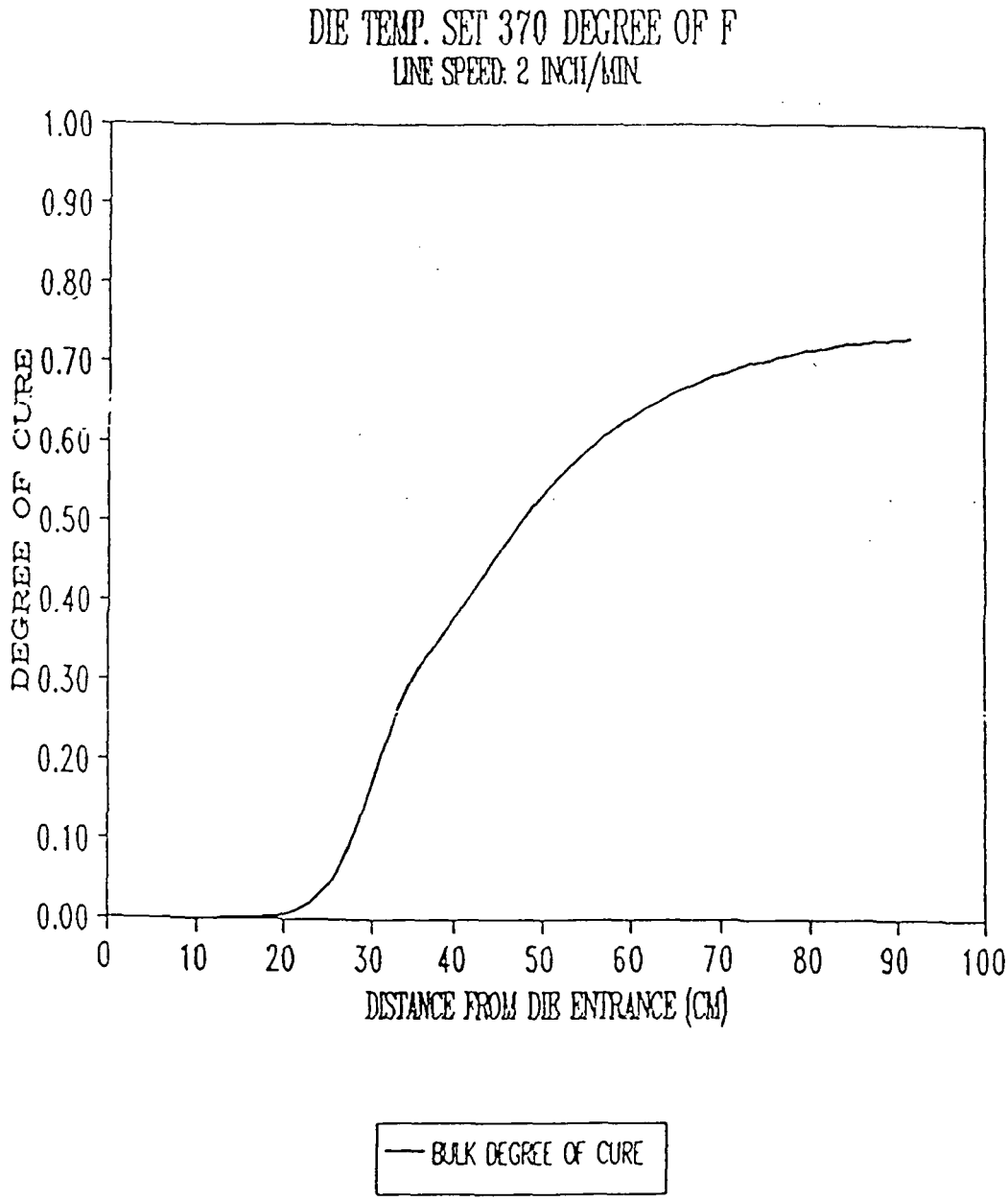
DIE TEMP. SET 370 DEGREE OF F
LINE SPEED: 2 INCH/MIN.
DEGREE OF CURE
1.00
0.90
0.80
0.70
0.60
0.50
0.40
0.30
0.20
0.10
0.00
0
10
20
30
40
50
60
70
80
90
100
DISTANCE FROM DIE ENTRANCE (CM)
BULK DEGREE OF CURE

Figure A-2

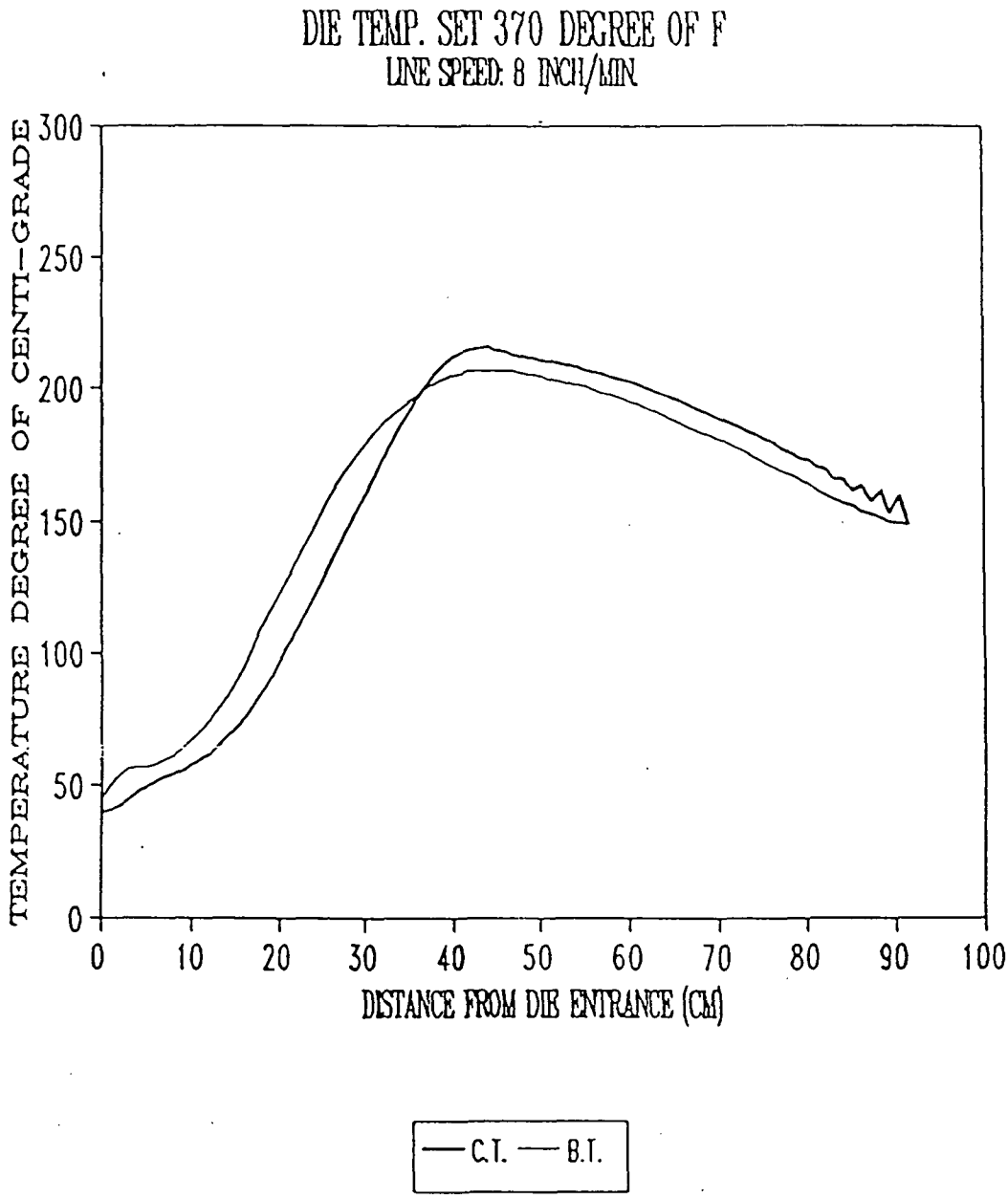
DIE TEMP. SET 370 DEGREE OF F
LINE SPEED: 8 INCH/MIN
TEMPERATURE DEGREE OF CENTI-GRADE
300
250
200
150
100
50
0
0
10
20
30
40
50
60
70
80
90
100
DISTANCE FROM DIE ENTRANCE (CM)
C.I.
B.I.

Figure A-3

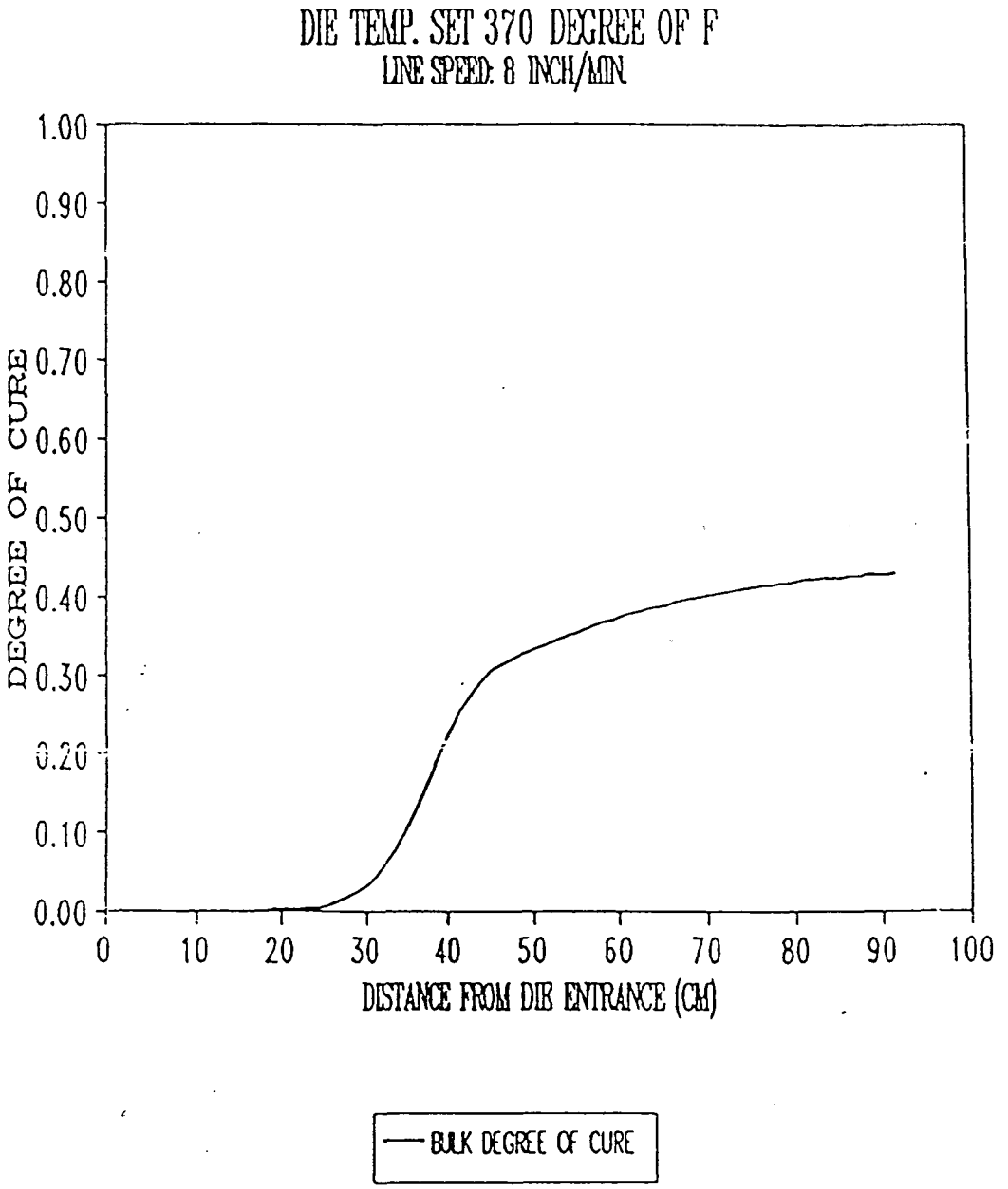
DIE TEMP. SET 370 DEGREE OF F
LINE SPEED: 8 INCH/MIN
DEGREE OF CURE
1.00
0.90
0.80
0.70
0.60
0.50
0.40
0.30
0.20
0.10
0.00
0
10
20
30
40
50
60
70
80
90
100
DISTANCE FROM DIE ENTRANCE (CM)
BULK DEGREE OF CURE

Figure A-4

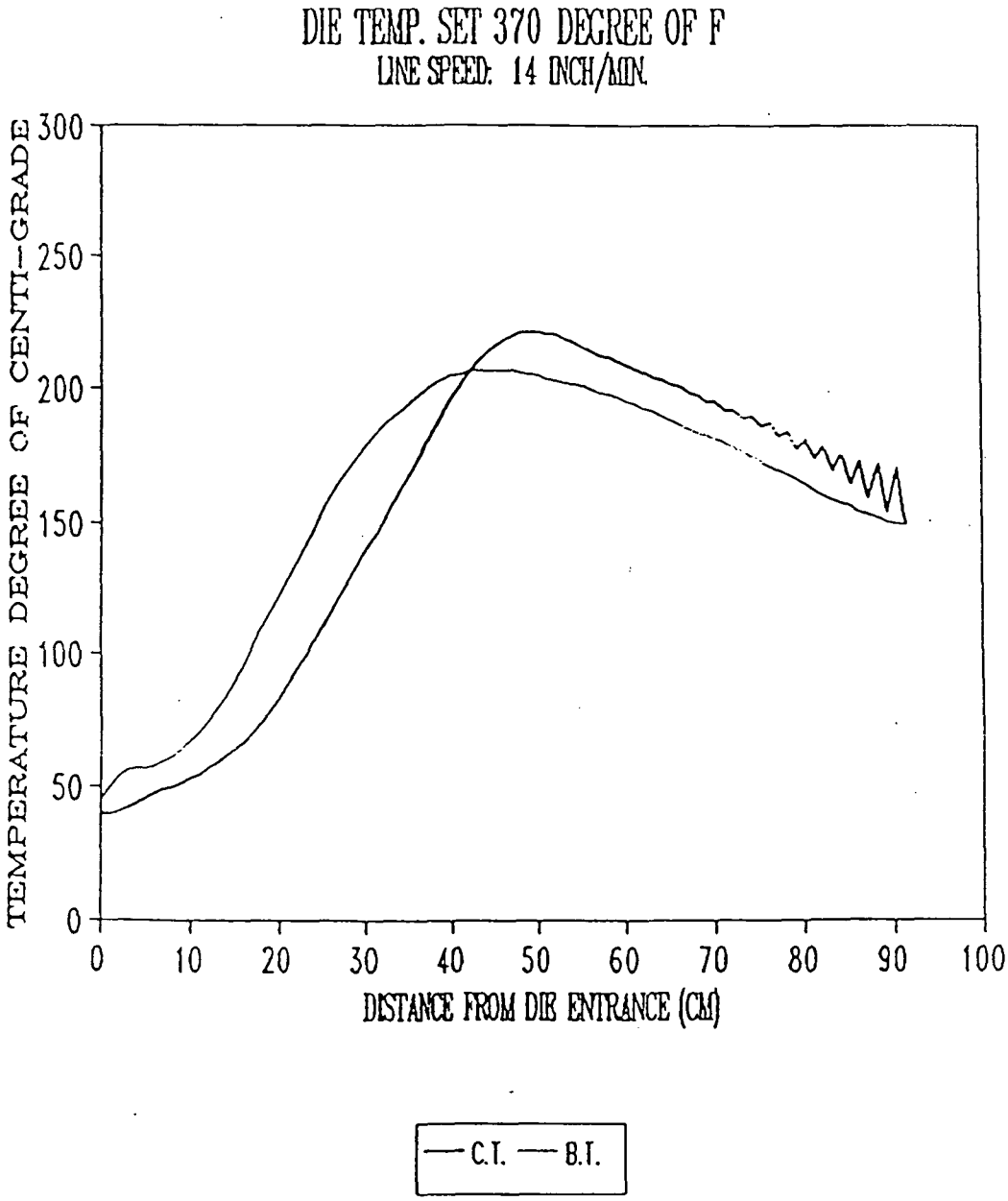
DIE TEMP. SET 370 DEGREE OF F
LINE SPEED: 14 INCH/MIN.
TEMPERATURE DEGREE OF CENTI-GRADE
300
250
200
150
100
50
0
0
10
20
30
40
50
60
70
80
90
100
DISTANCE FROM DIE ENTRANCE (CM)
C.T.
B.T.

Figure A-5

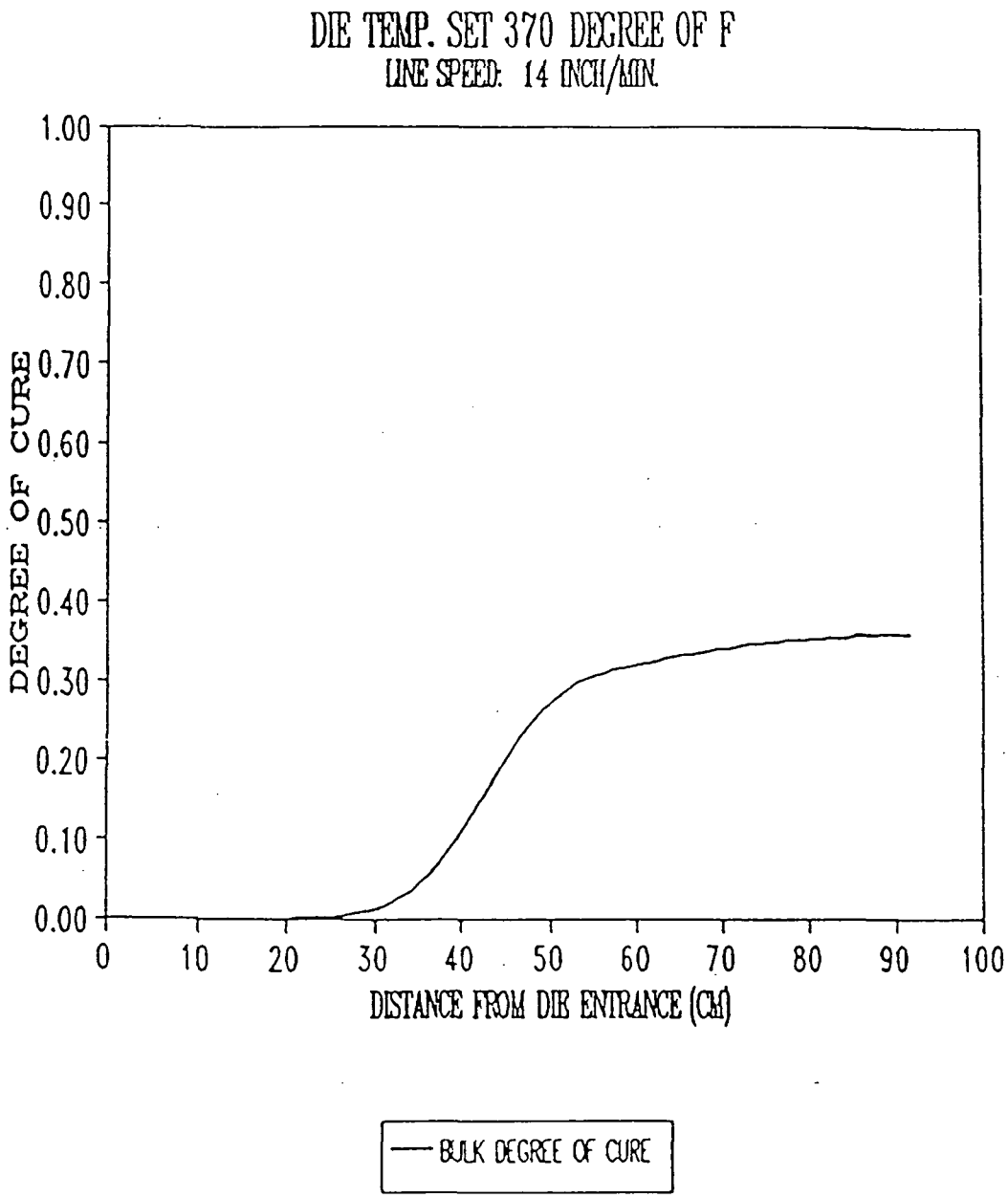
DIE TEMP. SET 370 DEGREE OF F
LINE SPEED: 14 INCH/MIN.
DEGREE OF CURE
1.00
0.90
0.80
0.70
0.60
0.50
0.40
0.30
0.20
0.10
0.00
0
10
20
30
40
50
60
70
80
90
100
DISTANCE FROM DIE ENTRANCE (CM)
BULK DEGREE OF CURE

Figure A-6

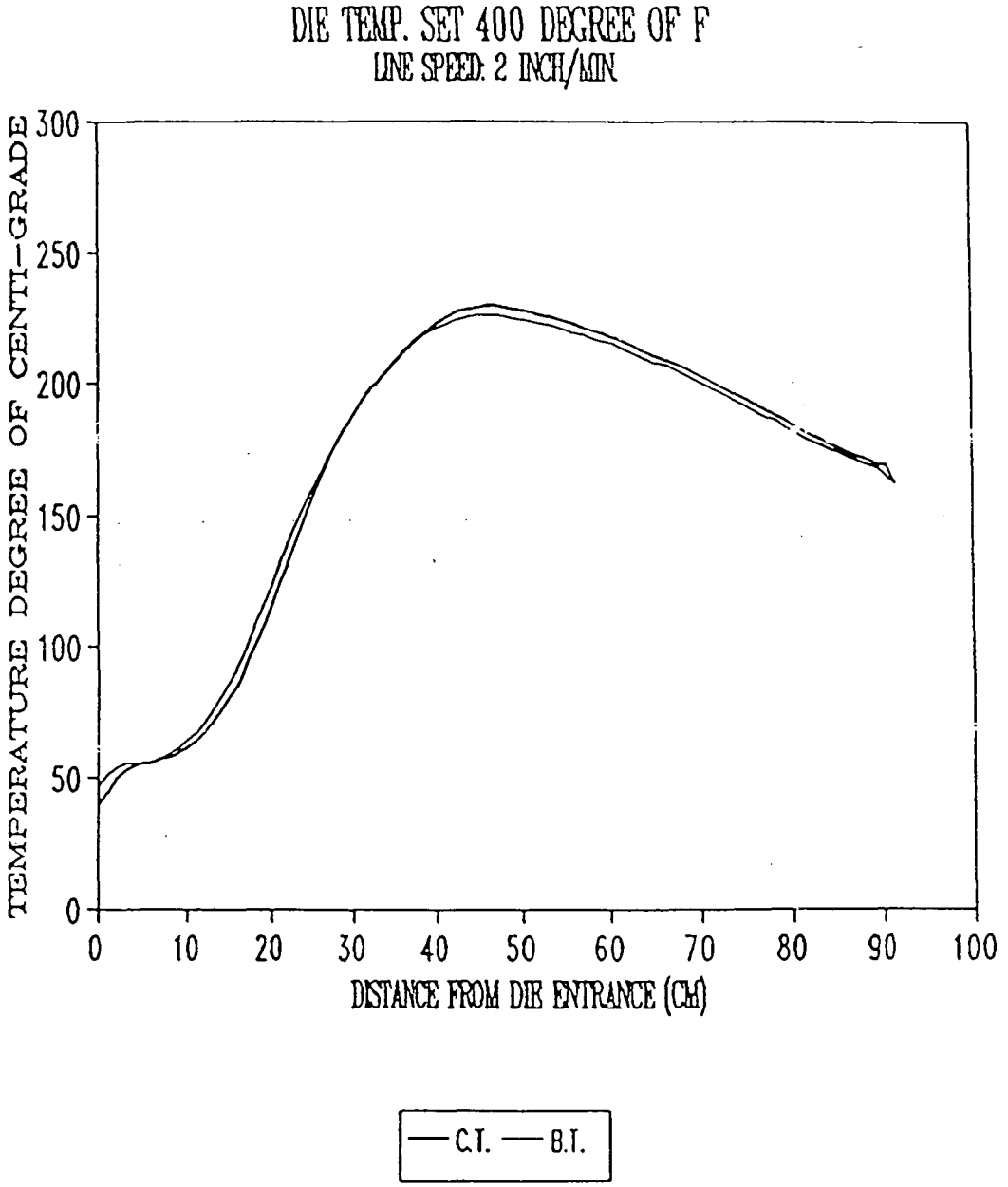
DIE TEMP. SET 400 DEGREE OF F
LINE SPEED: 2 INCH/MIN
TEMPERATURE DEGREE OF CENTI-GRADE
300
250
200
150
100
50
0
0
10
20
30
40
50
60
70
80
90
100
DISTANCE FROM DIE ENTRANCE (CM)
C.I.
B.I.

Figure A-7

C-2

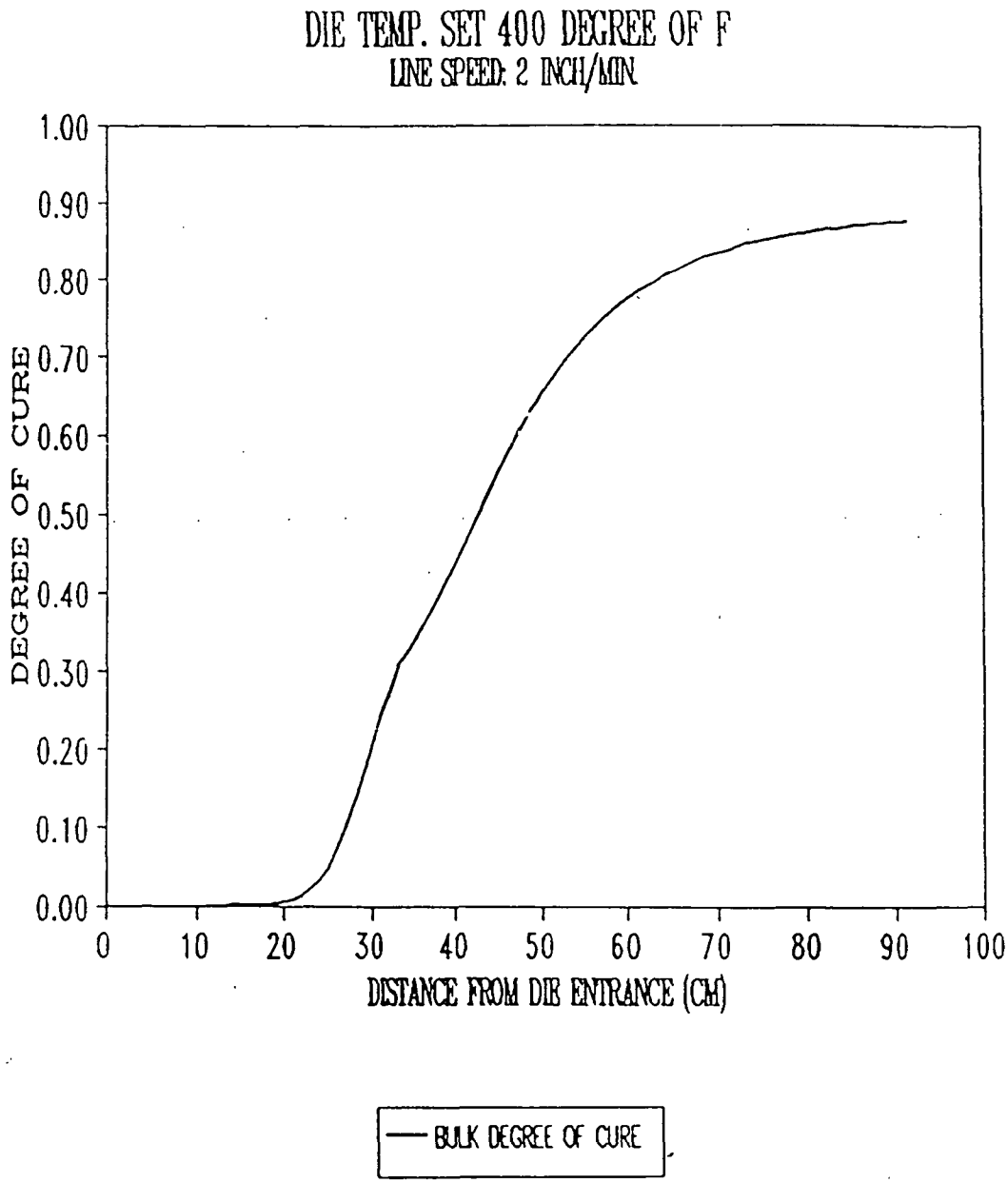
DIE TEMP. SET 400 DEGREE OF F
LINE SPEED: 2 INCH/MIN
DEGREE OF CURE
1.00
0.90
0.80
0.70
0.60
0.50
0.40
0.30
0.20
0.10
0.00
0
10
20
30
40
50
60
70
80
90
100
DISTANCE FROM DIE ENTRANCE (CM)
BULK DEGREE OF CURE

Figure A-8

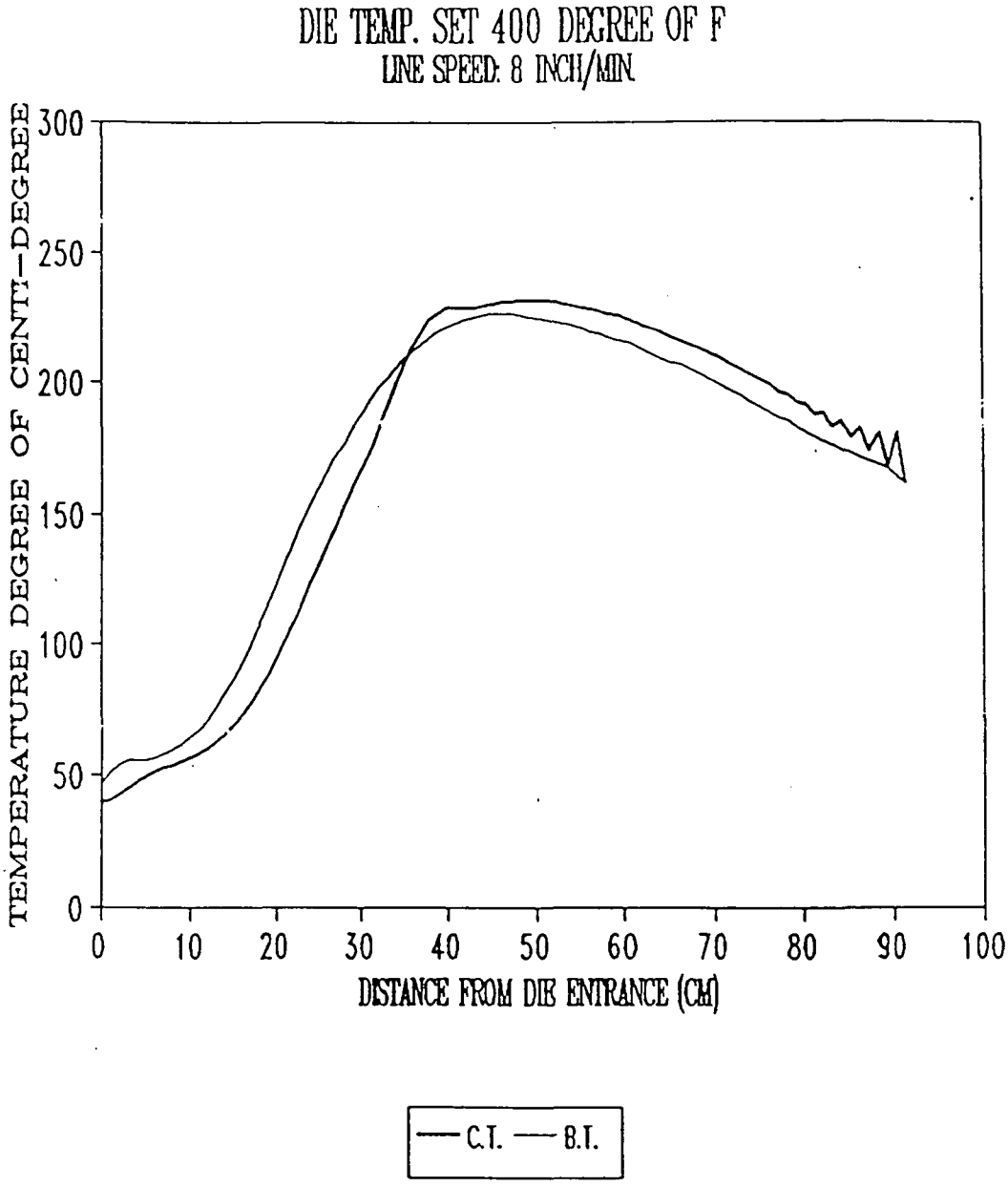
DIE TEMP. SET 400 DEGREE OF F
LINE SPEED: 8 INCH/MIN
TEMPERATURE DEGREE OF CENTI-DEGREE
300
250
200
150
100
50
0
0
10
20
30
40
50
60
70
80
90
100
DISTANCE FROM DIE ENTRANCE (CM)
C.T.
B.T.

Figure A-9

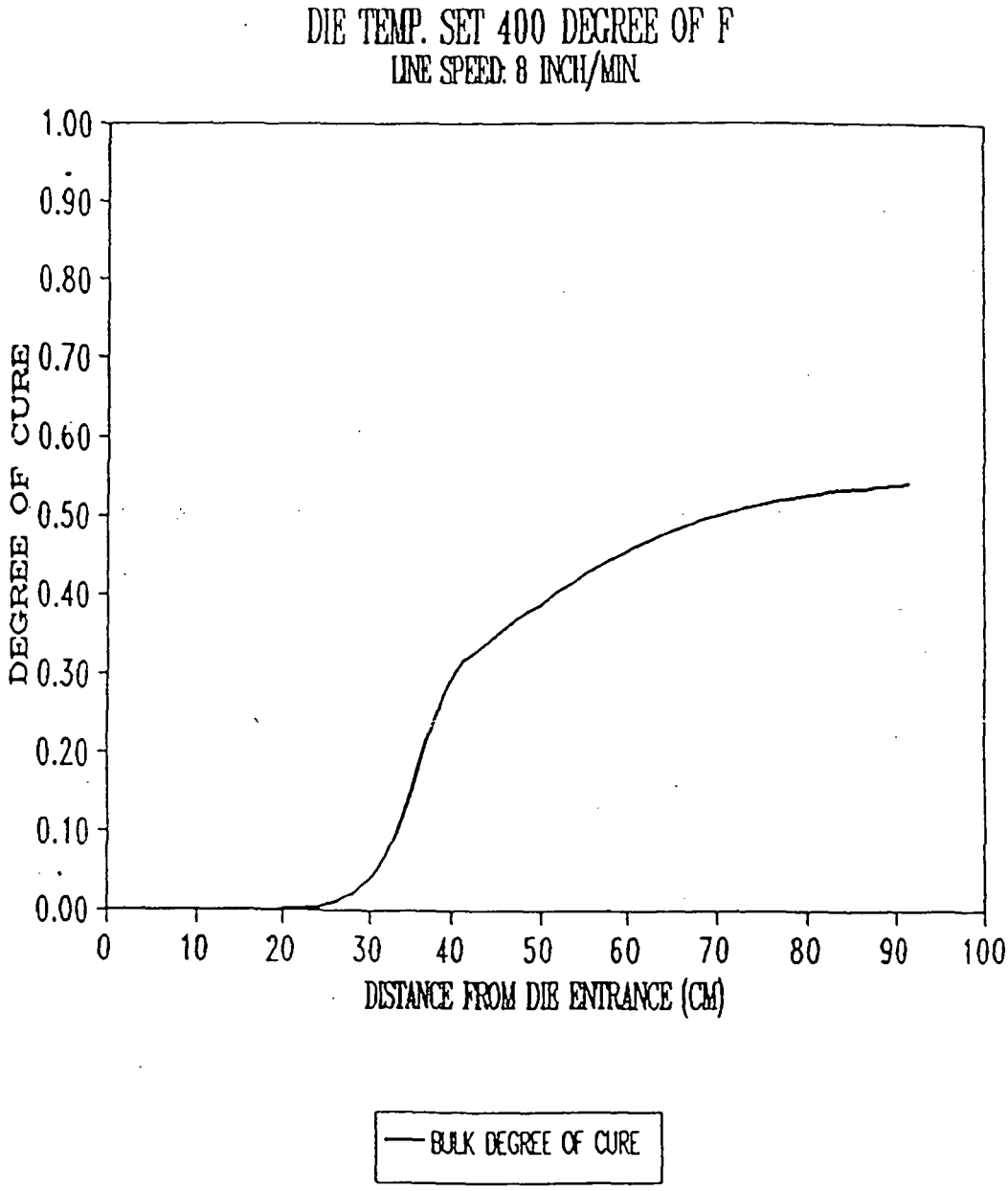
DIE TEMP. SET 400 DEGREE OF F
LINE SPEED: 8 INCH/MIN.
DEGREE OF CURE
1.00
0.90
0.80
0.70
0.60
0.50
0.40
0.30
0.20
0.10
0.00
0
10
20
30
40
50
60
70
80
90
100
DISTANCE FROM DIE ENTRANCE (CM)
BULK DEGREE OF CURE

Figure A-10

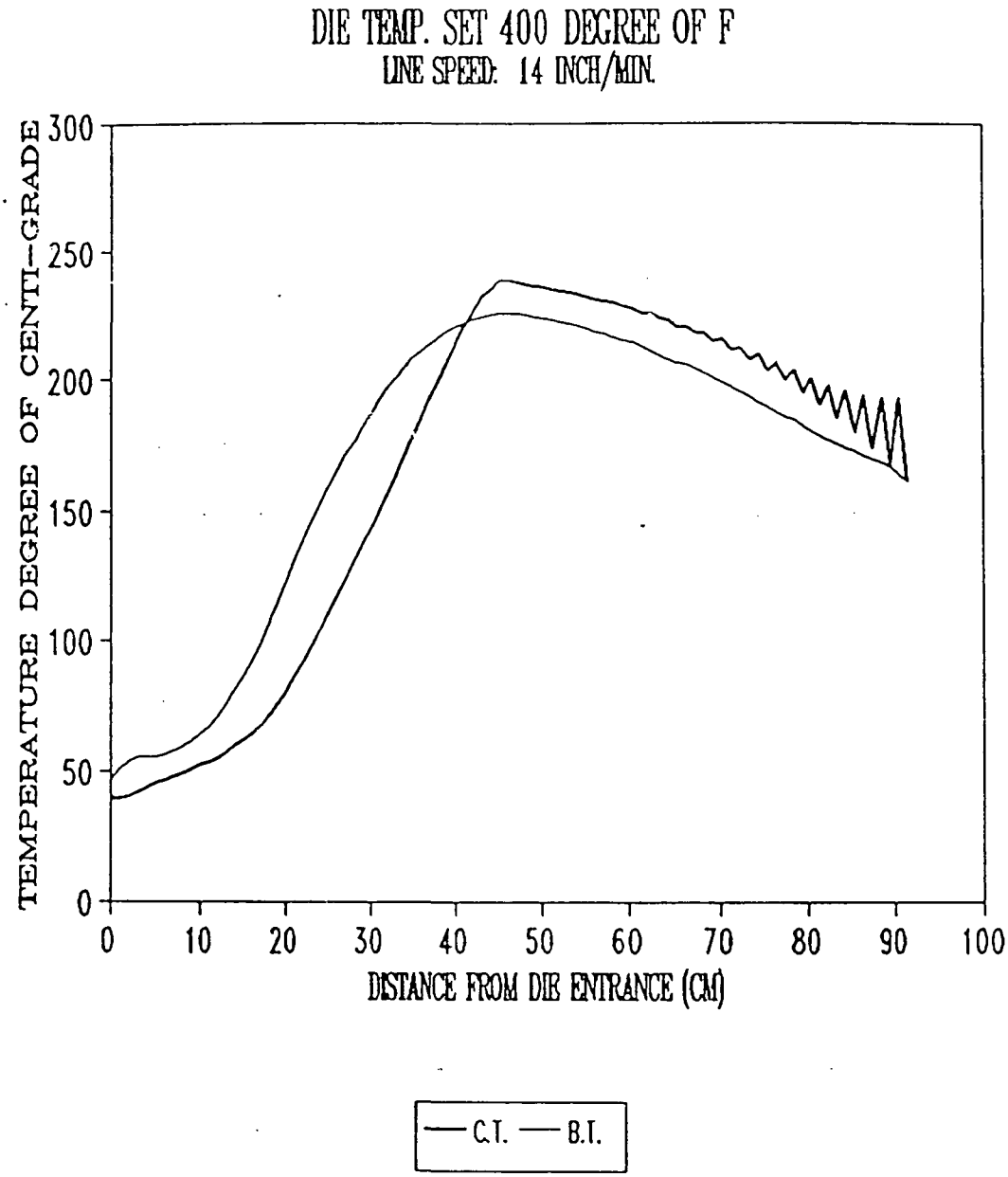
DIE TEMP. SET 400 DEGREE OF F
LINE SPEED: 14 INCH/MIN.
TEMPERATURE DEGREE OF CENTI-GRADE
300
250
200
150
100
50
0
0
10
20
30
40
50
60
70
80
90
100
DISTANCE FROM DIE ENTRANCE (CM)
C.T.
B.T.

Figure A-11

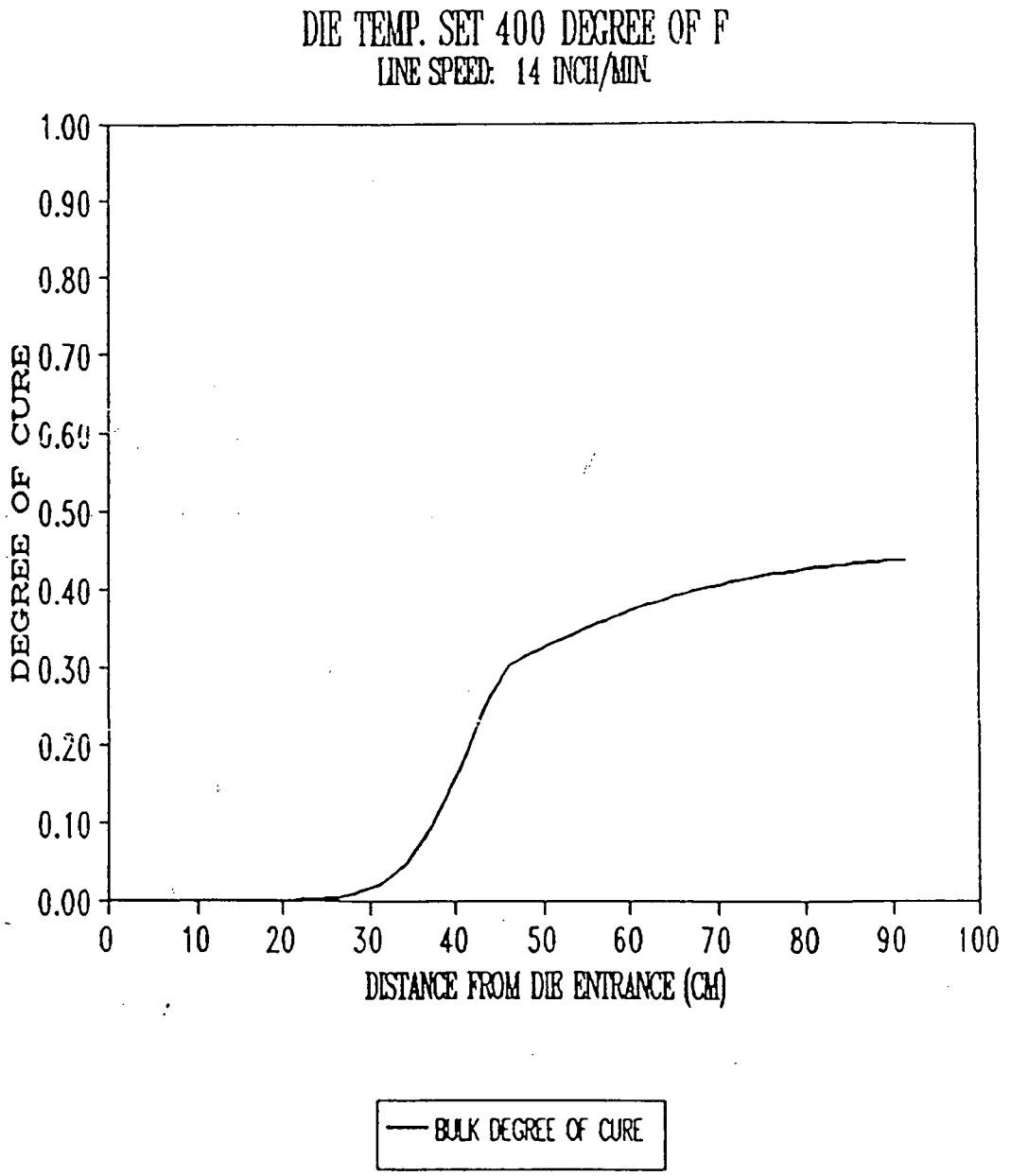
DIE TEMP. SET 400 DEGREE OF F
LINE SPEED: 14 INCH/MIN
DEGREE OF CURE
1.00
0.90
0.80
0.70
0.60
0.50
0.40
0.30
0.20
0.10
0.00
0
10
20
30
40
50
60
70
80
90
100
DISTANCE FROM DIE ENTRANCE (CM)
BULK DEGREE OF CURE

Figure A-12

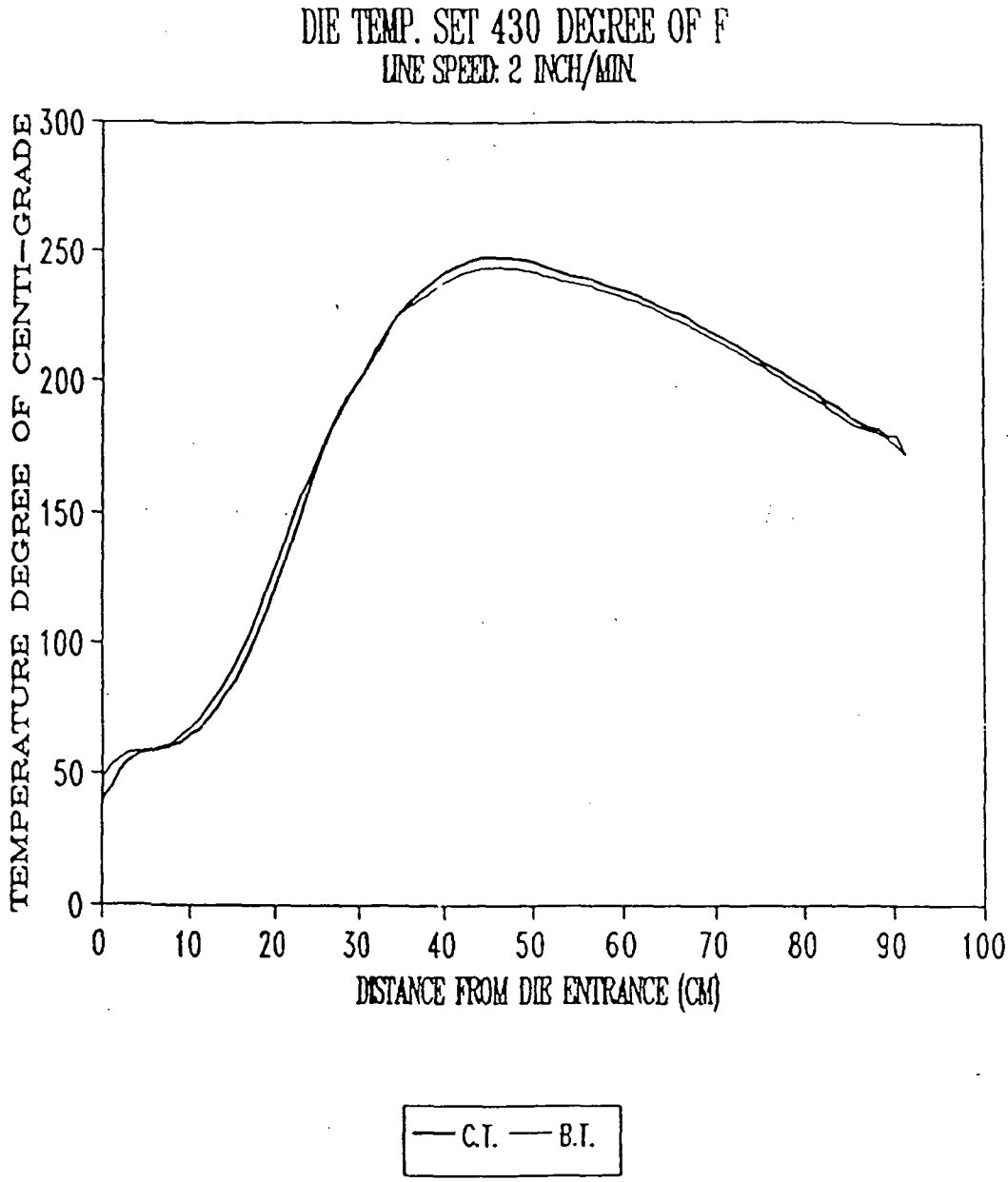
DIE TEMP. SET 430 DEGREE OF F
LINE SPEED: 2 INCH/MIN.
TEMPERATURE DEGREE OF CENTI-GRADE
300
250
200
150
100
50
0
0
10
20
30
40
50
60
70
80
90
100
DISTANCE FROM DIE ENTRANCE (CM)
C.T.
B.T.

Figure A-13

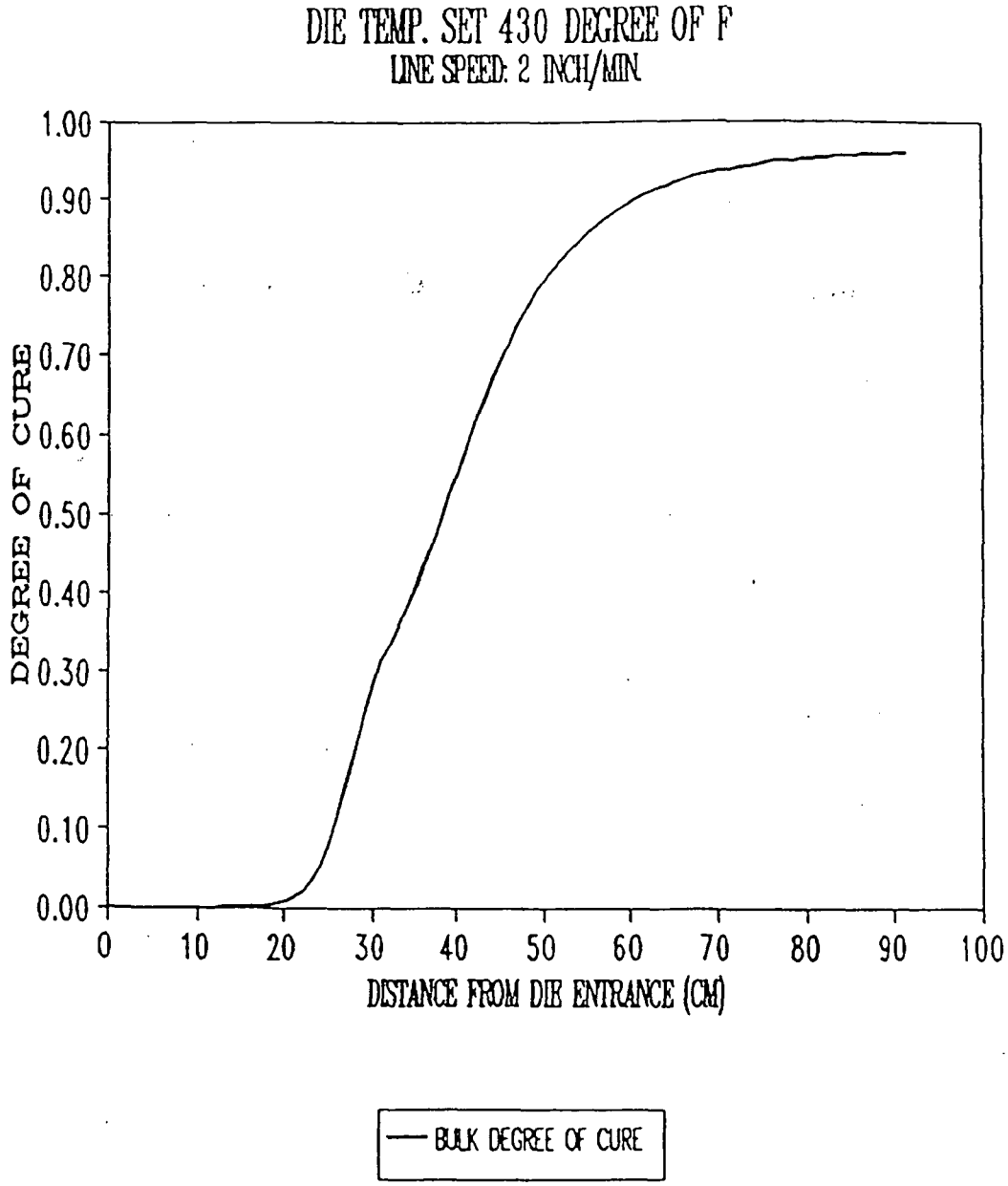
DIE TEMP. SET 430 DEGREE OF F
LINE SPEED: 2 INCH/MIN
DEGREE OF CURE
1.00
0.90
0.80
0.70
0.60
0.50
0.40
0.30
0.20
0.10
0.00
0
10
20
30
40
50
60
70
80
90
100
DISTANCE FROM DIE ENTRANCE (CM)
BULK DEGREE OF CURE

Figure A-14

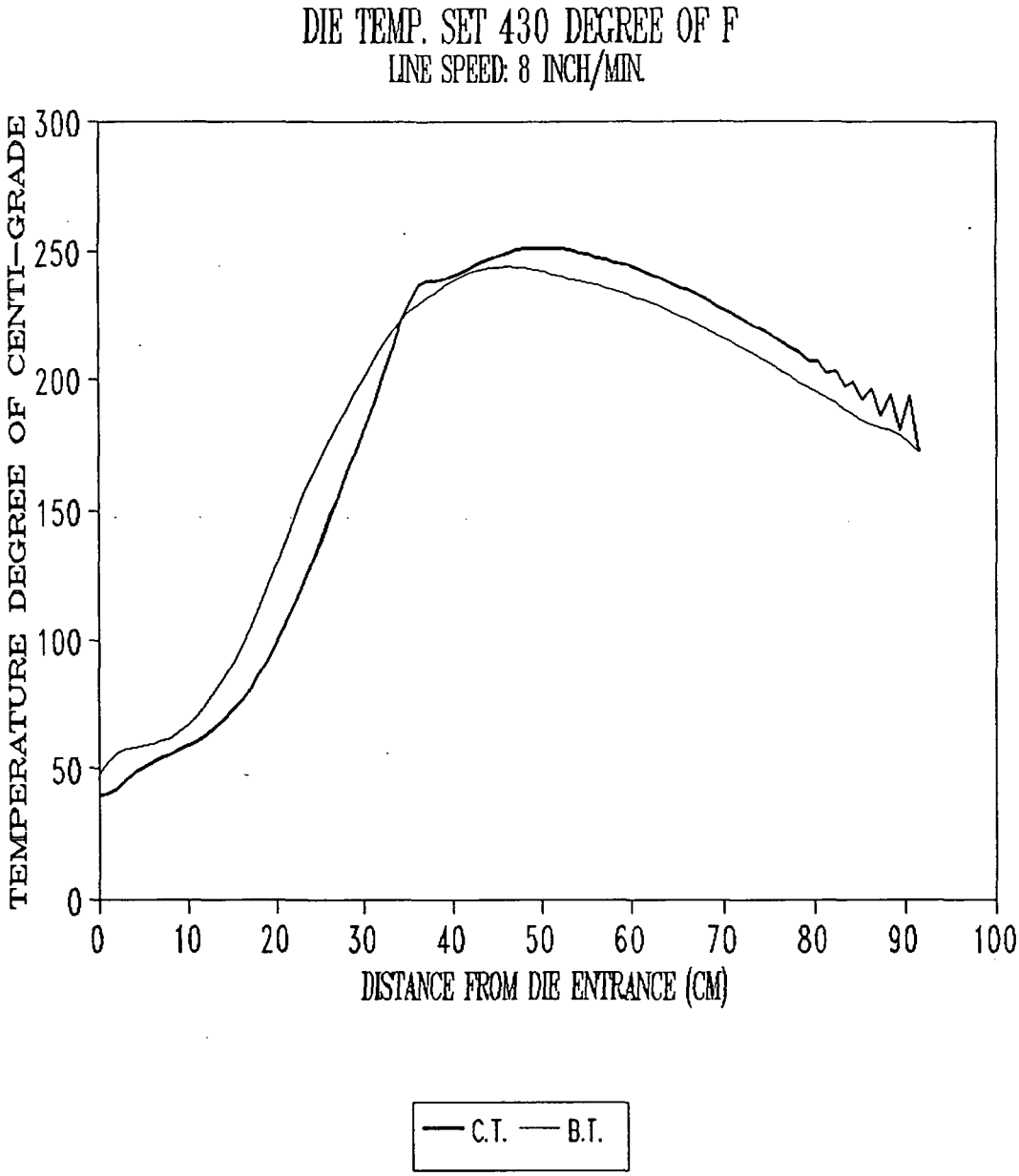
DIE TEMP. SET 430 DEGREE OF F
LINE SPEED: 8 INCH/MIN.
TEMPERATURE DEGREE OF CENTI-GRADE
300
250
200
150
100
50
0
0
10
20
30
40
50
60
70
80
90
100
DISTANCE FROM DIE ENTRANCE (CM)
C.T.
B.T.

Figure A-15

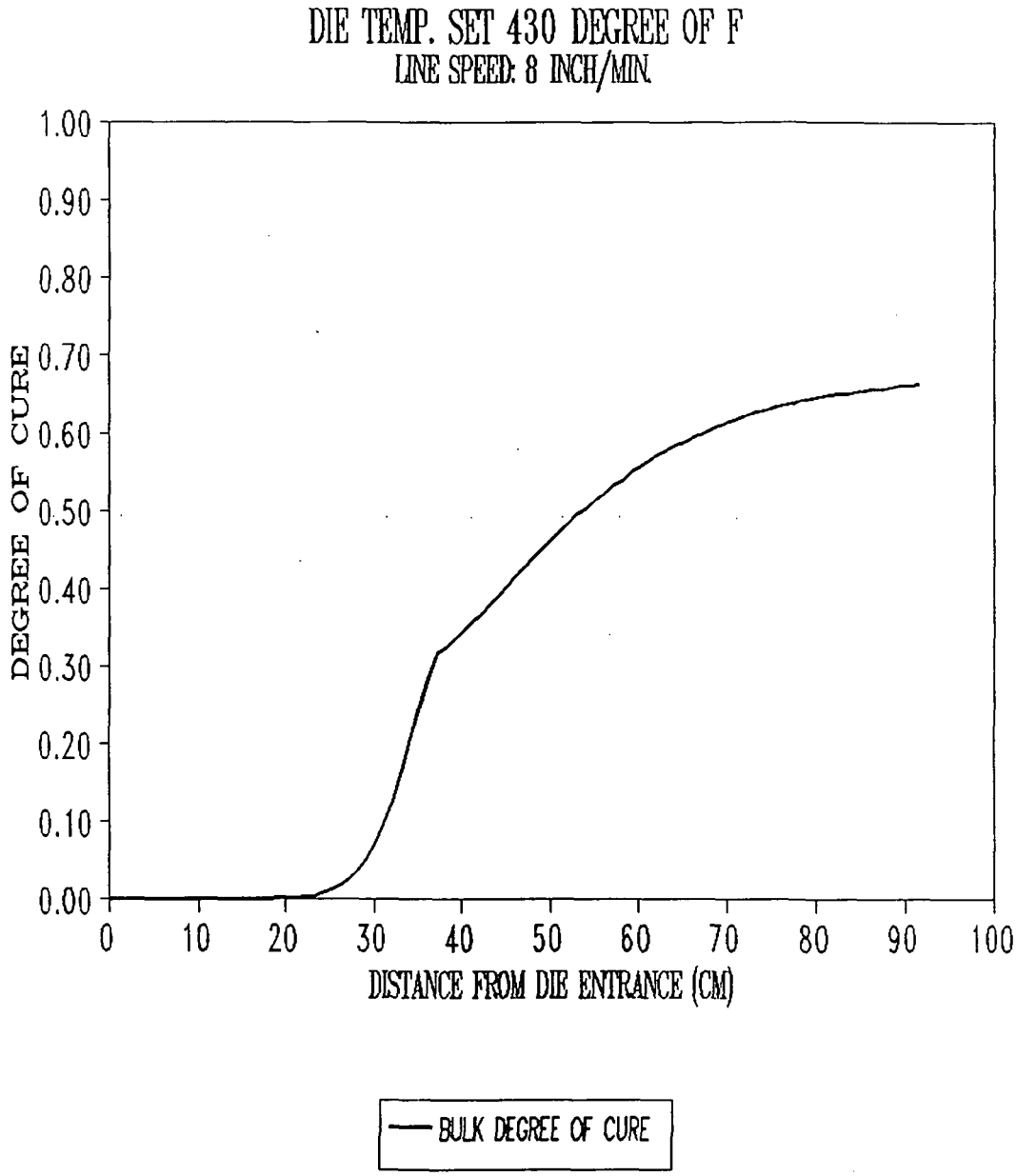
DIE TEMP. SET 430 DEGREE OF F
LINE SPEED: 8 INCH/MIN.
DEGREE OF CURE
1.00
0.90
0.80
0.70
0.60
0.50
0.40
0.30
0.20
0.10
0.00
0
10
20
30
40
50
60
70
80
90
100
DISTANCE FROM DIE ENTRANCE (CM)
BULK DEGREE OF CURE

Figure A-16

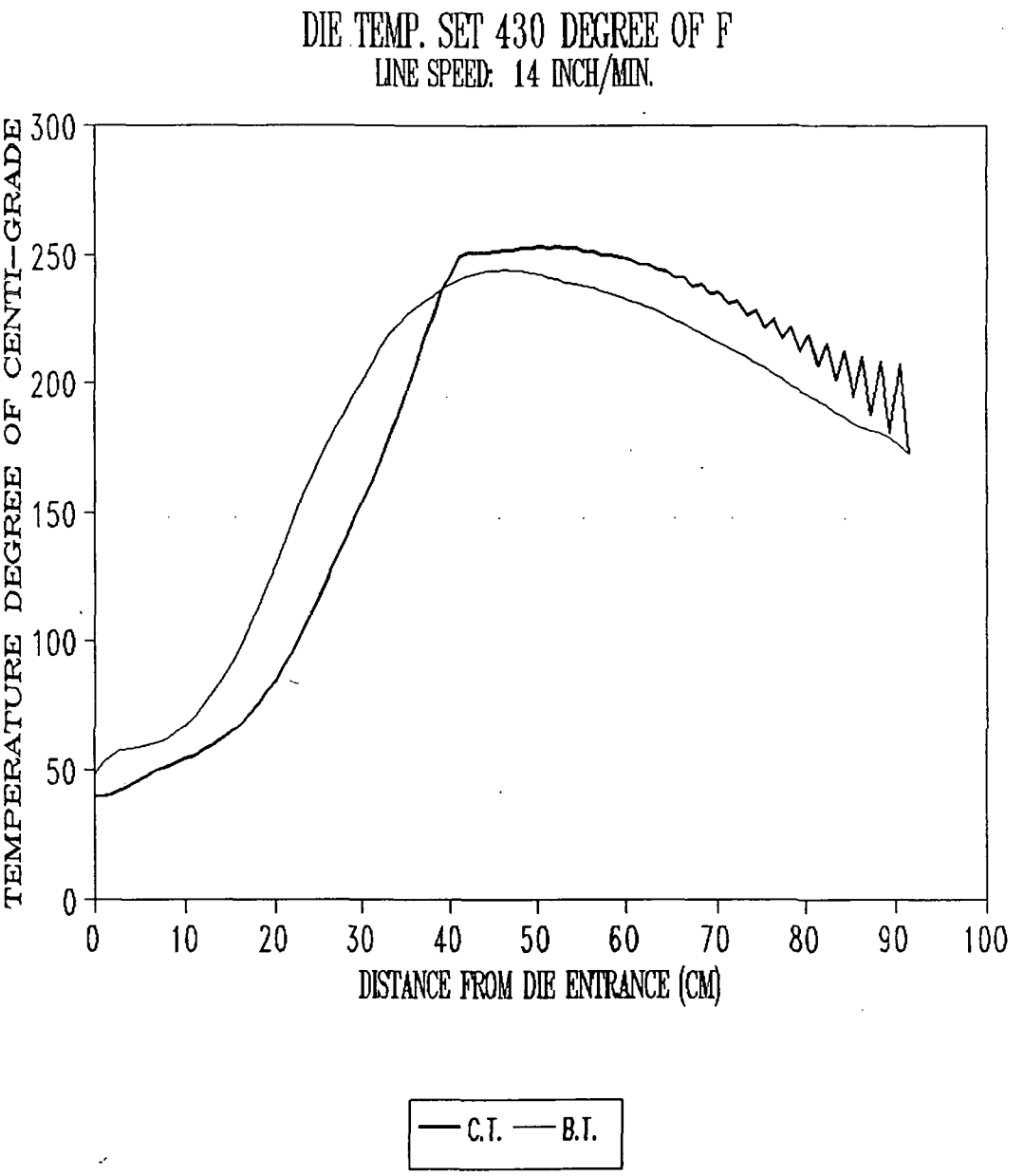
DIE TEMP. SET 430 DEGREE OF F
LINE SPEED: 14 INCH/MIN.
TEMPERATURE DEGREE OF CENTI-GRADE
300
250
200
150
100
50
0
0
10
20
30
40
50
60
70
80
90
100
DISTANCE FROM DIE ENTRANCE (CM)
C.T.
B.T.

Figure A-17

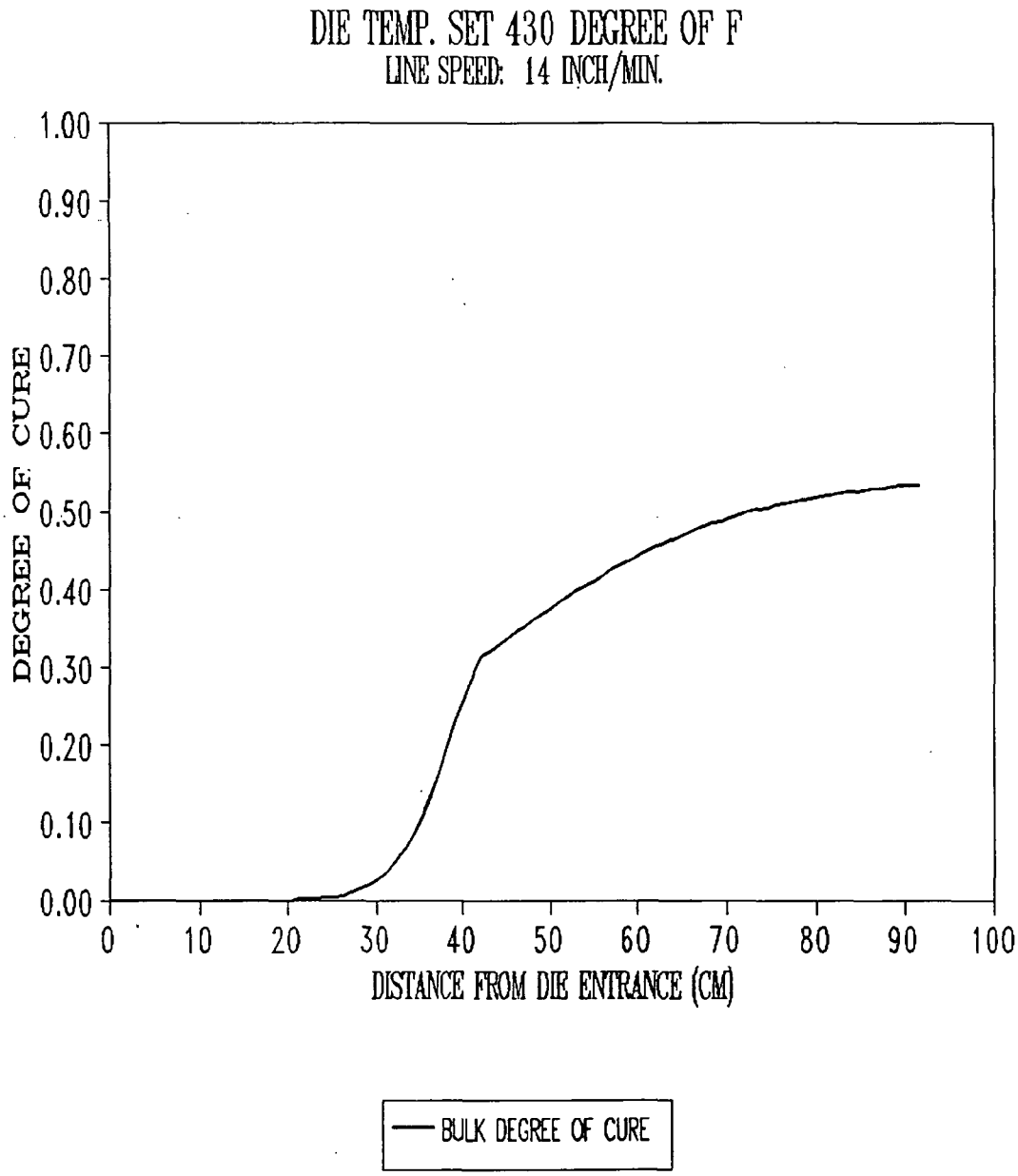
DIE TEMP. SET 430 DEGREE OF F
LINE SPEED: 14 INCH/MIN.
DEGREE OF CURE
1.00
0.90
0.80
0.70
0.60
0.50
0.40
0.30
0.20
0.10
0.00
0
10
20
30
40
50
60
70
80
90
100
DISTANCE FROM DIE ENTRANCE (CM)
BULK DEGREE OF CURE

Figure A-18

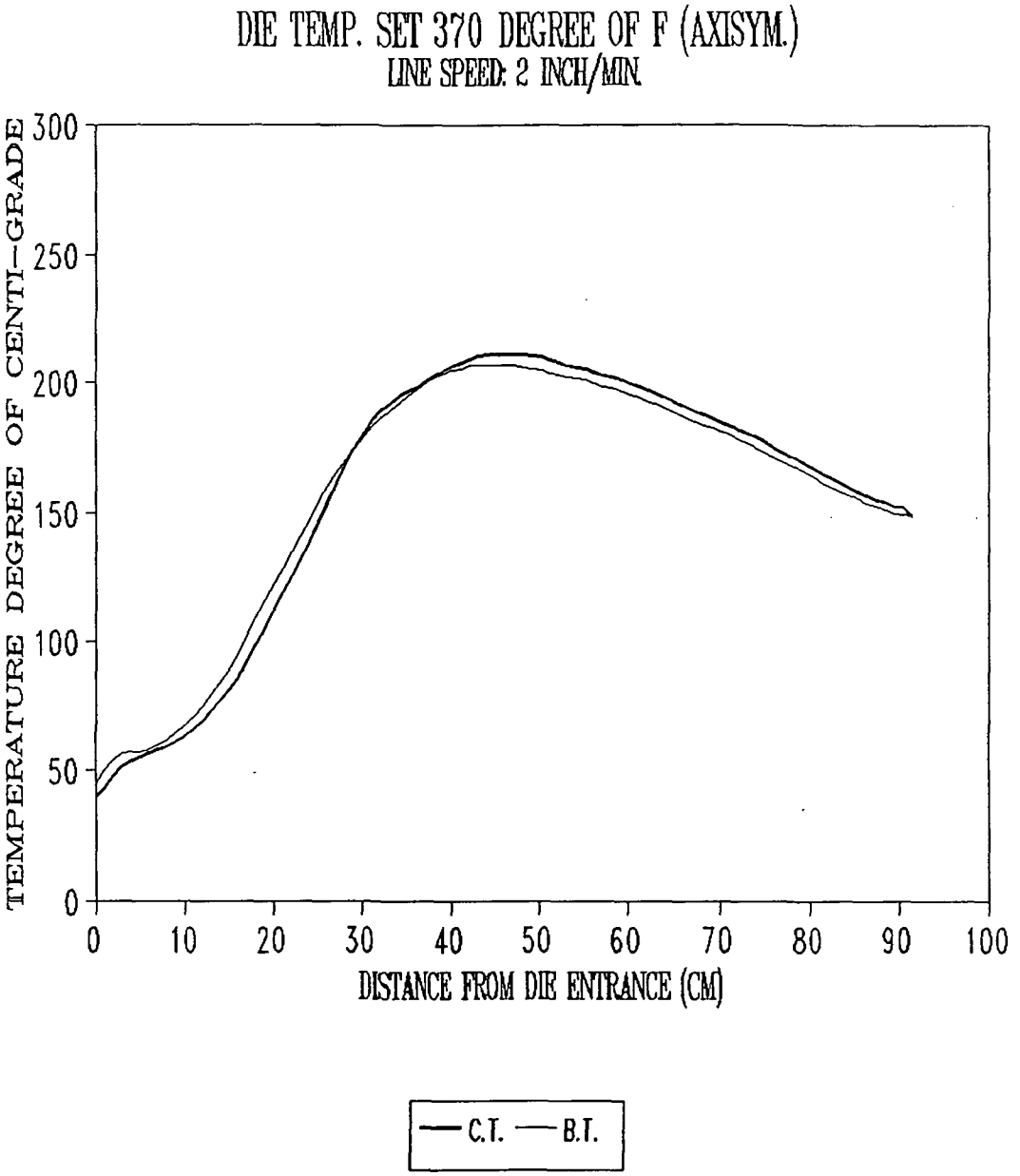
DIE TEMP. SET 370 DEGREE OF F (AXISYM.)
LINE SPEED: 2 INCH/MIN.
TEMPERATURE DEGREE OF CENTI-GRADE
300
250
200
150
100
50
0
0
10
20
30
40
50
60
70
80
90
100
DISTANCE FROM DIE ENTRANCE (CM)
C.T.
B.T.

Figure A-19

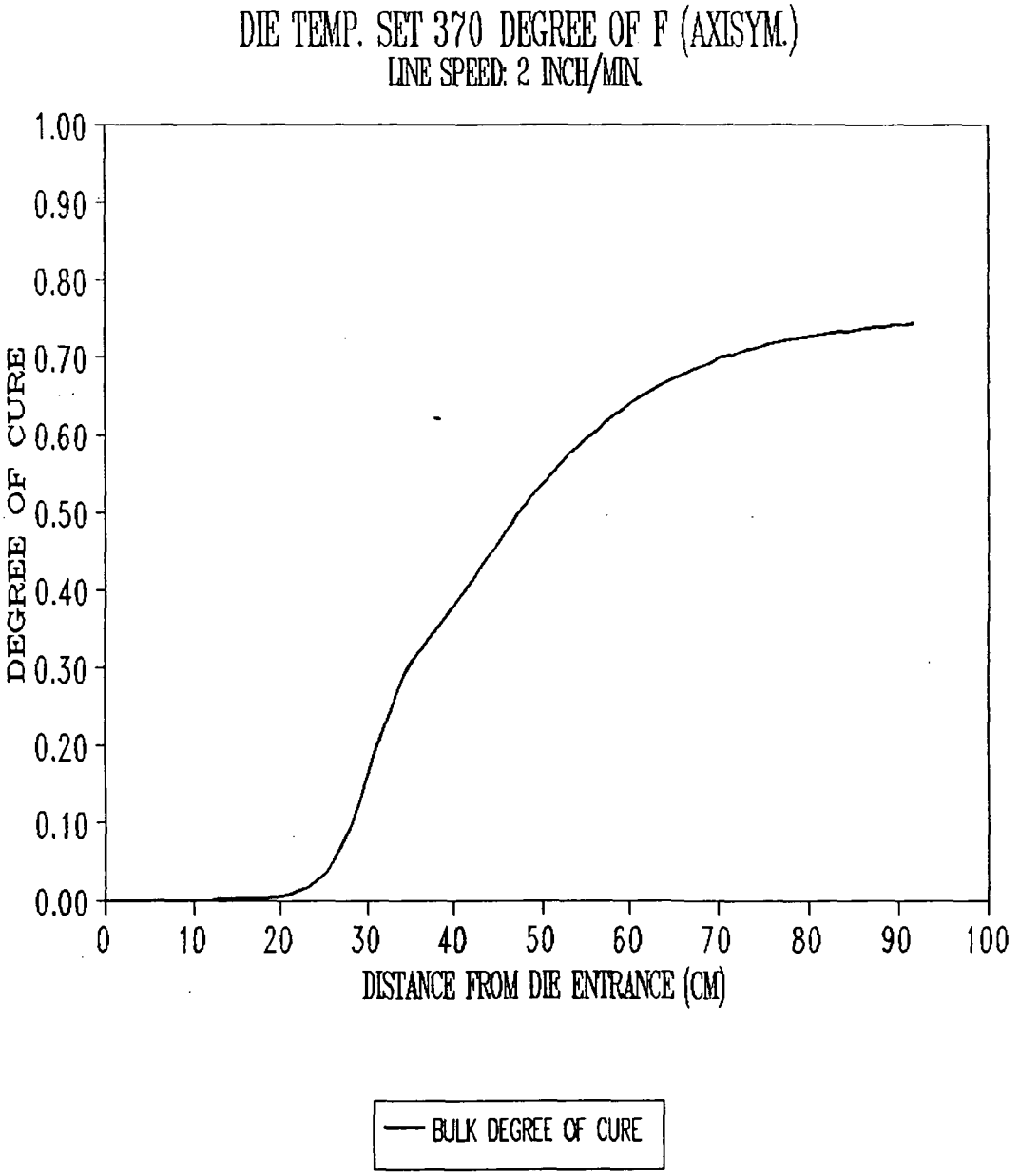
DIE TEMP. SET 370 DEGREE OF F (AXISYM.)
LINE SPEED: 2 INCH/MIN.
DEGREE OF CURE
1.00
0.90
0.80
0.70
0.60
0.50
0.40
0.30
0.20
0.10
0.00
0
10
20
30
40
50
60
70
80
90
100
DISTANCE FROM DIE ENTRANCE (CM)
BULK DEGREE OF CURE

Figure A-20

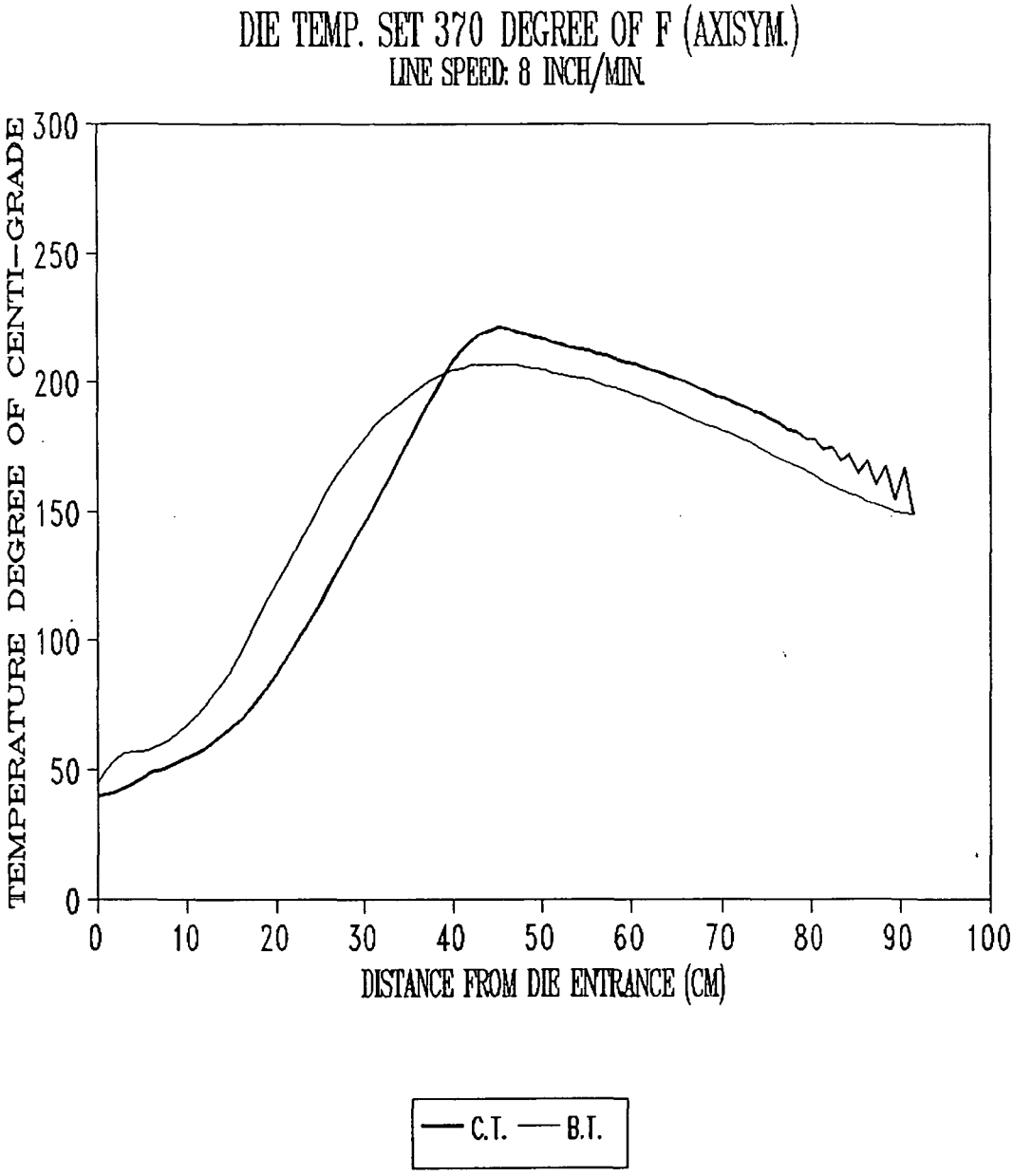
DIE TEMP. SET 370 DEGREE OF F (AXISYM.)
LINE SPEED: 8 INCH/MIN.
TEMPERATURE DEGREE OF CENTI-GRADE
300
250
200
150
100
50
0
0
10
20
30
40
50
60
70
80
90
100
DISTANCE FROM DIE ENTRANCE (CM)
C.T.
B.T.

Figure A-21

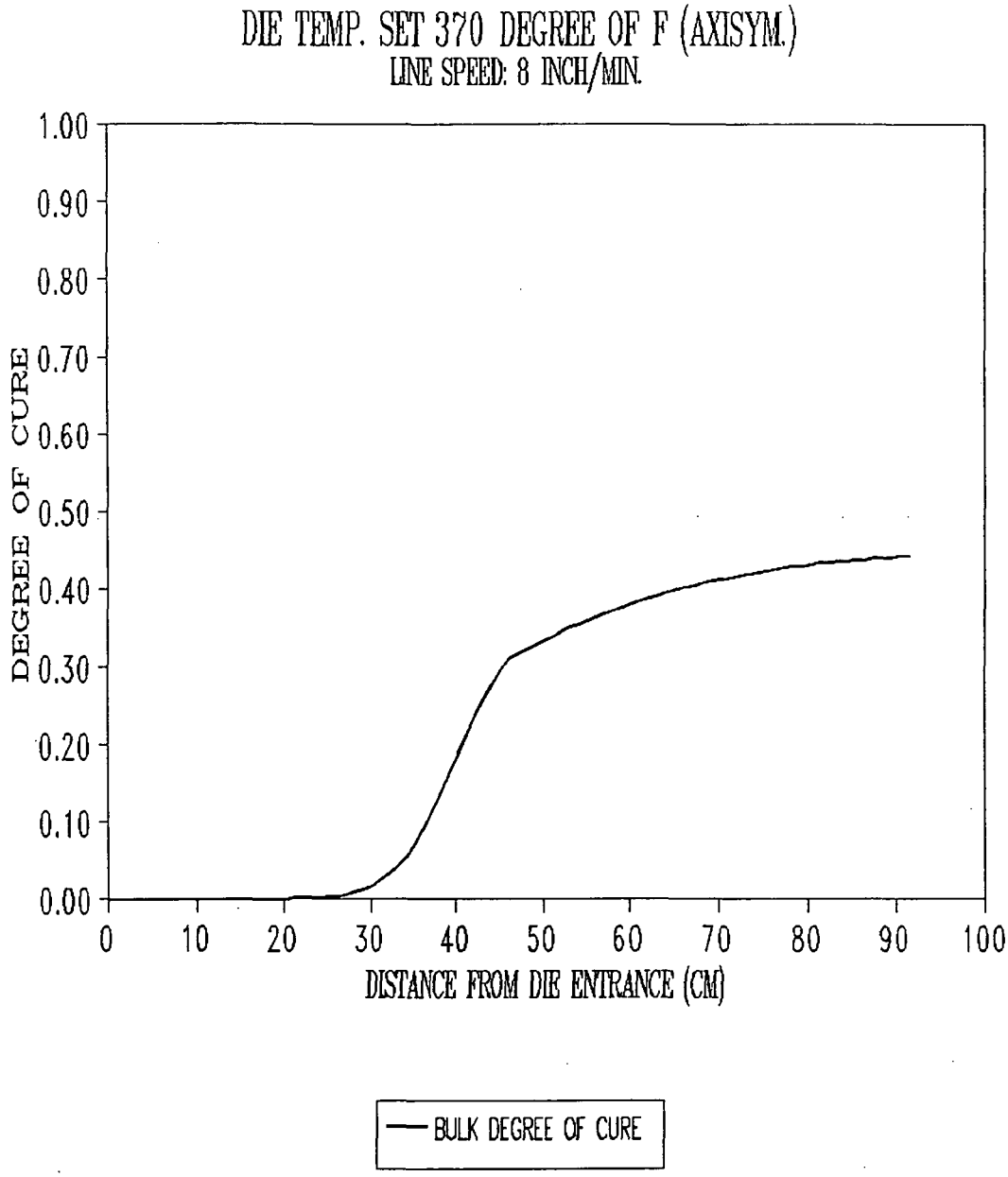
DIE TEMP. SET 370 DEGREE OF F (AXISYM.)
LINE SPEED: 8 INCH/MIN.
DEGREE OF CURE
1.00
0.90
0.80
0.70
0.60
0.50
0.40
0.30
0.20
0.10
0.00
0
10
20
30
40
50
60
70
80
90
100
DISTANCE FROM DIE ENTRANCE (CM)
BULK DEGREE OF CURE

Figure A-22

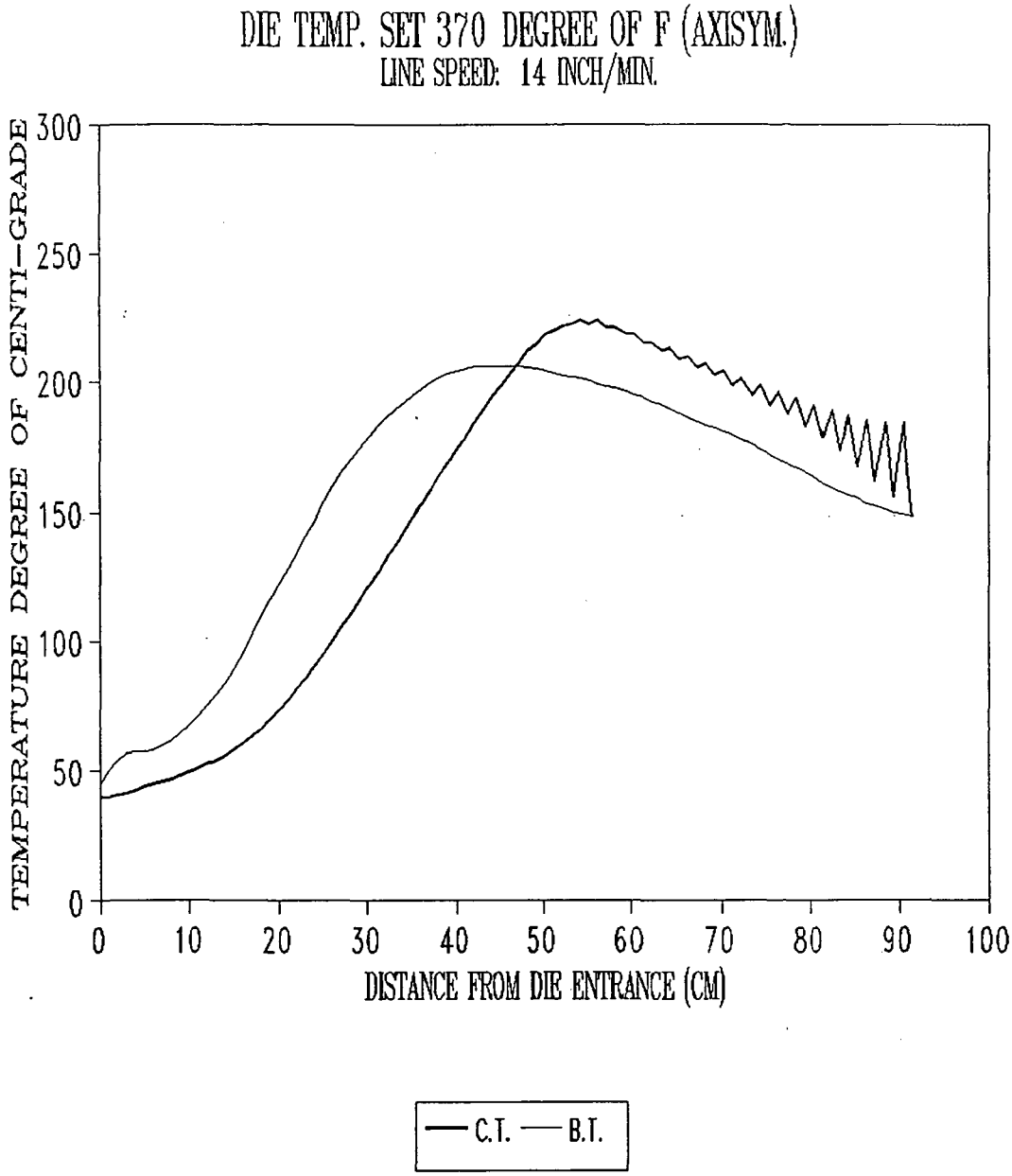
DIE TEMP. SET 370 DEGREE OF F (AXISYM.)
LINE SPEED: 14 INCH/MIN.
TEMPERATURE DEGREE OF CENTI-GRADE
300
250
200
150
100
50
0
0
10
20
30
40
50
60
70
80
90
100
DISTANCE FROM DIE ENTRANCE (CM)
C.T.
B.T.

Figure A-23

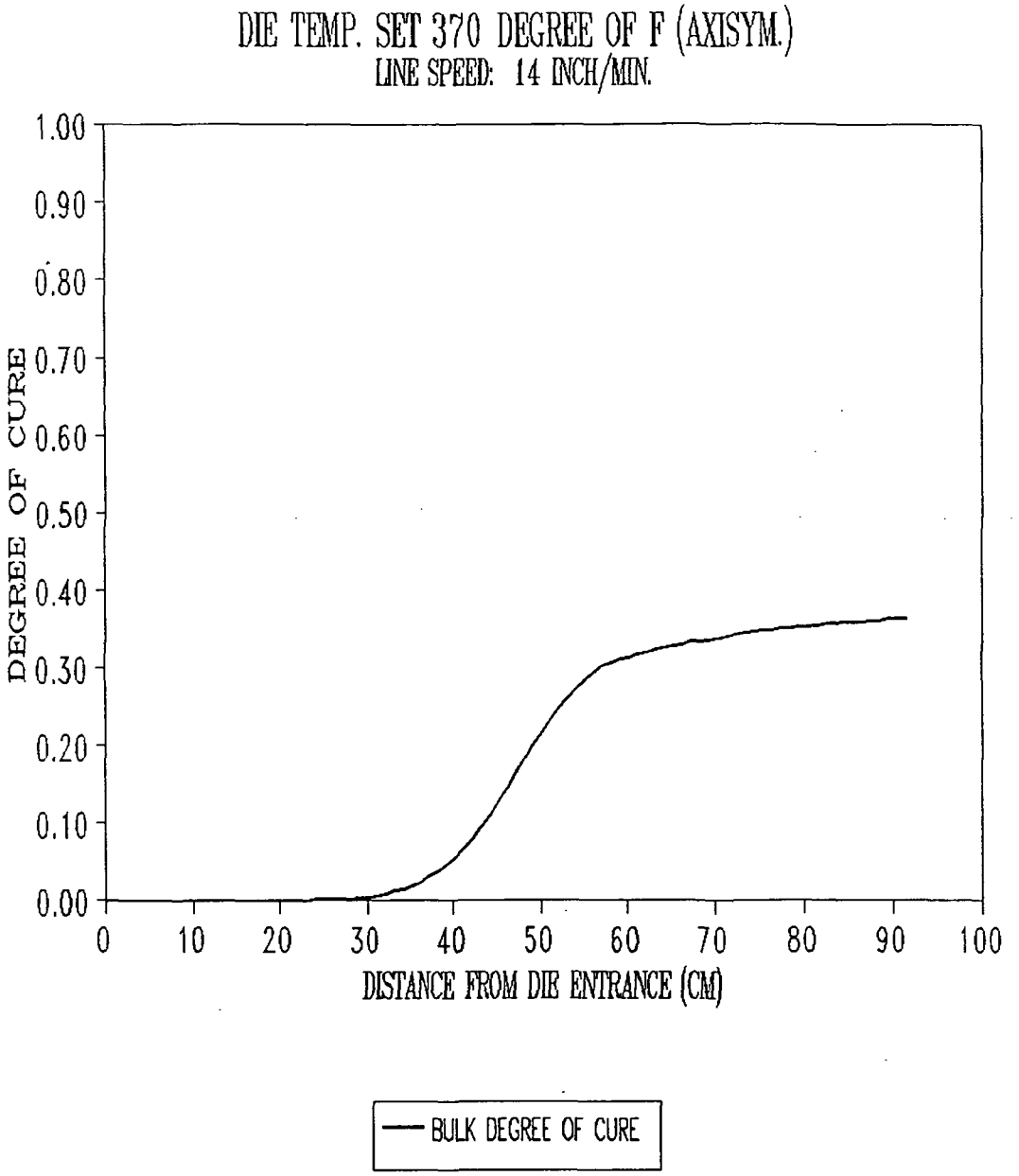
DIE TEMP. SET 370 DEGREE OF F (AXISYM.)
LINE SPEED: 14 INCH/MIN.
DEGREE OF CURE
1.00
0.90
0.80
0.70
0.60
0.50
0.40
0.30
0.20
0.10
0.00
0
10
20
30
40
50
60
70
80
90
100
DISTANCE FROM DIE ENTRANCE (CM)
BULK DEGREE OF CURE

Figure A-24

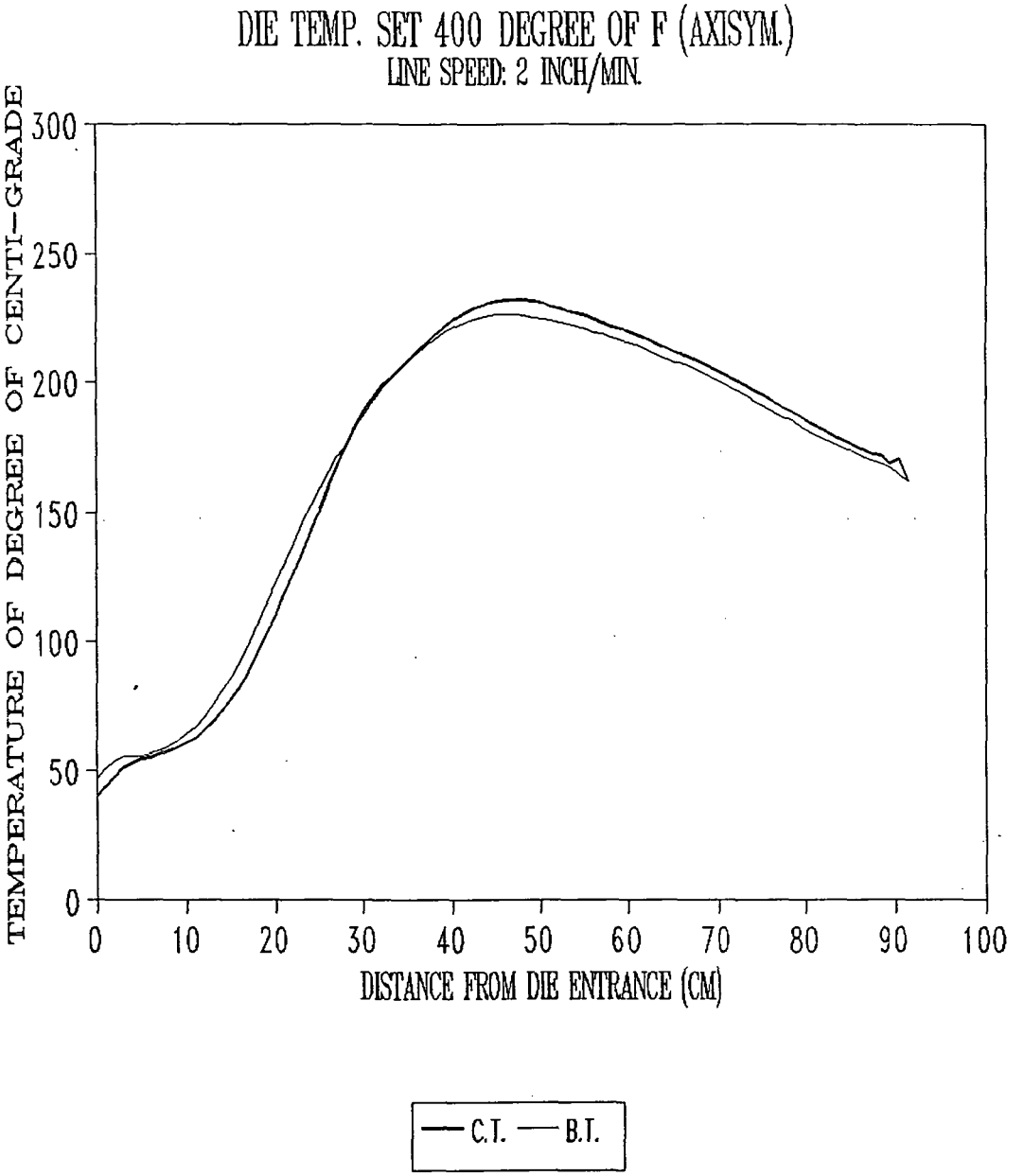
DIE TEMP. SET 400 DEGREE OF F (AXISYM.)
LINE SPEED: 2 INCH/MIN.
TEMPERATURE OF DEGREE OF CENTI-GRADE
300
250
200
150
100
50
0
0
10
20
30
40
50
60
70
80
90
100
DISTANCE FROM DIE ENTRANCE (CM)
C.T.
B.T.

Figure A-25

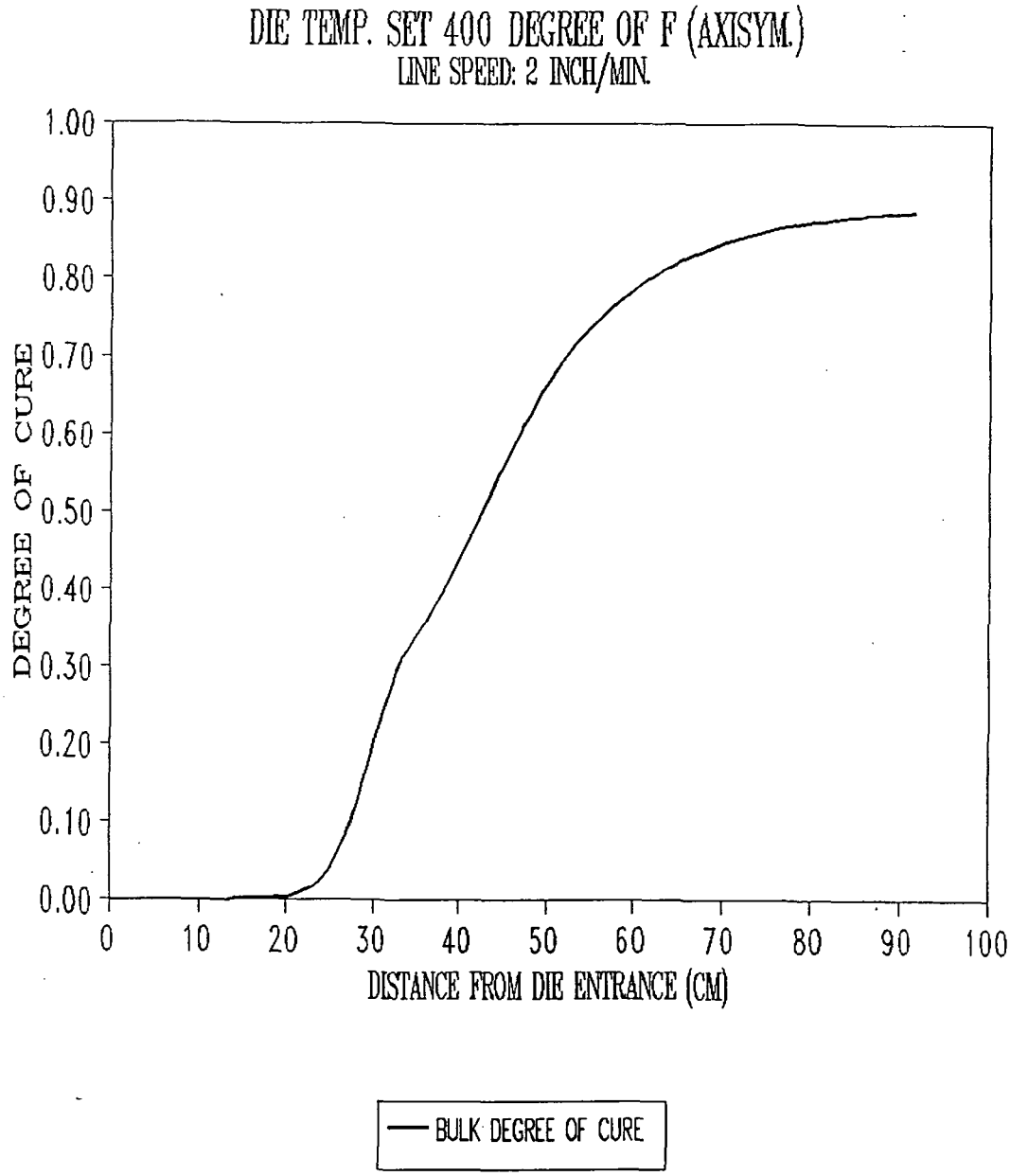
DIE TEMP. SET 400 DEGREE OF F (AXISYM.)
LINE SPEED: 2 INCH/MIN.
DEGREE OF CURE
1.00
0.90
0.80
0.70
0.60
0.50
0.40
0.30
0.20
0.10
0.00
0
10
20
30
40
50
60
70
80
90
100
DISTANCE FROM DIE ENTRANCE (CM)
BULK DEGREE OF CURE

Figure A-26

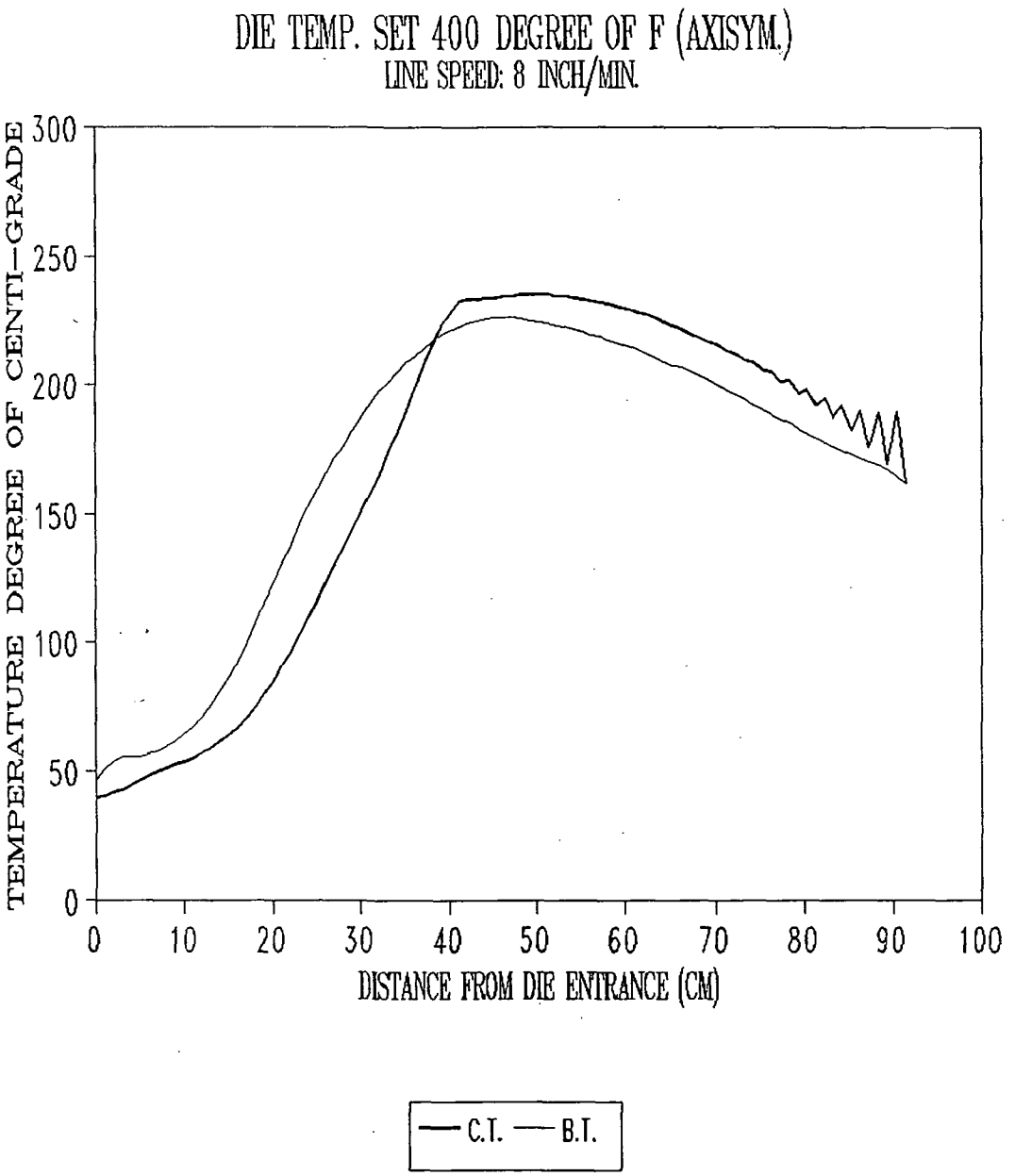
DIE TEMP. SET 400 DEGREE OF F (AXISYM.)
LINE SPEED: 8 INCH/MIN.
TEMPERATURE DEGREE OF CENTI-GRADE
300
250
200
150
100
50
0
0
10
20
30
40
50
60
70
80
90
100
DISTANCE FROM DIE ENTRANCE (CM)
C.T.
B.T.

Figure A-27

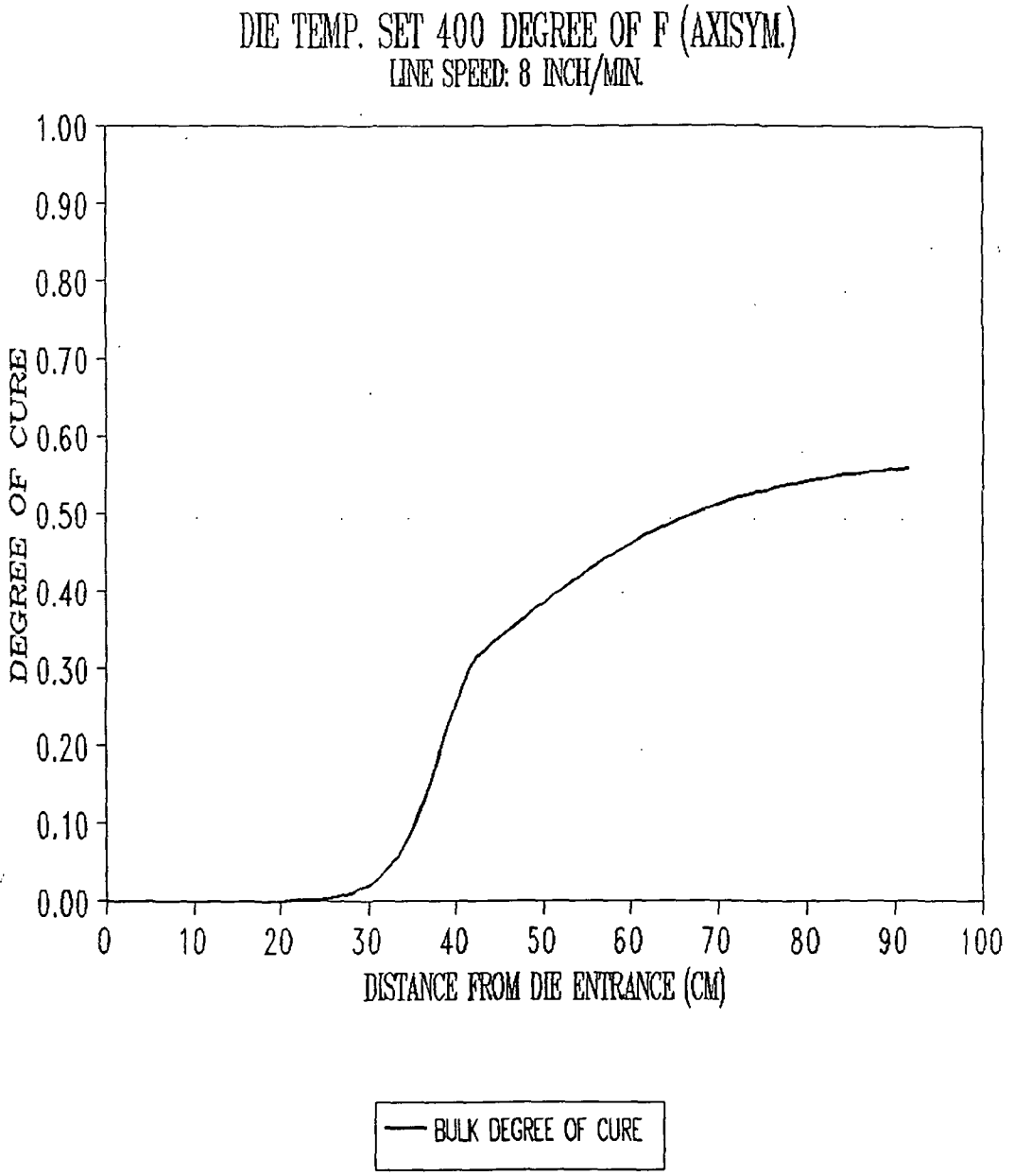
DIE TEMP. SET 400 DEGREE OF F (AXISYM.)
LINE SPEED: 8 INCH/MIN.
DEGREE OF CURE
1.00
0.90
0.80
0.70
0.60
0.50
0.40
0.30
0.20
0.10
0.00
0
10
20
30
40
50
60
70
80
90
100
DISTANCE FROM DIE ENTRANCE (CM)
BULK DEGREE OF CURE

Figure A-28

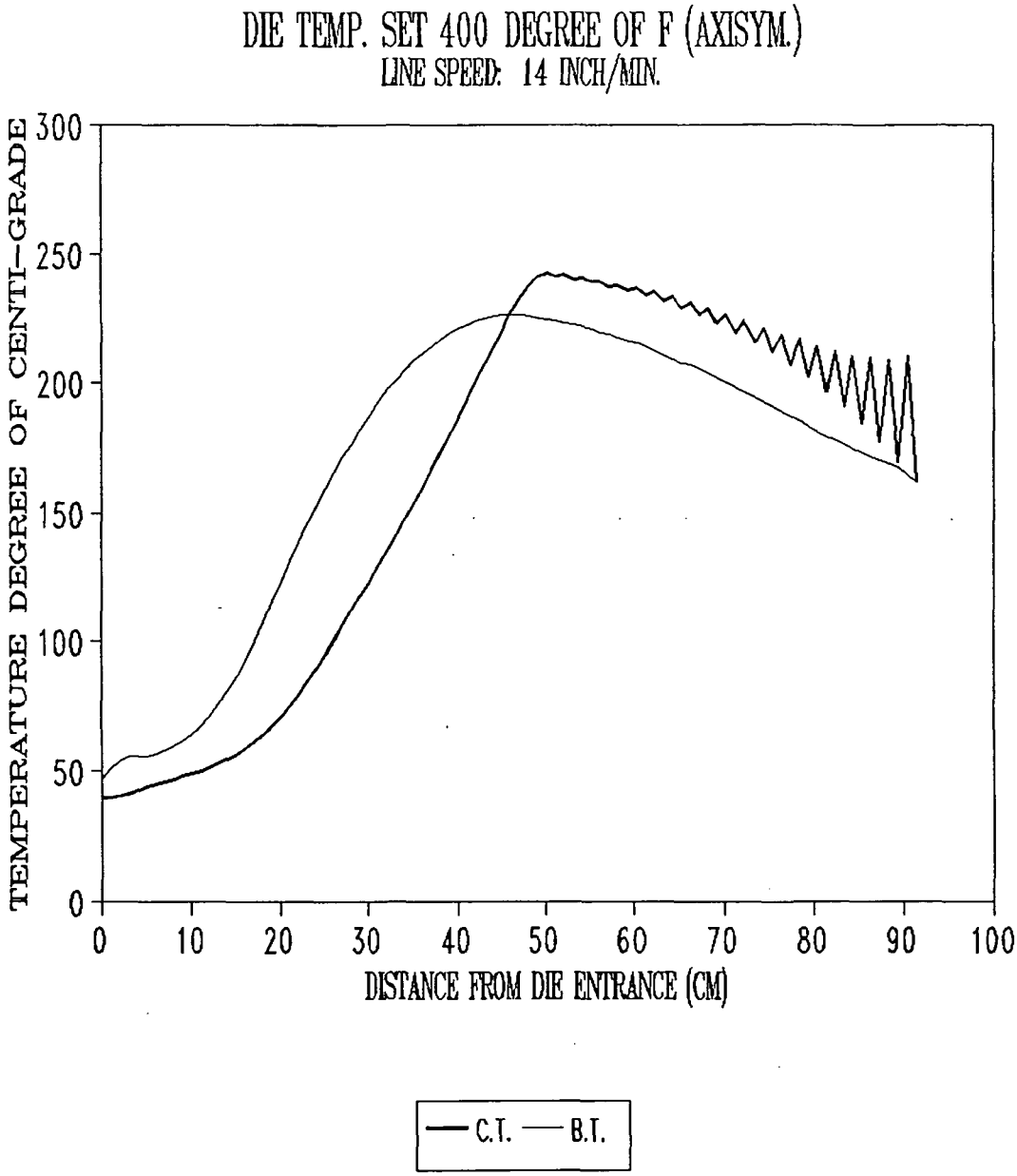
DIE TEMP. SET 400 DEGREE OF F (AXISYM.)
LINE SPEED: 14 INCH/MIN.
TEMPERATURE DEGREE OF CENTI-GRADE
300
250
200
150
100
50
0
0
10
20
30
40
50
60
70
80
90
100
DISTANCE FROM DIE ENTRANCE (CM)
C.T.
B.T.

Figure A-29

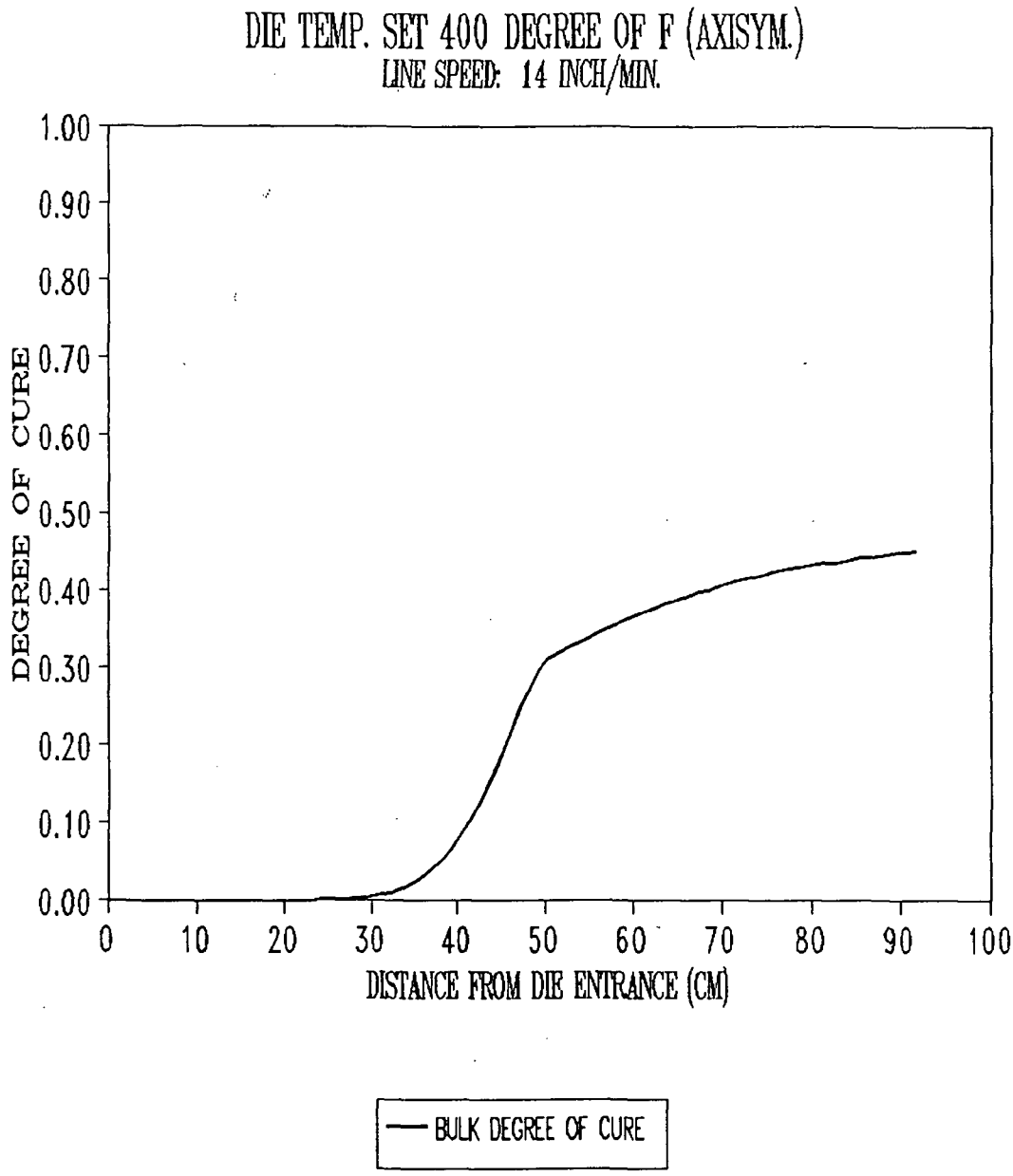
DIE TEMP. SET 400 DEGREE OF F (AXISYM.)
LINE SPEED: 14 INCH/MIN.
DEGREE OF CURE
1.00
0.90
0.80
0.70
0.60
0.50
0.40
0.30
0.20
0.10
0.00
0
10
20
30
40
50
60
70
80
90
100
DISTANCE FROM DIE ENTRANCE (CM)
BULK DEGREE OF CURE

Figure A-30

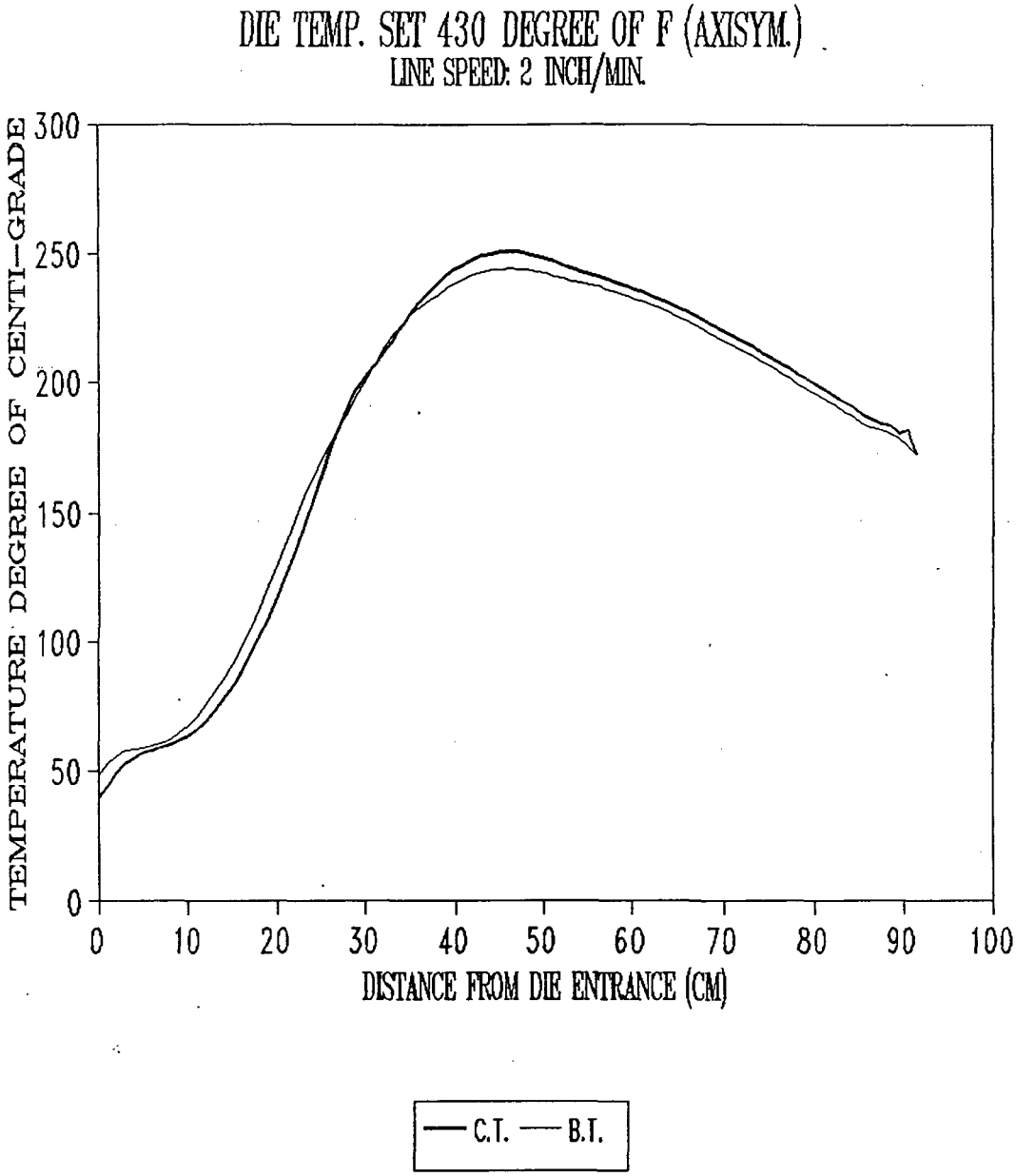
DIE TEMP. SET 430 DEGREE OF F (AXISYM.)
LINE SPEED: 2 INCH/MIN.
TEMPERATURE DEGREE OF CENTI-GRADE
300
250
200
150
100
50
0
0
10
20
30
40
50
60
70
80
90
100
DISTANCE FROM DIE ENTRANCE (CM)
C.T.
B.T.

Figure A-31

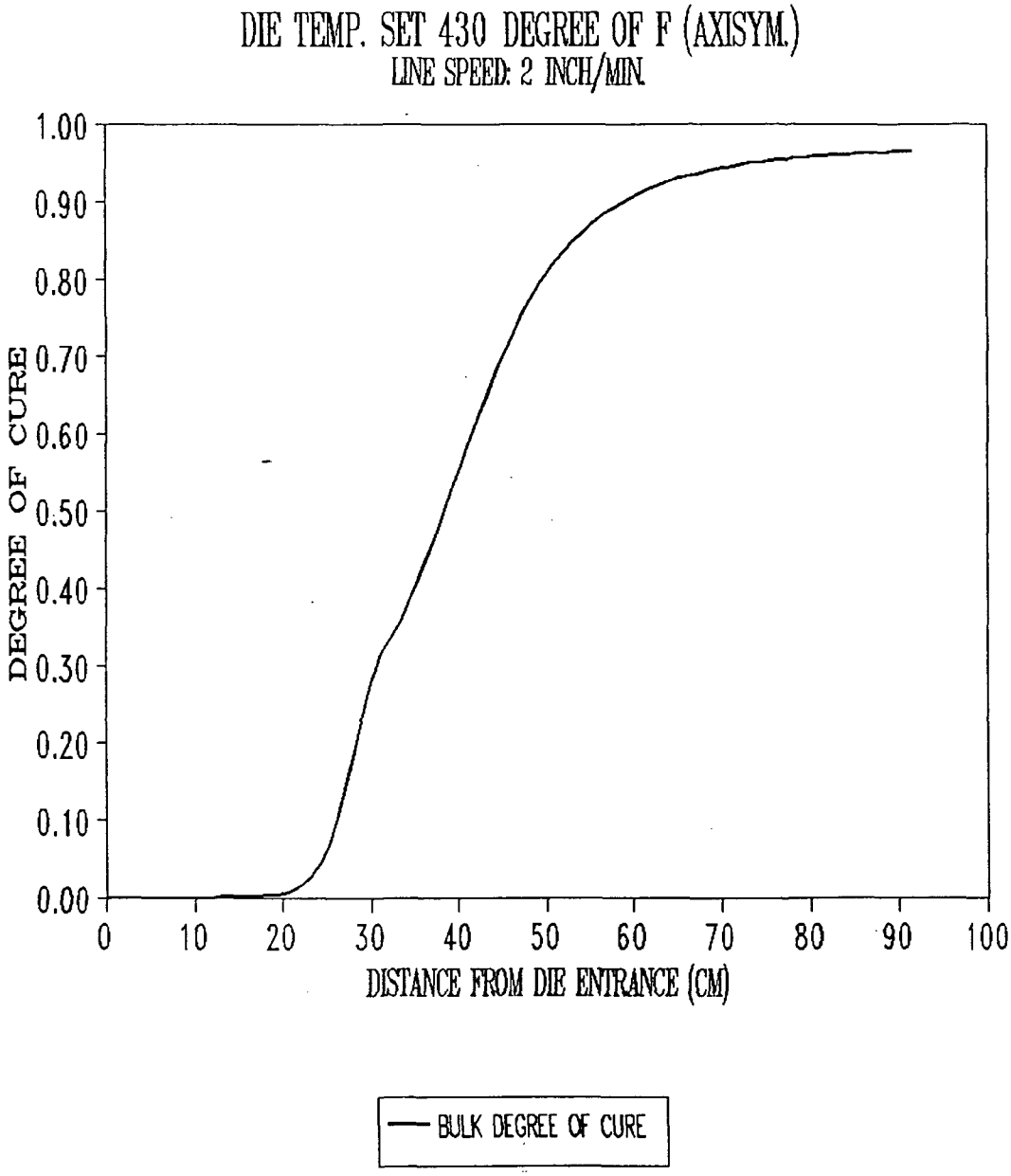
DIE TEMP. SET 430 DEGREE OF F (AXISYM.)
LINE SPEED: 2 INCH/MIN.
DEGREE OF CURE
1.00
0.90
0.80
0.70
0.60
0.50
0.40
0.30
0.20
0.10
0.00
0
10
20
30
40
50
60
70
80
90
100
DISTANCE FROM DIE ENTRANCE (CM)
BULK DEGREE OF CURE

Figure A-32

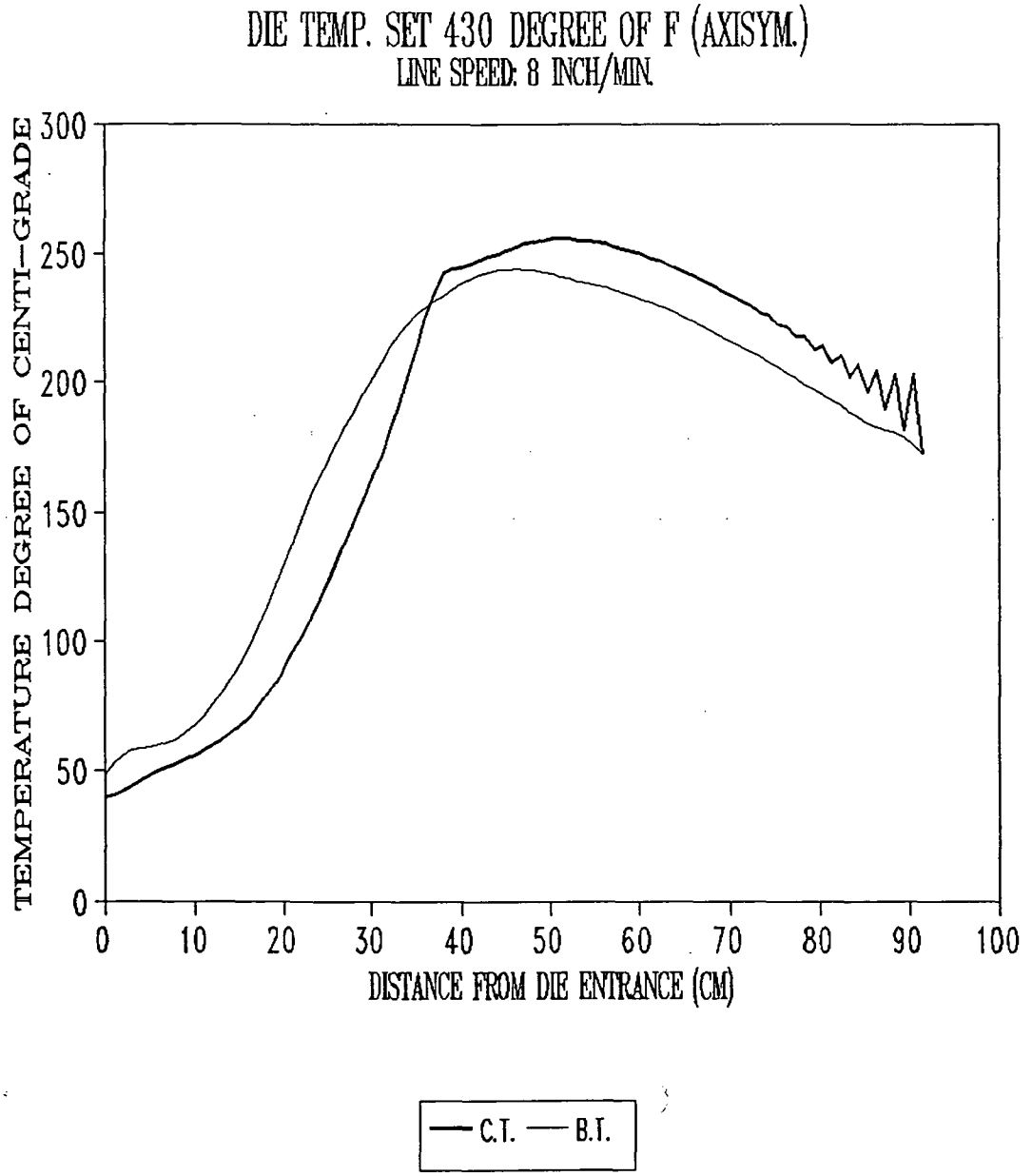
DIE TEMP. SET 430 DEGREE OF F (AXISYM.)
LINE SPEED: 8 INCH/MIN.
TEMPERATURE DEGREE OF CENTI-GRADE
300
250
200
150
100
50
0
0
10
20
30
40
50
60
70
80
90
100
DISTANCE FROM DIE ENTRANCE (CM)
C.T.
B.T.

Figure A-33

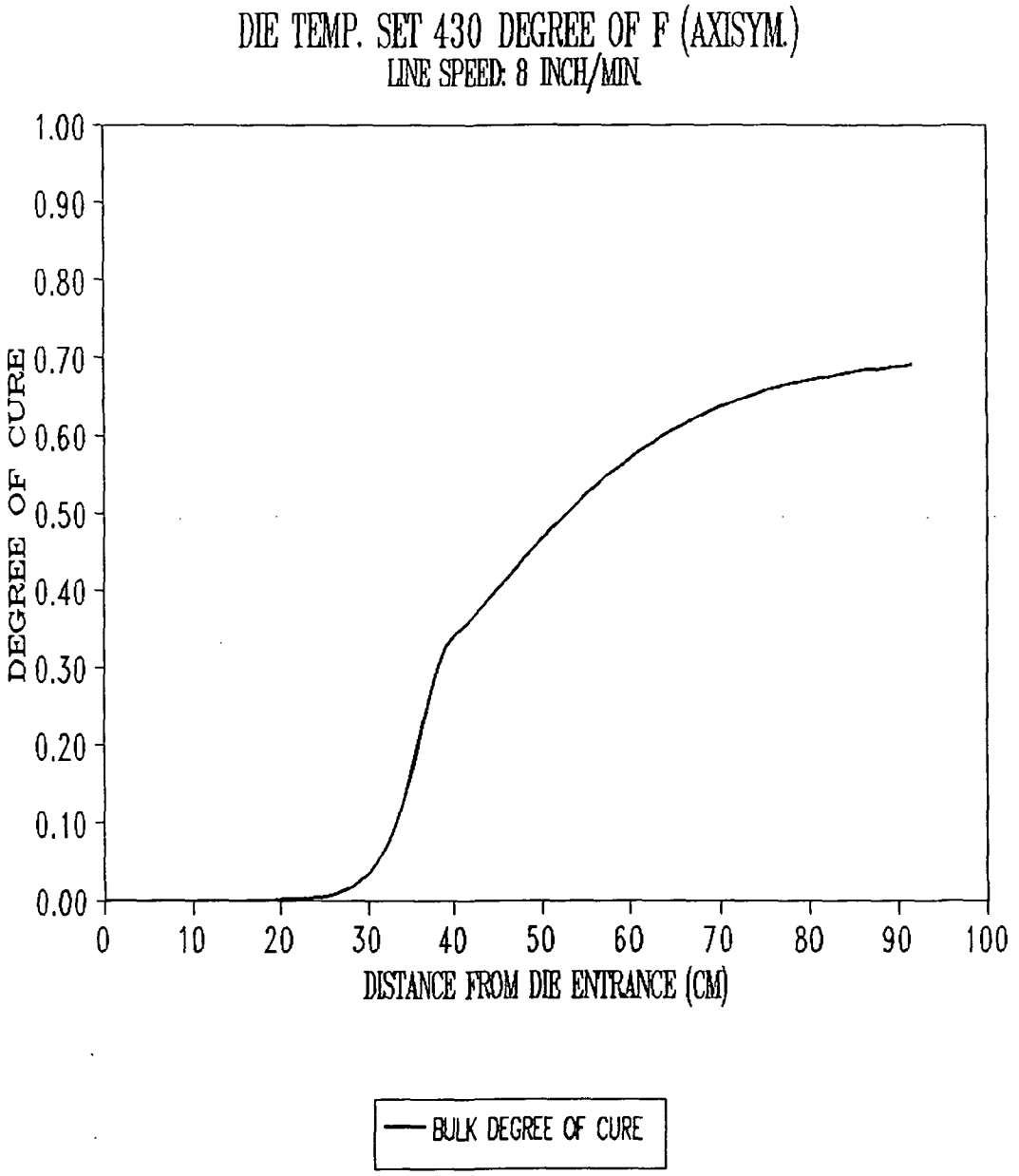
DIE TEMP. SET 430 DEGREE OF F (AXISYM.)
LINE SPEED: 8 INCH/MIN.
DEGREE OF CURE
1.00
0.90
0.80
0.70
0.60
0.50
0.40
0.30
0.20
0.10
0.00
0
10
20
30
40
50
60
70
80
90
100
DISTANCE FROM DIE ENTRANCE (CM)
BULK DEGREE OF CURE

Figure A-34

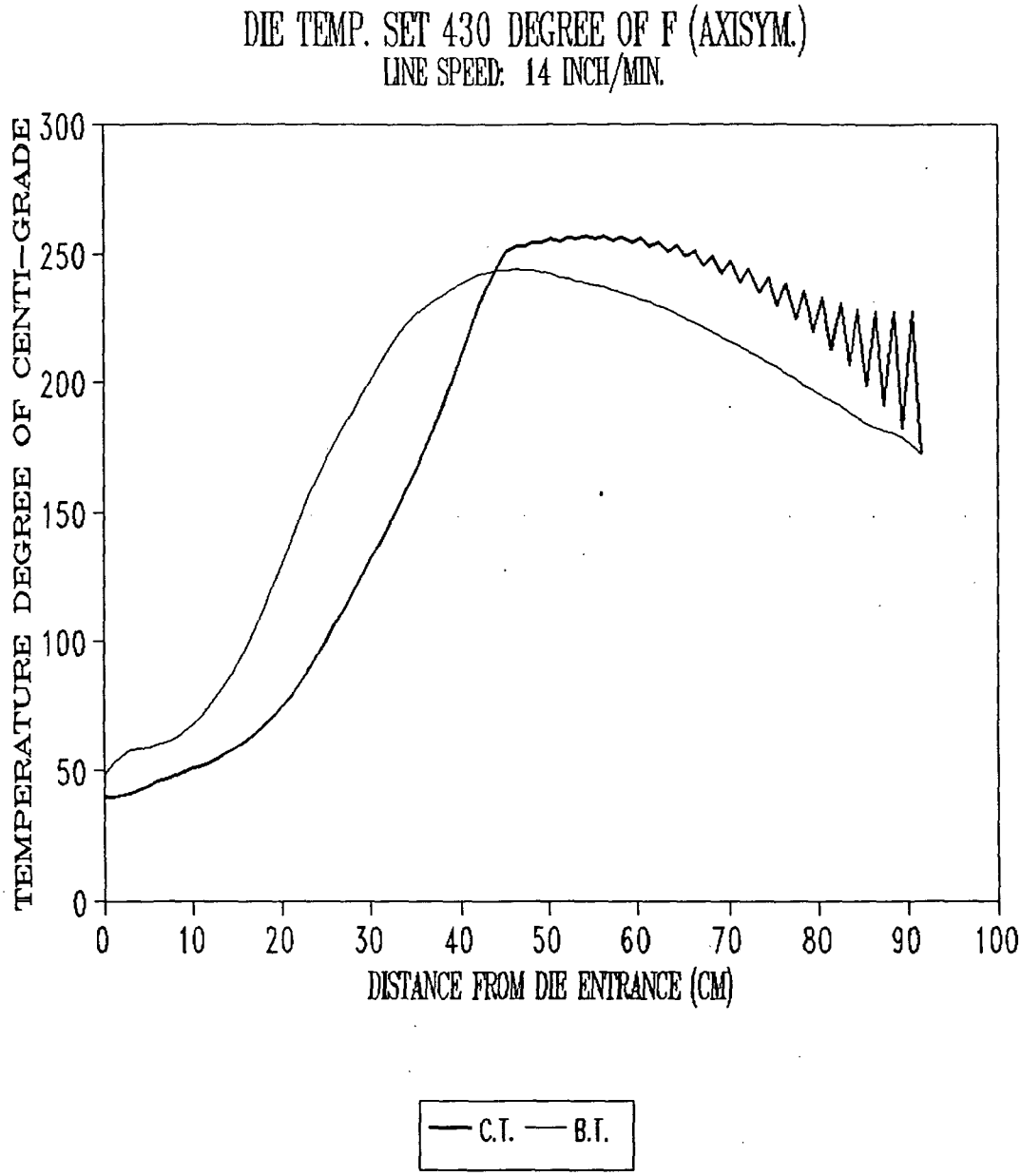
DIE TEMP. SET 430 DEGREE OF F (AXISYM.)
LINE SPEED: 14 INCH/MIN.
TEMPERATURE DEGREE OF CENTI-GRADE
300
250
200
150
100
50
0
0
10
20
30
40
50
60
70
80
90
100
DISTANCE FROM DIE ENTRANCE (CM)
C.T.
B.T.

Figure A-35

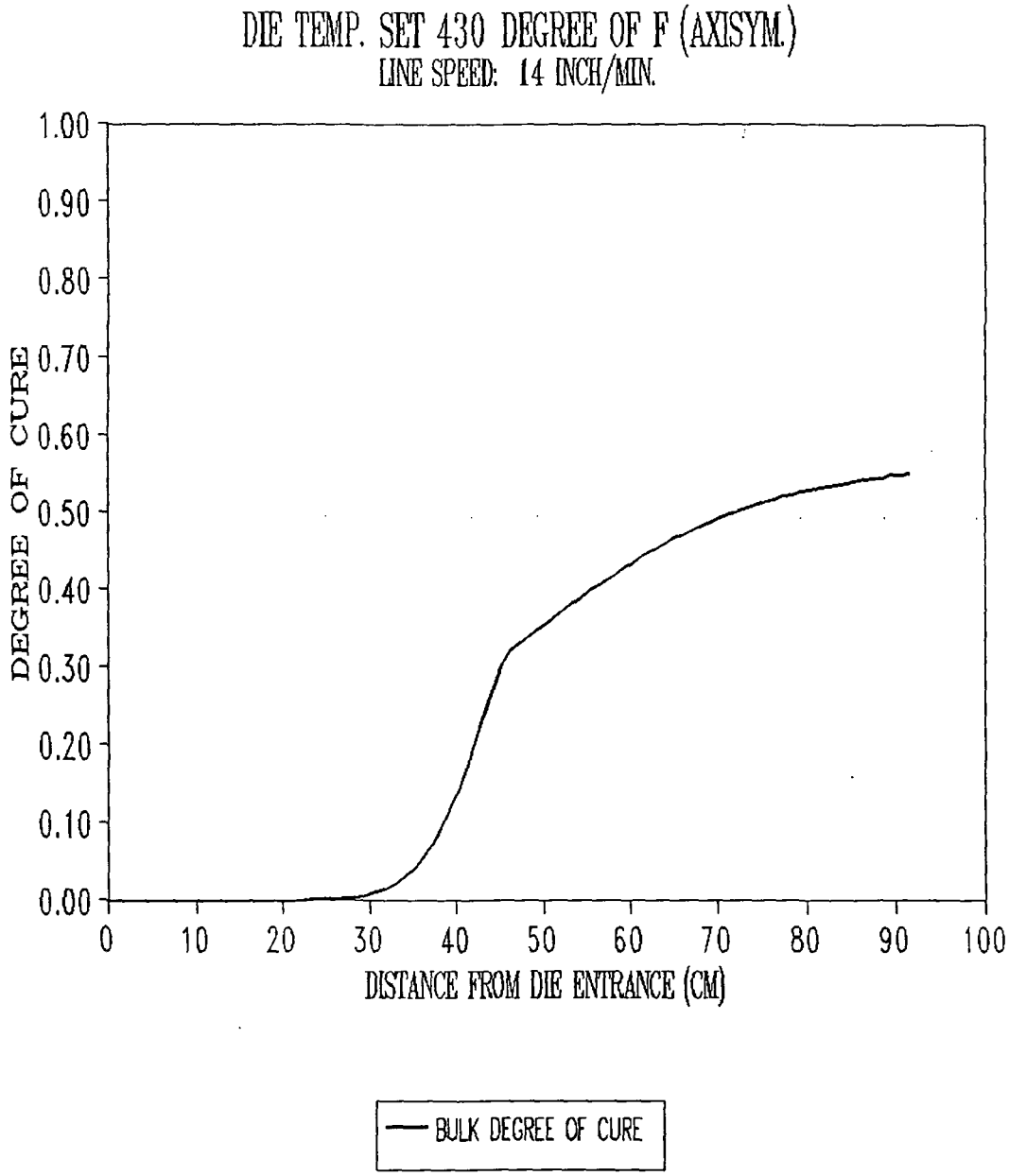
DIE TEMP. SET 430 DEGREE OF F (AXISYM.)
LINE SPEED: 14 INCH/MIN.
DEGREE OF CURE
1.00
0.90
0.80
0.70
0.60
0.50
0.40
0.30
0.20
0.10
0.00
0
10
20
30
40
50
60
70
80
90
100
DISTANCE FROM DIE ENTRANCE (CM)
BULK DEGREE OF CURE

Figure A-36

NASA National Aeronautics and Space Administration

Report Documentation Page

1. Report No.	2. Government Accession No.	3. Recipient's Catalog No.

4. Title and Subtitle

Pultrusion Process Characterization

5. Report Date

September 25, 1991

6. Performing Organization Code

7. Author(s)

James G. Vaughan
Robert M. Hackett

8. Performing Organization Report No.

10. Work Unit No.

9. Performing Organization Name and Address

School of Engineering
The University of Mississippi
University, MS 38677

11. Contract or Grant No.

NAS8-37193

13. Type of Report and Period Covered

Final
7 Aug. 90 - 6 Aug. 91

12. Sponsoring Agency Name and Address

National Aeronautics and Space Administration
Marshall Space Flight Center, AL 35812

14. Sponsoring Agency Code

15. Supplementary Notes

16. Abstract

17. Key Words (Suggested by Author(s))

Pultrusion, Modeling, Finite Element, Characterization

18. Distribution Statement

19. Security Classif. (of this report)	20. Security Classif. (of this page)	21. No. of pages	22. Price
Unclassified	Unclassified		

NASA FORM 1626 OCT 86